# PVA-Based Scaffolds for Controlled Release of Neuroprotective Compounds

by

Zachary Blaine Visser

Submitted in partial fulfilment of the requirements
for the degree of Master of Applied Science

at

Dalhousie University
Halifax, Nova Scotia
July 2021

Dalhousie University is located in Mi'kma'ki,
the ancestral and unceded territory of the Mi'kmaq.
We are all Treaty people.

# TABLE OF CONTENTS

## List of Tables

## List of Figures

## Abstract

To restore function lost by damage to the nerve fibers, nerve regeneration must take place. Poor clinical outcomes are still observed for many autografting surgeries, stem cell therapies, and growth factor treatments. Biomaterials-based tissue engineering approaches to nerve repair utilize nerve guides. These nerve guides can be made of a variety of materials, using various fabrication processes and design concepts. The use of these nerve guides in conjunction with neurotrophic factors, gene therapies, cell transplants, and extracellular matrix proteins has shown improved experimental results for promoting nerve regeneration. Here, contact drawn poly(vinyl alcohol) fibers were cross-linked with glyoxal, to increase resistance to dissolution and hydrolytic degradation in an aqueous environment for application as a component of a nerve guide. Quercetin (an anti-inflammatory plant flavonoid) was loaded into fibers in a dose-dependent manner prior to contact drawing and reached a maximum cumulative release of 56 ± 6%. Fibers were characterized via IR spectroscopy. Glyoxal cross-linking and quercetin loading effects on fiber formation behavior and fiber diameters were investigated. Initial cytotoxicity screening against PC12Adh cells indicated novel PVA fiber formulations were not cytotoxic. The contact-drawn, glyoxal cross-linked, quercetin-loaded PVA fibers demonstrated potential for release of quercetin – a known neuroprotectant. Incorporation of these PVA fibers into a nerve guide may have potential to alleviate scar tissue formation and fibrosis following surgical intervention, improving outcomes for patients suffering from nerve damage.

## List of Abbreviations Used

| | |
|---|---|
| **6-OHDA** | **6-Hydroxydopamine** |
| **7,8-DHF** | **7,8-Dihydroxyflavone** |
| **aCSF** | **Artificial cerebrospinal fluid** |
| **ASIA** | **American Spinal Injury Association** |
| **ATP** | **Adenosine triphosphate** |
| **ATR** | **Attenuated total reflection** |
| **CNS** | **Central nervous system** |
| **DMSO** | **Dimethyl sulfoxide** |
| **ECM** | **Extracellular matrix** |
| **EDTA** | **Ethylenediaminetetraacetic acid** |
| **FBS** | **Fetal bovine serum** |
| **FTIR** | **Fourier transform infrared (spectroscopy)** |
| **HCl** | **Hydrochloric acid** |
| **IR** | **Infrared (spectroscopy)** |
| **NGC** | **Nerve guidance conduit** |
| **NMR** | **Nuclear magnetic resonance** |

| | |
|---|---|
| **P2E2O** | **Poly(2-ethyl-2-oxazoline)** |
| **PBS** | **Phosphate-buffered saline** |
| **PC12Adh** | **Cell line from pheochromocytoma of rat adrenal medulla** |
| **PDMS** | **Polydimethylsiloxane** |
| **pH** | **Power of hydrogen** |
| **PNS** | **Peripheral nervous system** |
| **PVA** | **Poly(vinyl alcohol)** |
| **SCI** | **Spinal cord injury** |
| **SEM** | **Scanning electron microscopy** |
| **TRKB** | **Tropomyosin receptor kinase B** |
| **UV-Vis** | **Ultraviolet-visible (spectroscopy)** |
| **wt** | **Weight** |

# 1. Introduction

## 1.1 Significance and Prevalence of Nerve Injuries

Spinal cord injuries (SCIs) affect many people around the globe, including an estimated 320,000 North Americans (1). In Canada, SCIs affect more than 85,000 Canadians, including over 4,300 new cases every year (2). These injuries are separated into traumatic and non-traumatic cases, with a nearly even split of 51 and 49% respectively (2). The affected Canadians are 2.6 times more likely to be hospitalized than Canadians who do not live with a SCI (2). Furthermore, the lifetime financial cost of partial paraplegia is an estimated $1.5 million, whereas the average cost for tetraplegia is $3.0 million (3). While these figures seem relatively small considering Canada has a population of over 37 million, this still represents an annual economic burden of around $2.67 billion for those who survive their initial hospitalization (3). These figures present a large economic burden for the health care system – but the toll on the emotional, mental, social, and physical livelihoods of the patients and their families is immeasurable. The number of individuals affected by peripheral nerve damage (neuropathy) is much larger; it is estimated that 25-30% of Canadians will suffer some degree of neuropathy in their lifetime (4).

To restore function lost by damage to nerve tissue, nerve regeneration must take place. Unfortunately, nervous tissue has poor regenerative capacity; it is essentially nonexistent for the nerve fibers of the spinal cord (5). There is greater regenerative potential for peripheral nerves, yet there is still a relatively limited intrinsic regenerative capability when compared to many other tissues. Nevertheless, there is great potential for tissue engineering in this field. Clinical outcomes can be drastically improved for patients suffering some degree of neuropathy. Yet,

there are many challenges and barriers to overcome in the development of a clinically relevant technique/procedure.

### 1.2 Understanding Neurobiology of Nerve Injuries

An overview of neurobiology, neuroanatomy, and cellular biology (especially related to nerve injuries and the processes involved) is required to understand and appreciate the challenges facing regenerative medicine and tissue engineering for nerves. As for general neuroanatomy, the nervous system is subdivided into the central nervous system (CNS) and the peripheral nervous system (PNS) (6). The CNS includes the brain and spinal cord and is considered the command center of the nervous system. The PNS includes a variety of spinal and cranial nerves (6). The nervous system is considered to function in sensory input, integration of data, and motor output. This is accomplished by means of a communication network (i.e., the nervous system) that conducts electrical impulses across tissue (7).

Neurons can be classified by the afferent (sensory) and efferent (motor) neurons of the PNS (as indicated previously), with the third functional classification being interneurons of the CNS that form connections between neurons (8). These neurons are classified according to the number of processes associated with the neuron, which stem from the soma of the neuron. On the other hand, neuroglia are much smaller than neurons and function in various roles in the nervous system. Neuroglia include microglial cells (resident macrophages of the CNS), astrocytes (star-shaped macroglial cells, abundant in CNS, crucial to axon guidance and synaptic support), oligodendrocytes (CNS cells that form myelin sheaths to increase speed of action potential travel), Schwann cells (PNS equivalent of oligodendrocytes), and satellite glial cells (line the surface of neuron cell bodies in ganglia) (9). Other types of neuroglia include various progenitor cells and support cells associated with various efferent neurons. Surrounding each nerve, there

are three layers of connective tissue including endoneurium, perineurium, and epineurium (10). These layers are important in understanding the extent of a nerve injury.

### 1.3 Classification Systems of Nerve Injuries

Classification of peripheral nerve injuries is key in determining the appropriate treatment strategy. A classification system developed by Seddon was detailed in 1943 and expanded by Sunderland in 1951 (11,12). Both classification systems indicate the degree of damage based on the extent of tissue damage and extent of transection. Seddon's classifications include three main classes: neurapraxia, axonotomesis, and neurotmesis (also Class I, II, and III respectively, Figure 1) (12). Neurapraxia is indicated by the temporary interruption of conduction without loss of axonal continuity. This includes sensory-motor problems distal to the site of injury, an absence of Wallerian degeneration (the cellular process which prepares the injury for regeneration), and all three layers of connective tissue (endoneurium, perineurium, and epineurium) being intact (12). Axonotemesis can be identified as a loss of complete continuity, yet the connective tissue is maintained. In this case, Wallerian degeneration is present, there are sensory and motor defects, nerve conduction is inhibited, and the process of axonal regeneration can occur without surgical intervention (12). Finally, neurotmesis indicates a total disruption of the entire nerve fiber and can be partial or complete. Like axonotomesis, Wallerian degeneration occurs and a loss of conduction results in motor and sensory defects, yet surgical intervention is required for regeneration to occur following neurotmesis (12).

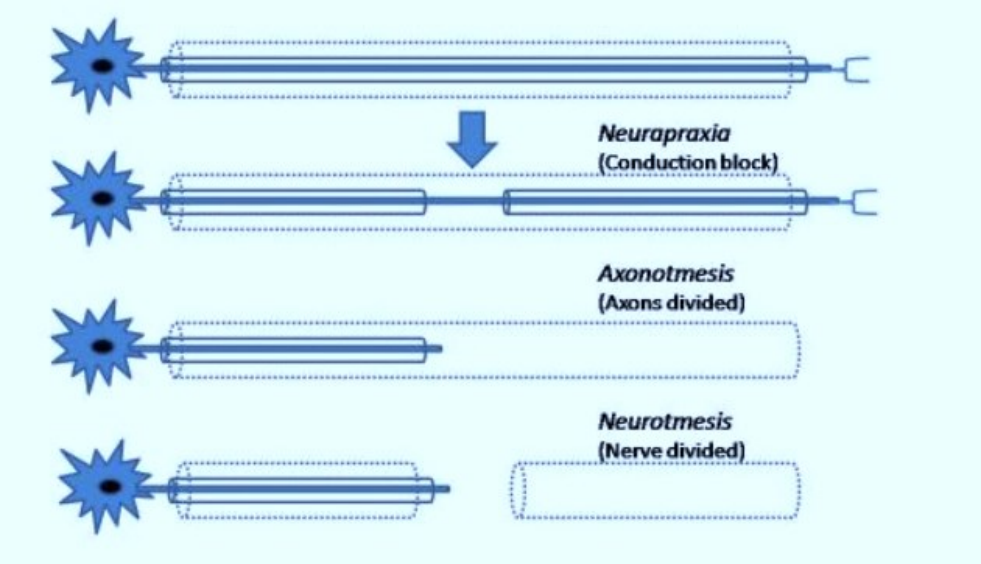


**Figure 1 Seddon's classification of peripheral nerve injuries (13).**

As for Sunderland's classification scheme, the first two degrees match up to Seddon's neurapraxia and axonotomesis, respectively (11). The subsequent three classifications subdivide the injury situation relative to Seddon's definition of neurotmesis. In these three classifications (third, fourth, and fifth degree), the layers of connective tissue indicate the degree of damage. Sunderland's third degree involves damage to the endoneurium, the fourth degree only includes an intact epineurium, and the fifth degree is defined by a complete transection of the nerve (11). Note that Wallerian degeneration occurs in all classifications except neurapraxia.

Another classification scheme was developed by the American Spinal Injury Association (ASIA) (14). In this scale, the rankings proceed from ASIA A through E, where subsequent letter indicates a less severe injury. Thus, the ASIA E indicates a normal spinal cord with no indication or detectable form of crush and/or lesion (14). Letter D indicates an incomplete motor injury, where more than half the muscle groups potentially effected maintain their antigravity capabilities (those muscles which help to maintain an upright balanced posture) (14). ASIA C is also an incomplete motor injury, but in this case less than half the muscles are still antigravity

(14). ASIA B indicates complete loss of motor function and limited sensory function (14). Finally, ASIA A indicates a complete motor and sensory loss (14).

### 1.4 Wallerian Degeneration in the PNS and CNS

Wallerian degeneration is a complex physiological response due to a nerve injury. Following nerve fiber damage, (usually a cut or crush) active degeneration occurs distal to the site of the injury (i.e., further from the neuronal soma) (15). This process occurs in both the peripheral and central nervous system to varying degrees and via different mechanisms. In the peripheral nervous system, there are many chemical messengers (e.g., transforming growth factor β1 and tissue necrosis factor alpha) responsible for this process, many of which are secreted by Schwann cells (15). These messengers induce apoptotic mechanisms originating in the distal portion of the axons (relative to the injury), activating resident macrophages, and recruiting additional macrophages to clear myelin and other cellular debris (Figure 2) (16).

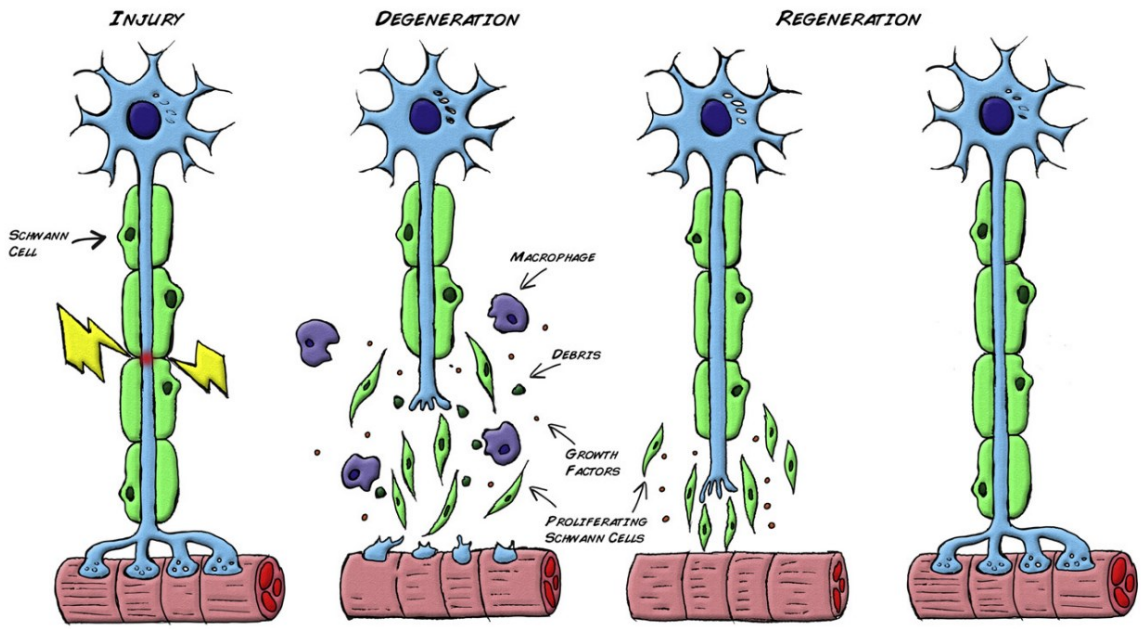


**Figure 2 Ongoing cellular actions during Wallerian degeneration (17).**

The event described above lead to axonal degeneration, dedifferentiation of Schwann cells, and subsequent clearing of cellular debris. This occurs more quickly in the peripheral nervous system for three main reasons: degradation rate is dependent on the diameter of the axon (larger axons take longer to degenerate), expedited clearance of cellular debris (much easier for macrophages to be recruited in the PNS), and Schwann cells can survive independent of axonal stimulation (18). On the other hand, oligodendrocytes of the CNS undergo apoptosis or enter a state of latency without electrical activity (18). Thus, oligodendrocytes fail to accomplish what Schwann cells can in the PNS, and the role of Wallerian degeneration must be facilitated by microglia. It has been observed that an overexpression of these messengers can lead to fibrosis (as opposed to regeneration), potentially causing a permanent loss of function (18). The Schwann cells will eventually align in tubes known as Büngner bands, which express surface markers to guide regenerating fibers (19). The transected/damaged nerve will send out sprouts from the

proximal portion that grow at approximately 1 mm per day, eventually reinnervating the target tissue (19). Misguided growth, scar tissue formation, and a significant gap may all limit the success of axonal regeneration (20). These can often be alleviated through surgical intervention, with the nerve autograft being the current gold standard.

### 1.5 Overview of Approaches to Nerve Regeneration and Repair

For most nerve injuries, the damaged nerve can be sutured end-to-end in a tension free primary neurorrhaphy (21). In cases where there is a significant gap, many alternatives exist: allografts, direct repair, autografts, nerve conduits, and end-to-end sensory repair. A nerve autograft is used to close the gap and the donor nerve (sourced from a second surgery on the same patient) is sutured on both proximal and distal ends to connect the damaged nerve (21). Nerve allografts have also been used in this instance, where the donor nerve is sourced from a second patient rather than the same individual (21). This technique has been used when there is significant damage to the nerve tissue that would otherwise be irreparable. Even though many of these techniques were introduced in the late 1870's, they have been significantly improved through the development and advancement of microsurgical techniques. Treatment for spinal cord injuries requires various measures to at a bare minimum, maintain the injury (i.e., prevent further damage). Surgery may often be performed to treat spinal cord compressions, or to stabilize the spinal cord to prevent future deformity and pain.

The role of biochemical signals that promote/inhibit nerve growth in the spinal cord has also been explored. Unfortunately, growth factors (and similar signaling molecules) alone do not provide desirable levels of neuronal regeneration (22). Stem cell therapies have also attracted interest; however, the safety and efficacy of these treatments have not been determined (23). Cell therapies, gene therapies, and other molecular therapies have also been explored to help restore

motor function and sensory function following a nerve injury. These techniques are relatively new and still not well understood. Furthermore, these techniques rely on the knowledge and understanding of molecular pathways and specific cellular responses. Recently, biomaterials-based approaches have exploded in popularity as a novel technique for nerve guidance and repair (24). These techniques have potential to provide clear benefits to the tissue engineering approach – the addition/loading of growth factors, various extracellular matrix proteins, and even transplanted cells could provide crucial cues and components necessary for a successful nerve guidance conduit (Figure 3).

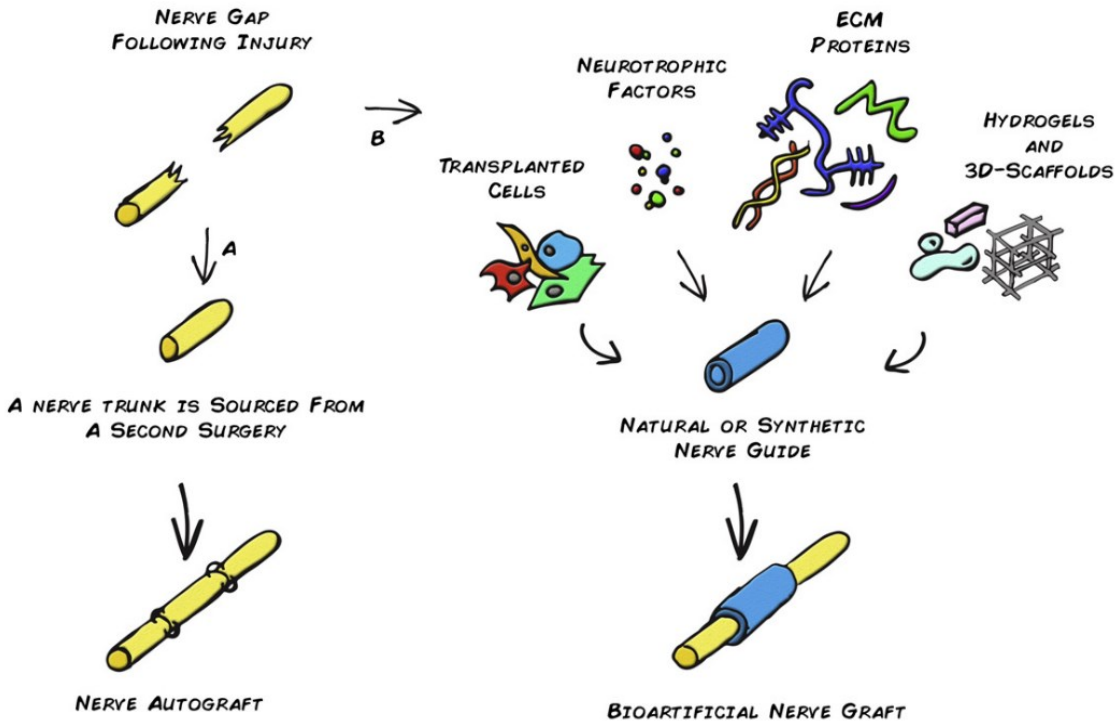


**Figure 3 Schematic showing the proposed biosynthetic nerve graft as opposed to the traditional nerve autograft (17).**

There have been a variety of nerve guidance conduits that have supported nerve growth and attachment (both in research and clinical settings), including some that have better clinical outcomes than the nerve autograft. Tissue engineering of nerves (both peripheral and central) has

been an area of interest for various researchers and is often viewed as the holy grail of regenerative medicine. There are a variety of differences in physiology, cellular function and organization, and neuroanatomy between the PNS and CNS, both have their own challenges and limitations when it comes to developing a tissue engineering approach for these tissues. Assessment of peripheral nerve approaches can provide foundations of nerve tissue engineering which may help translate into a more informed approach for the CNS. The peripheral nervous system has a much higher capacity for nerve regeneration. However, the pathophysiology of injuries to the PNS are much simpler than that of the CNS, and although similar techniques and scaffolds may be applied, the process is intrinsically different at the cellular level. Thus, it is likely more complex and robust treatment options will likely be necessary solutions for the CNS.

### 1.6 Biomaterial Approaches to Nerve Regeneration and Repair

Biomaterials have become increasingly important as a potential route for promoting nerve regeneration following traumatic nerve injury. The most common approach involves the use of biosynthetic nerve guides in place of donor nerves, coined nerve guidance conduits (NGCs, Figure 4) (25–27). These devices have also been referred to as tissue engineered nerve guides (28–30). For consistency, these guides will be herein referred to as nerve guidance conduits or NGCs. The basis of the NGC is a sheath of natural or synthetic biomaterial which encapsulates the injured section of the nerve via suturing. The basic requirements of an NGC include formation of a physical barrier from the external environment whilst also providing guidance for regenerating axons across the gap. This also helps provide a localized environment for endogenous and exogenous growth factors, hormones, cytokines, and extracellular matrix (ECM) factors. These factors could even be loaded into or on the surface of the materials within

the interior of the NGC. The most variable and arguably largest indicator of success for any NGC is the internal composition of the sheath; a few of these strategies are listed in Figure 4.

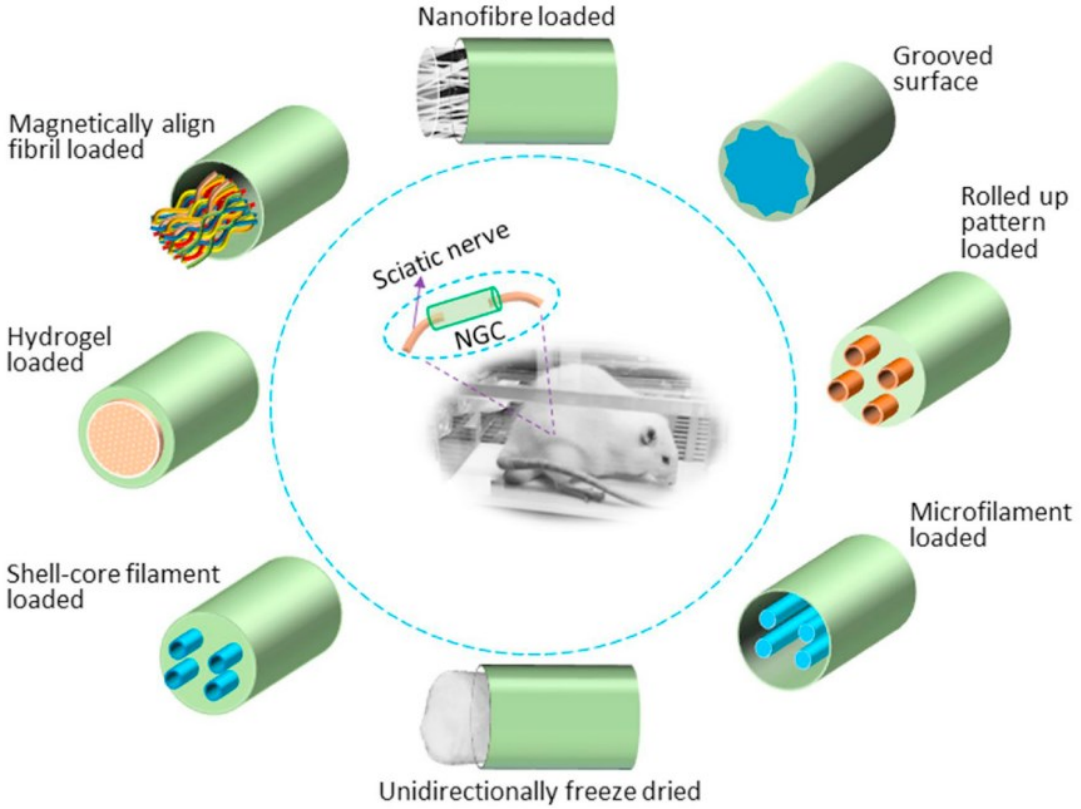


**Figure 4 Biomaterial strategies for creating nerve guide conduits – synthetic nerve guides to promote nerve regeneration following traumatic nerve injuries (31).**

There have been a variety of material compositions including synthetic materials like polyglycolic acid, silicone, polylactic acid, and polycaprolactone as well as natural materials like chitosan, collagen, and laminin (25,31). Glass fabrics, ceramics, and metallic materials have also been purposed for neural scaffolding (32,33). Natural materials tend to mimic tissues and help to provide proper guidance cues whereas synthetic materials are much simpler to fabricate, access, and modify. Synthetic polymers can also be biostable or biodegradable, meaning they either become incorporated within the regenerating nerve tissue or they degrade and make way for regenerating nerve tissue. There are many benefits and drawbacks to the potential biomaterials,

indicating a composite NGC which takes advantage of different materials may be beneficial. In addition to modifying composition, materials can be chemically or physically adapted to form unique biomaterials with specific functions. In addition to chemical and physical changes, the fabrication method can impart various guidance properties and enhanced mechanical properties. An ideal guidance material could be one which allows incorporation of specific integrins or binding motifs for cellular interactions, and which can be selectively modified (by chemical or physical means) to control a variety of factors including degradation rate, swelling, and hydrophilicity. In this sense, a template material for further modification may be suitable for this purpose.

Loading various adjuvants can increase the local response of regenerating axons, helping to facilitate integral cellular functions within the regenerating nerve. For example, the addition of $Ca^{2+}$ to a fibrin-forming solution can produce conductive fibers for neural tissue engineering (34). Various magnetically aligned collagen materials have also been proposed to enhance axon guidance (35). Axon guidance is an essential process in formation of neuronal connection during development and regeneration. Axonal growth stems from the growth cone and must reach the target through guidance from chemical messengers (36). The use of physical guidance strategies via NGC intervention helps to prevent misguided axonal growth (37,38). Cross-linkers can also modify the material characteristics and change the micro- and macromechanical properties of the material. These types of modification have been shown to increase the resistance to degradation and provide proper topographical guidance cues. Degradation is a difficult factor to control since the ideal degradation profile will be determined by the regeneration rate which can be extremely variable and may require more stringent design protocols determined through case-by-case analysis. Some of the various fabrication techniques employed for NGC materials include

injection molding, fused deposition, soft-lithography, immersion precipitation, dip-coating, microextrusion bioprinting, and inkjet bioprinting (39). All these methods used in fabrication of internal compositions for NGCs, with varying challenges and outcomes. The idea of a multifunctional, composite NGC conduit may be a more likely solution to combat the challenges facing nerve regeneration and repair. Hence, it is important to consider a fabrication method that is compatible with this approach. Fabrication must be compatible with potential adjuvant loading and production of a biocomposite scaffold/network with various materials. Attention has also been placed on production of synthetic filaments or fibers based on analogous structure to nerve tissue and the guidance potential of such structures (40,41).

The use of fibrous materials to promote nerve regeneration is based on the idea that fiber fabrication methods can produce materials which possess the ability to facilitate nerve guidance through topographical guidance cues. In conjunction with a nerve guidance conduit, the proper fibrous scaffold can provide the proper nano- (macromolecular), micro-(cellular), and macromechanical guidance. Electrospinning whilst using a grounded rotating collector allow for formation of highly aligned, parallel fibers of different polymers (42). This alignment allows for formation of small grooves which can provide individual guidance channels for regenerating axons. Polycaprolactone and poly(lactic glycolic acid) fibers, and polyethyleneimine can be incorporated in arranged electrospun polymer fibers within a nerve guide to promote guidance along grooves (40,43). In addition to microgrooves, fibers promoting guidance can also be coated or loaded with ECM proteins or growth factors. Laminin coated conduits based on poly(l-lactide-co-glycolide) fibers and yarns can help to promote nerve guidance through cooperation of topographical structure and biological cues (41). Fibers can also be natural materials rather than synthetic polymers, like the nerve growth factor functionalized silk nanofibers for nerve

reconstruction in a rat model (44). Fibers provide a great potential template for production of a larger fibrous scaffold. Fiber fabrication can be modified to influence pore size and control cellular interactions, create micro- and nanogroove structures to promote axonal guidance, and act as a vehicle for various proteins, growth factors, and small molecules. Thus, biomaterial fibers can affect the nano- (macromolecular), micro- (cellular), and macrolevel interactions that influence the success of nerve guidance conduit approaches, prompting the need to develop efficient approaches (such as contact drawing described below) for fabrication of functionalized biomaterials.

### 1.6.3 Optimizing Material Characteristics of Biomaterial Fibers

The nerve guide has some desirable qualities (user needs) that can act as design inputs for fiber development (Table 1). The design inputs will hopefully become the design outputs necessary for the nerve guide through iterative design processing and verification (45). Although these properties were not validated for a medical device for this project, user needs were important to consider during the design process (45). Other important user needs may be more appropriately associated with the nerve guide and not biomaterial fibers. For this project, the focus was on the material characteristics and the fiber development.

**Table 1 User needs and corresponding design inputs for fiber development.**

| User needs | Design Inputs |
|---|---|
| Biocompatible (nervous tissue environment) | Polymer fibers and by-products of degradation are non-cytotoxic, non-pyrogenic, non-immunogenic in the response of nervous tissue implantation |
| Biodegradable/biostable | Polymers are sufficiently modified to degrade over a time period suitable for nerve attachment and growth *in situ* **or** do not degrade and can be incorporated into regenerating tissue without causing a chronic foreign body response |
| Non-friable | Mechanical properties which prevents material being crushed or turned into a powder when handled |
| Pliable | Mechanical properties corresponding to fibers which can be extended or compressed without compromising the fiber or material integrity |

These user needs and corresponding design inputs will help to guide the iterative design process in making biomaterial fibers that can support nerve growth and guidance. This is not an exhaustive or comprehensive list and as various user needs present themselves, the corresponding design inputs should be included in the design process. These inputs may not be necessary until the fibers are being assembled into bundles and arranged into a nerve guide, and thus may not be necessary requirements at this stage of development. Nevertheless, they are important considerations when designing novel biomaterial formulations and fabrication processes. Furthermore, various mechanical properties (both macro and micromechanical properties) will be of specific interest to the development, so that a pliable, non-friable nerve guide can be constructed with the fibers. The specific inputs appropriate to satisfy these conditions is specific to the material and application, as without further experimentation and mechanical testing, the explicit range of acceptable values cannot be determined.

These criteria can be compared to nerve guides which have reached clinical trials or are in the process of being approved for human studies (46–48). For the most part, the material specifications for the nerve guides listed in 510(k) summaries include both characteristics of the

material and desired responses *in vivo*. The *in vivo* response requirements detail a noncytotoxic, nonpyrogenic, nonirritating, and nonsensitizing nerve guide whereas the material characteristics denote a soft, pliable, nonfriable, porous tube (46–48). The intended use of the nerve guides is introduction of an interface between the nerve and surrounding tissue, creating a localized environment for axonal growth across a nerve gap (47). Referring back to the nerve injury classification scheme, the intended use scenario involves nerve discontinuities, which indicate neurotmesis according to Seddon and depending on the depth of discontinuity one of three classifications (third-fifth degree) for Sunderland. Some of the available nerve guides indicate more ambiguous indication of application – indicated for peripheral nerve discontinuities where gap closure can be achieved by flexion of the extremity (47). On the other hand, some guides list use for complete discontinuities of up to 20 mm (46).

## 1.7 Contact Drawing of Viscous Polymer Solutions

### 1.7.1 Contact Drawing versus Other Fiber Fabrication Methods

Polymers can be dissolved into aqueous solutions for fabrication of various biomaterials – including porous scaffolds, hydrogels, or polymeric fibers. The prominent methods for fabrication of fibers are wet-spinning, electrospinning, melt spinning, direct spinning, and extrusion spinning (49,50). Electrospinning seems to be the leading choice for fabrication of fibrous materials for tissue engineering applications. Many types of electrospun materials have been proposed for neural tissue engineering, including hemin-doped serum albumin scaffolds, polyvinylidene fluoride-based scaffolds, and polycaprolactone-gelatin scaffolds to name a few (27–29). Aside from wet-spinning and electrospinning, many of these techniques require high temperatures or hot air for formation of fibers. One of the major benefits of electrospinning and wet-spinning processes is that they occur at room temperature – providing an expanded range of

pharmaceuticals and biologics that can be incorporated. Electrospinning and wet-spinning are similar (aside from the electrical field required) and can effectively form fibers of various natural and synthetic biomaterials. In this highly active field, the demand for mass production of these materials is likely to be a considerable challenge for these spinning techniques. Multiple extrusion tips and/or spinnerets may help to alleviate this issue, although the equipment and set-up required for this process can become cumbersome (53,54). Contact drawing provides a seemingly too good to be true" solution to this process as it allows formation of hundreds to thousands of biomaterial fibers at room temperature in seconds (Figure 5).

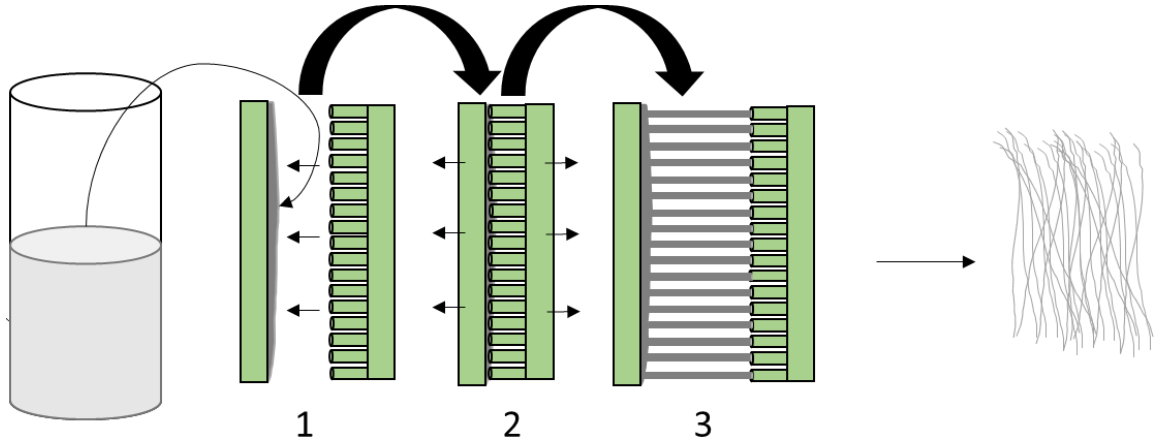


**Figure 5 Contact drawing of viscous polymer solutions.**
1) A viscous polymer paste is placed on a flat surface and a pin array is pressed into the polymer paste. 2) The pin array and flat surface are pulled in opposite directions with parallel alignment to the pins. 3) Polymer entanglement drives formation of stable liquid bridges which become fibers as they dry.

Polymers without suitable solvent systems may not be appropriate for pursuing within contact drawing methods, although this is the case for many of the other techniques as well. One of the benefits of contact drawing is the ability to use viscous polymer solutions to form fibers, where the viscosity of these solutions could clog the nozzles used in wet-spinning and electrospinning (54,55). Moreover, the necessary equipment is a fraction of the price and size when compared to the set-up required for electrospinning or wet-spinning, making contact

drawing a more accessible techniques for researchers (42,54,55). Furthermore, electrospinning may produce fabrication defects within the polymer fibers formed (49,56). The use of water as the solvent (aqueous polymer formulations) is also desirable since the recovery of industrial solvents is a large issue for mass production of other biomaterials. Some proteins and other biologics are incompatible with other fiber fabrication processes due to the high temperature and electric fields that can cause denaturation and inactivation of these adjuvants (50). Furthermore, the method accommodates one-pot additions of these adjuvants to the polymer system prior to contact drawing for homogenous distribution within the fibers. This incorporation may be physical or chemical in nature, providing routes for controlled release. As the material swells or degrades, the physical or chemical interactions holding the adjuvants in place may weaken and allow release of the loaded material. This provides a much simpler route of loading as compared to the other techniques discussed previously. Cross-linking agents or other modifying agents can be also added prior to contact drawing.

### 1.7.2 Contact Drawing is Driven by Polymer Entanglement

Contact drawing is driven by the process of polymer entanglement – a process where polymer chains are constrained in their movement with respect to each other. To understand polymer entanglement, we need to describe polymer motion. Reptation is the motion of long, linear macromolecules like polymer chains. The motion was analogous to slithering snakes for Pierre-Gilles de Gennes who coined the term in 1971 (57). He described the effect of polymer chain entanglements as a function of molecular mass and chain relaxation time (57). Specifically, entanglements with other polymer chains restrict polymer chain motion to a thin tube-like area (57–59). Relaxation time refers to the time required for a chain to completely escape this tube-

like area (57). Assuming that the polymer chain cannot be broken, the entangled chains must be pulled or flow through the restrictions (Figure 6).

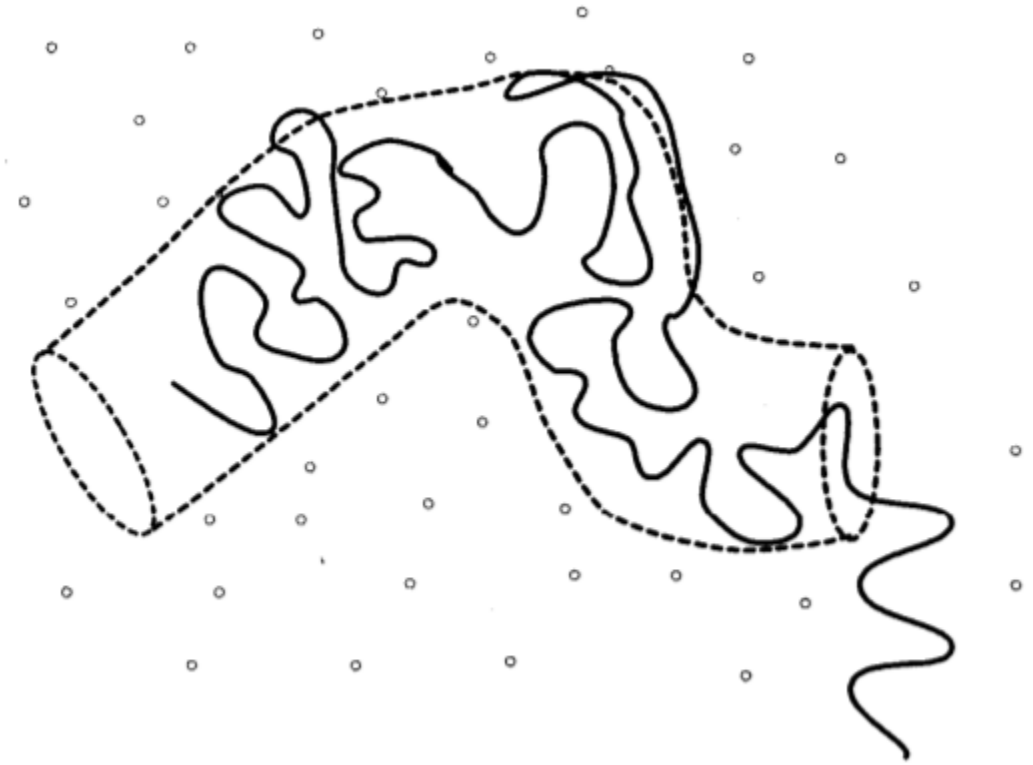

**Figure 6 Reptation theory depicts tube-like areas of motion for entangled polymers.** In this figure, other polymer chains are depicted as points so indicate the complexity of three dimensional entanglements (59).

Molecular mass is one of the strongest determinants of relaxation time for entangled polymer systems (60). Increasing the molar mass will effectively increase the chain length and thus increase the number of tangles within the system. Cross-linking is one method for modifying entangled polymer systems since cross-linking forms covalent linkages between polymer chains – increasing the effective molar mass of the polymer distribution. Cross-linking density, type of cross-linker (chemical, thermal, physical), size of cross-linker (steric hinderance), and strength/stability of the cross-linker can all affect polymer entanglement

(57,58,60). Although chemical cross-linking can affect polymer entanglement, these covalent linkages between or among chains are unique from the interactions which describe polymer entanglement. These non-covalent interactions are often classified as either topological or cohesional (for amorphous polymers) (61). The former being a steric hinderance of chains in a three-dimensional space where the latter is a molecular interaction between chains which may act like a physical cross-link (61).

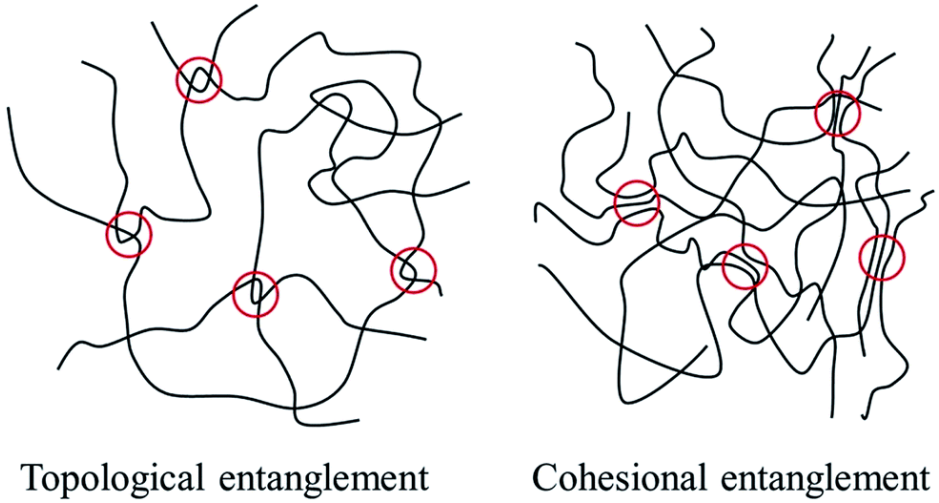


**Figure 7 Two main classifications of polymer entanglements in amorphous systems** (61)**.** Note that these are two-dimensional representations of polymer entanglement which exist as three-dimensional systems. This is an oversimplification of polymer entanglement.

Polymer entanglements are the driving factor behind fiber formation through contact drawing (62). Understanding this process and how it affects fiber formation for a given polymer system can be important in optimizing fiber formation for novel fiber formulations. Contact drawing is a fabrication technique that can be used to design polymeric fibers for a specific application, like nerve regeneration and repair.

## 1.8 Research Questions, Aims, and Objectives

The current prognosis for almost any spinal cord injury is some loss of function, ranging from partial motor loss to complete loss of sensory and motor function (for those individuals who survive their related traumas). Furthermore, people with spinal cord injuries are at elevated risks for various complications including pneumonia, pressure ulcers, and deep vein thrombosis. The goal of this research aims to progress toward a clinical outcome for those affected individuals that may include a partial or complete functional recovery. Through a biomaterials-based approach, this research aims to provide new strategies that will improve upon current approaches to nerve injury.

### 1.8.1 Polymer Selection

Various peripheral nerve approaches have shown promising results for various biomaterials, extracellular matrix components, cellular therapies, and even gene therapies. The goal of this research was to develop a novel biomaterial fiber approach for potential use in an NGC. The nature of the biomaterial and possible modifications will be explored to maximize intended use. For use surrounding a nerve injury, the polymer of choice will have to be significantly cross-linked (thermal, physical, or chemically) to produce a material which slowly degrades in an aqueous environment since these polymers are all readily soluble in water. A variety of synthetic polymer candidates were considered for this task, with unique side groups and thus many potential chemical modifications (Table 2). This shortlist was part of a patent proposal relating to the templating of collagen and other materials though loading into polymer systems prior to contact drawing (63).

**Table 2 Potential polymers for biomaterial based-nerve guide.**

| Polymer | Supplier | Average MW (kDa) | Cost ($/g or $/mL) | Modifiable Group(s) |
|---|---|---|---|---|
| **Dextran** | Pharmacosmos, Dextran Products Ltd. | 500 | 2.79/g | Hydroxyl |
| **Hydroxypropyl Cellulose** | Sigma Aldrich | 80 | 0.91/g | Hydroxyl |
| **Poly(2-ethyl-2-oxazoline)** | Sigma Aldrich | 500 | 0.39/g | Amide |
| **Poly(4-styrenesulfonic acid-co-maleic acid)** | Sigma Aldrich | 20 | 0.20/g | Sulfonic acid/sulfonate, carboxylic acid/carboxylate |
| **Poly(diallyldimethyl ammonium chloride)** | Sigma Aldrich | 450 | 1.59/g | Carboxylic acid |
| **Poly(acrylic acid)** | Sigma Aldrich | 400-500 | 0.04/mL | Ammonium |
| **Poly(methyacrylic acid)** | Sigma Aldrich | 9.5 | 0.05/mL | Carboxylate |
| **Poly(methyl vinyl ether-alt-maleic acid)** | Sigma Aldrich | 216 | 0.65/g | Ester, carboxylic acid |
| **Poly(vinyl alcohol)** | Sigma Aldrich | 31 & 205 | 0.23/g | Hydroxyl group |
| **Poly(vinylpyrrolidone)** | Sigma Aldrich | 360 | 0.98/g | Amide, heterocyclic ring |

These polymers were all characterized as polymers which could form fibers from aqueous systems and then be rehydrated to wash away the templating polymers whilst leaving the collagen fibers behind. To modify these polymers for the intended use (slowly degrading material in aqueous environment), a significant drop in hydrophilic character was required to decrease dissolution and hydrolytic degradation of the polymer. Thus, polymers containing reactive, hydrophilic side chains were identified as strong candidates. Furthermore, the reactive species should be able to participate in cross-linking reactions where the reaction occurs between

or among polymer chains to increase cross-linking density of the polymer system and create a water-stable polymer fiber. Hydroxyl linkages provide a route for formation of acetal, hemiacetal, or other potential linkages among themselves depending on the cross-linker. On the other hand, cross-linking reactions between sulfonates and carboxylates either do not proceed or do not form very stable linkages when reacting with each other. Amide linkages can also form strong interactions among polymer chains through formation of various linkages including esters, imides, or other potential linkages once again depending on the cross-linking agent. A few of the polymers fitting the favourable moieties for cross-linking included the hydroxyl containing poly(vinyl alcohol) (PVA) and dextran, and the amide containing poly(2-ethyl-2-oxazoline) (P2E2O). It should be noted that the list contains a multitude of polymers fitting these criteria considering the polymers were all relatively soluble in aqueous solutions. The other criteria for initially shortlisting the polymer list for preliminary experiments was the average molecular weight and corresponding ease of fiber formation. Fiber formation tends to be easier for higher molecular weight polymers like dextran (500 kDa), P2E2O (500 kDa), and the higher molecular weight PVA (205 kDa), providing a starting point for learning and mastering the contact drawing technique.

Degradation time is important since rapid degradation can result in swelling and loss of structural stability, whereas too slow degradation can lead to compression and a potential chronic foreign body reaction (64). Although ambiguous, degradation must be consistent with the time required for axons to regenerate across a nerve gap. This is dependant on the size of the nerve gap and the rate of regeneration and thus has some case-by-case variance. This is also an important consideration for the central nervous system due to a lack of intrinsic regeneration. It is likely that the polymeric biomaterial will need to be modified to last for longer than the 10

days shown by Alhosseini *et al*. These polymers (Dextran, P2E2O, PVA) all have potentially modifiable side chain moieties within the polymer networks. Cross-linkers which can act on these reactive side chains can be used to increase the resistance to degradation and produce a biomaterial which slowly degrades *in vivo*. Furthermore, cross-linking may provide a route for controlled release – fine tuning the cross-linking density can correspondingly affect the timeline over which a material degrades *in vivo*. As the material degrades, the physical and/or chemical interactions responsible for incorporation of the small molecule will become weaker, allowing the adjuvant to be released. In theory, increased cross-linking density could be used for a more sustained release, whereas decreasing the cross-linking density could cause a burst release.

### 1.8.2 Quercetin as a Model Drug for Controlled Release

There are a variety of molecular mechanisms at play within a regenerating nerve, and some research groups have looked at incorporating various proteins, small molecules, and other additives to nerve guides to facilitate nerve cell attachment and promote overall nerve regeneration (25,26,37). Various extracellular (ECM) components and proteins can allow for the scaffold to be biomimetic and quite bioabsorbable, in addition to providing topographical guidance cues. ECM components provide natural cellular attachment cues to guide regenerating shoots of the proximal end of a nerve lesion. These cells express specific integrins that bind to ECM proteins to promote myelination through their interaction (65). A variety of ECM components have been shown to play a major role in nerve guidance and attachment, including fibronectin, laminin, collagen, and vitronectin (65,66). Neurotrophic and growth factors can also be loaded into the nerve guides. Brain-derived neurotrophic factor, ciliary neurotrophic factor, fibroblast growth factor, glial cell-derived neurotrophic factor, nerve growth factor, vascular endothelial growth factor, insulin-like growth factor 1, platelet derived growth factor, leukemia

inhibitory factor, glial growth factor, and neurotrophin-3 have all shown specific affinity for ECM components and promising activity for nerve tissue (26,67). Contact-drawn dextran fibers have been used for templating ECM proteins (63). This biomaterial fabrication approach produced collagen fibers that could direct myoblast cell growth in 2D and 3D cell culture models (63). ECM proteins were also employed in a variety of loading methods, conduit materials, and animal models for nerve guidance conduits, hoping to take advantage of this similar property (27,68). Most of the factors showed improved results in comparison to nerve guides that did not contain the growth factors. No adverse events were noted, although some cases reported no significant difference in regeneration. Protein loading in biomaterials can cause considerable fabrication challenges: microstructure manipulation, physical/chemical interactions, fabrication techniques, and retention of mechanical properties.

Other potential adjuvant loading has focused on small molecules such as pharmaceuticals proposed to be useful in promoting regeneration of nerves. These small molecules can have similar benefit and efficacy to larger proteins (like ECM and growth factor proteins) whilst providing a less challenging route to incorporation in biomaterials. Drug-eluting biomaterials can improve drug efficacy through targeted release (local response), controlled release (kinetics), and increased dispersity for poorly soluble materials. Although there are no clinically approved pharmacotherapies, research groups have hypothesized the use of drug interventions to help treat and manage nerve injuries. For example, Flora *et al*. looked at the use of a selective phosphodiesterase-4 inhibitor, Rolipram, for treatment of subacute spinal cord injuries (69). There are a variety of clinical trials testing various interventions to improve neurological function following nerve damage. These include (but are not limited to) Minocycline, human growth hormone, Riluzole, BA-210, AC-105, Dalfampridine, Escitalopram, and SUN-13837

(70). Almost all these interventions hope to improve the motor function of those affected by spinal cord injuries (70). There are other potential small molecules that are currently in preclinical studies, most of which have functions specific to neuroprotection, anti-inflammation, and neuroregeneration. Some of these molecules include Rolipram, Oxycyte, and a variety of compounds with their tradenames protected by the various pharmaceutical companies which are working on them (69,70). Although ECM proteins and other various proteins like neurotrophic factors can be beneficial for nerve guides, this project will focus on small molecule addition to nerve guides. These small molecules will be much smaller than proteins, so loading of these molecules will be important so that a slow, local release can be achieved. The specific chemical moieties of the drugs/nerve guide polymer will be important considerations for controlling the release kinetics and delivery *in situ*. The slow release is important since the nerve repair timeline is extensive, and we would like the desired effect of the drug to continue as the axons regenerate and the nerve guide is slowly degraded.

This project will look at investigating the effects of loading a model small molecule into biomaterial fibers for neuroprotection and regeneration. A suitable small molecule must be compatible with the polymer of choice, PVA. Any chemical or physical cross-linking to the polymer of choice should also be considered when selecting the small molecule. Finally, the molecule of choice should be beneficial in a nerve regeneration environment – the intended target should combat a known issue/problem facing current nerve regeneration techniques. A few known small molecules according to these criteria include Deoxygedunine, 7,8-Dihydroxyflavone (7,8-DHF), Quercetin, and Tacrolimus (left to right, Figure 8). Tropomyosin receptor kinase B (TRKB) is the high affinity catalytic receptor for several neurotrophins, which are small protein growth factors that induce the survival and differentiation of distinct nerve cell

populations (71,72). Both Deoxygedunine and 7,8-DHF are examples of TRKB agonists. Quercetin is a plant flavanol from the flavonoid group of polyphenols (73). Quercetin acts as an antioxidant, preventing oxidative damage from free radicals and other reactive species (73,74). Tacrolimus has been used in the past as an immunosuppressant to prevent organ rejection f; (75).

**Deoxygedunine** **7,8 DHF** **Quercetin** **Tacrolimus**

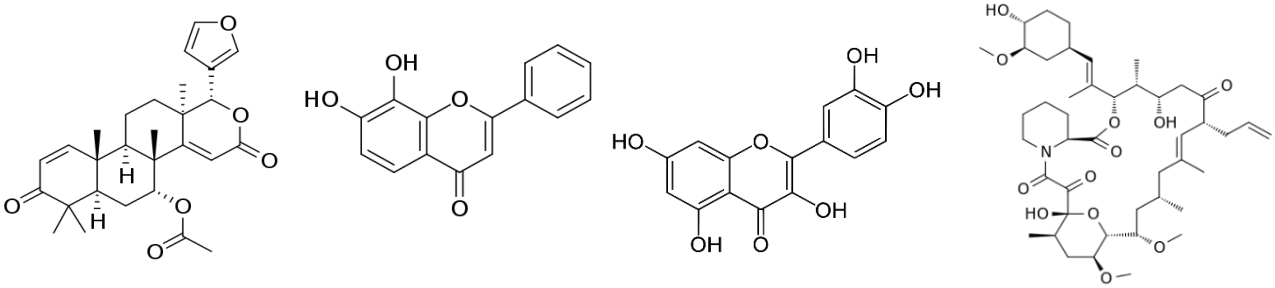

**Figure 8 Potential small molecule adjuvants for loading into biomaterial fibers.**

Based on the molecules seen above, Quercetin and 7,8-DHF are both free of any chiral centers. The presence of chiral centers could present a problem for incorporation of Deoxygedunine or Tacrolimus into a biomaterial using cross-linking to modify the synthetic polymer. It is possible that the chiral centers could be modified if the small molecule itself becomes chemically modified during incorporation, potentially resulting in production of the enantiomer of the drug/prodrug or a racemic mixture during release. This may lead to effectively rendering the drug useless (enantiomer is benign), decreasing the efficacy (enantiomer binds to receptor but does not elicit proper biological response), or producing a toxic response (enantiomer has antagonistic effect or acts improperly on another target). Of the simpler molecules, TRKB agonists like 7,8-DHF have a variety of neuronal cell responses in their downstream pathways once activated including survival, differentiation, and synaptic plasticity; however, the efficacy of this loading and release (within a biomaterial context) is dependent on

proper expression of the appropriate receptors – TRKBs (72). On the other hand, Quercetin is an antioxidant with the capacity to act in an unmediated fashion to prevent oxidative damage to many cell types (73,76). The plant flavanol is also fluorescent, providing a method for quantifying and/or identifying the small molecule following incorporation within a biomaterial. Based on these arguments, Quercetin presents as a viable model small molecule to load into contact-drawn biomaterial fibers.

Misguided growth and scar tissue formation is a major limitation regarding nerve regeneration, and is often believed to be one of the leading causes of failures with respect to injury prognosis (25). To avoid scar tissue formation, the foreign body response which causes the fibrosis can be alleviated though prevention of the apoptotic cell death that triggers fibrosis (99). This was the intended goal through the addition of quercetin to PVA fibers. Quercetin is a known antioxidant and neuroprotectant when preventing oxidative damage in a nervous tissue environment and can potentially avoid scar tissue formation which may lead to misguided and terminated growth of regenerating axons.

# 2. Materials and Methods

## 2.1 Polymer Selection – Preliminary Screening

Viscous polymer solutions from stock polymer powders were prepared in distilled water. Solutions of dextran (500 kDa, obtained from Dextran Products Ltd.), poly(2-ethyl-2-oxazoline) (500 kDa, obtained from Sigma-Aldrich), and poly(vinyl alcohol) (31 kDa, obtained from Sigma Aldrich) were prepared by combining known amounts of the stock polymers and adding distilled water to reach a desired weight percentage. Dextran and P2E2O were dissolved into 50% (wt/wt) solutions and PVA was dissolved into a 12.5% (wt/wt) solution. These stock polymers solutions were then incubated in a water bath (37°C) until a homogenous solution was observed (~24 h). Once the polymers had dissolved the solutions were stored at room temperature. All of these polymers have been previously reported as fiber-forming polymers so initial experimentation involved exploring how to pull fibers using 3D printed devices. These 3D printed devices (similar to the pin array shown in Figure 5) consisted of columns in an array with variable column widths and spacing between columns.

### 2.1.1 Contact Drawing of Viscous Polymer Solutions

Fibers were pulled for dextran (50% wt), poly(2-ethyl-2-oxazoline) (P2E2O, 50% wt), and poly(vinyl alcohol) (12.5% wt). To pull fibers, 1 mL aliquots of prepared polymer solutions were evenly spread over the flat surface of a 3D-printed block using a wooden applicator. A corresponding 3D-printed array was pressed against the block coated with the viscous polymer solution. The blocks were pulled apart from one another and stable liquid bridges became dry fibers between the two 3D-printed devices. Fibers were then deposited onto a collecting substrate (e.g., microscope slide, PDMS, or over the opening of a beaker) depending on intended use. The

most challenging polymer to form fibers with at the given concentrations was PVA (31 kDa). The higher molecular weight Mowiol® 40-88 (205 kDa) PVA was obtained from Sigma-Aldrich. This polymer took longer to dissolve into a homogenous aqueous solution (7-10 days at 37°C) but was much better suited to forming fibers via contact drawing.

## 2.2 Glyoxal Cross-linking – Secondary Screening

After reviewing numerous potential cross-linkers and methods within the literature, glyoxal was chosen as the cross-linking agent. The rationale here was choosing a cross-linker with reactions conditions which would be compatible with the contact drawing process. First, the cross-linker could act on side chains present in the polymer short-list provided. Glyoxal is an excellent choice since it can act on both free hydroxyl and free amine groups to form acetal linkages or Schiff bases, respectively (77). Cross-linkers were subsequently screened for reactions that proceed (or can proceed) at room temperature in an aqueous environment. Glyoxal proceeds via nucleophilic addition of alcohol or amino to the electrophilic dialdehyde and a protic solvent (required for proton transfer) and acidic conditions are required for the reaction mechanism (Figure 9). Furthermore, the reaction should not produce toxic by-products or have potential for sequestering any potential cytotoxic agents due to the intended use of the polymeric fibers. Although the dialdehyde cross-linker is a known cytotoxin, free glyoxal can be easily inactivated in many biomaterials through glycine washes or other agents with free amines or alcohols to react with the residual glyoxal (78).

### 2.2.1 Reaction Scheme

This cross-linking reaction can be kinetically controlled via temperature, where increasing the temperature will increase the rate of reaction. The acidic conditions have two main purposes – proton transfer helps to protect against self polymerization of glyoxal chains

(potentially cytotoxic upon hydrolysis) and acting as a catalytic agent to speed up the reaction. The temperature and proton concentration will be important considerations in combining this reaction with contact drawing. This is because as the cross-links form, polymer entanglement will increase, and this process directly influences fiber formation. Keeping the reaction conditions at room temperature will slow down the reaction and allow fiber formation to occur.

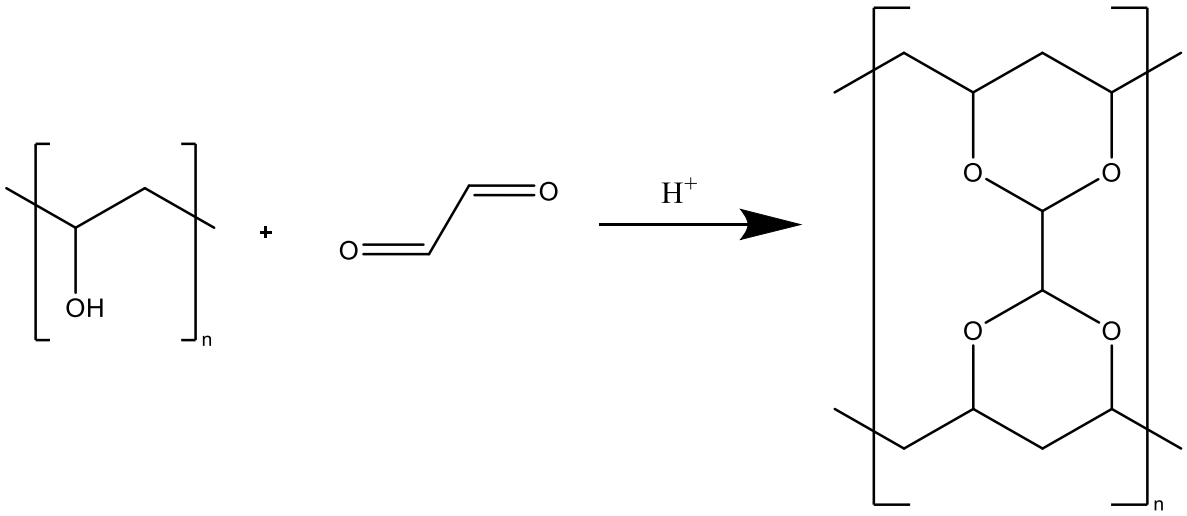


**Figure 9 Reaction scheme for glyoxal cross-linking of poly(vinyl alcohol) chains.**

The pH and any unreacted glyoxal of the fibers can be balanced post cross-linking via a glycine buffer wash. This step was completed for any fibers intended for use in cell-based assays or experiments meant to elucidate *in vivo effects*. The washing step was completed with a 10 mM glycine solution prepared in phosphate buffered saline (PBS) to deactivate any residual glyoxal.

### 2.2.2 Cross-linking Contact Drawn Fibers and Rehydration Experiments

For initial studies, glyoxal was incorporated into viscous polymer solutions prior to contact drawing in a one-pot addition method. Fibers were pulled from aliquots of the viscous polymer solution without any modifications. Fibers were also pulled 5 min after the addition of 5% glyoxal solution (40% wt/wt, obtained from Sigma-Aldrich) by total weight. Glyoxal

chemistry was completed according to similar reactions for a poly(vinyl alcohol) precipitate formation (77). The pH was lowered to 4.0 through dropwise addition of HCl prior to glyoxal addition. One difference from the glyoxal chemistry previously reported was the completion of the reaction at room temperature instead of 60°C. After allowing the fibers to dry overnight, solubility screening experiments were completed for the dextran (50% by weight), P2E2O (50% by weight), and PVA (12.5% by weight) fibers and the same fibers following cross-linking with glyoxal. Fibers were visualized using the 20X objective of a Nikon Eclipse Ti optical microscope following the addition of distilled water. Videos were collected for 1 minute following the addition of distilled water.

### 2.2.3 Optimization of Cross-linking Protocol for Contact Drawn Fibers

Cross-linking reactions were continued with PVA in the hopes of producing a biomaterial fiber for intended use in a nervous tissue engineering application. Alhosseini *et al*. showed promising proliferation of PC12 nerve cells on electrospun fibers of PVA cross-linked with glutaraldehyde (79). Unfortunately, this study also indicated the scaffolds were almost completely dissolved 10 days into a degradation study (scaffold immersed in PBS solution buffered at pH = 7.4) (79). Depending on the nature and size of the gap, this may be too rapid for the timeline for reinnervation. This timeline could also be variable due to the gap, location, and nature of the injury.

To increase the resistance to degradation and hydrolysis *in vivo*, the degree of cross-linking should be increased. The method of cross-linking could also influence the efficiency of the reaction. Fibers were pulled for aliquots of PVA with and without addition of the previously reported glyoxal additions. Glyoxal addition was increased to 20% (mol effective) and the reaction was allowed to progress for 15 min prior to fiber pulling. These fibers were allowed to

dry overnight and then placed in vapor chambers containing 50 mL of glyoxal (40% wt/wt) for subsequent cross-linking. Chambers were heated to 60°C in an oil bath for 24 h. Once fibers were allowed to dry overnight for a second time, solubility experiments were completed to assess cross-linking methods. Fibers were visualized using the 20X objective of a Nikon Eclipse Ti optical microscope following the addition of distilled water. Images were collected prior to rehydration, at 3, 12, and 48 h post rehydration, and after fibers were allowed to dry following the experiment.

### 2.3 Small Molecule Loading

After shortlisting the small molecule adjuvants, quercetin was selected as the model small molecule. The naturally occurring plant flavonoid is touted for anti-oxidant properties and has been shown to act as a neuroprotectant through sequestration of reactive oxygen species (e.g., free radicals) known to cause damage to neuronal cells (73,74,76). The issue with loading quercetin into the PVA polymer system is that quercetin is relatively insoluble under aqueous conditions. To alleviate this issue, quercetin powder (Sigma-Aldrich) was prepared as a concentrated 100 mM stock solution in dimethyl sulfoxide (DMSO). This stock solution could then be combined with the viscous PVA paste prior to contact drawing. The PVA mixture was thoroughly mixed for 2 min after the addition of quercetin to aid in homogenous distribution of the small molecule. Fibers were pulled (as per the contact-drawing protocol) for quercetin additions leading up to 200 μM final concentrations within PVA solutions. At concentrations greater than 200 μM, the polymer network seemed to become gel-like and was too viscous for liquid bridges to form. Fibers were pulled with 0, 50, 100, and 150 μM final concentrations of quercetin. These fibers were cross-linked with the same glyoxal cross-linking protocol as optimized previously, with both one-pot and vapor assisted glyoxal cross-linking.

### 2.3.1 Analysis of Quercetin Loading via Fluorescence Microscopy

PVA fibers containing 0, 50, 100, and 150 μM final concentrations of quercetin were pulled according to previously developed contact drawing and glyoxal cross-linking protocols. These fibers were collected on glass slides and then rehydrated in distilled water. Fibers were visualized using the 20X objective of a Nikon Eclipse Ti optical microscope. Epifluorescence microscopy images were collected for each loading condition. Quercetin is an active fluorophore that can be excited by blue light (460 nm) with a corresponding emission $\lambda_{max}$ of 544 nm (80,81). Thus, quercetin loading can be quantified via fluorescence microscopy using a blue excitation filter (B2-E, 450-490 nm) and green emission/barrier filter (520-560 nm). Images were collected under identical exposure conditions.

Fluorescent images were processed using an ImageJ macro to quantify and compare fluorescent images among quercetin loading conditions. This macro incorporated similar aspects from ImageJ analysis protocols outlined by Hartig *et al*. and Nichelle *et al.* (82,83). Images were first split into color channels. The green channel was converted to binary and corresponding integrated densities were obtained to normalize to fiber density. Images were also processed to produce the corresponding micrographs devoid of fluorescent fibers to correct for autofluorescence of the background. These images were obtained through application of specific thresholds to the original images to allow the fibers to be removed from the images. This was optimized for each image according to the average greyscale value of the background. This allowed the ImageJ macro to act as a low pass filter (i.e., only image particles with integrated density values below a threshold remained) to obtain an integrated density measurement representative of the background autofluorescence. Representative images help to illustrate this image processing workflow in Figure 10.

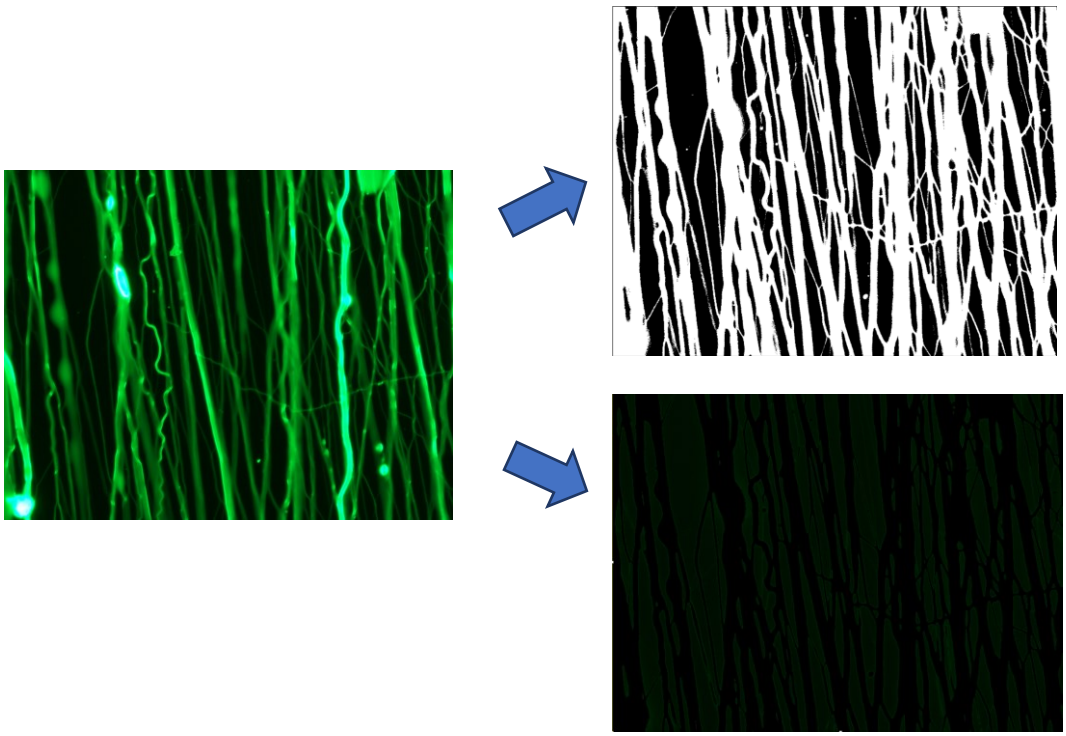

**Figure 10 Representative images showing the workflow for processing raw fluorescence images to obtain images for background and fiber density corrections.**
Raw images obtained from fluorescence microscopy (shown on the left) were adapted into images shown on the right to correct for background density (bottom right) using intensity filters to remove fibers (the signal) from the image and retain background fluorescence (which represents the noise). Fibers were also corrected for fiber density to correct for number and size of fibers included in the image frame among loading conditions.

The percent fluorescence for each loading condition was then calculated using the raw integrated density of the green channel image and the corresponding background and fiber coverage integrated densities as follows:

$$\%\, Fluorescence = \frac{raw\ int.dens. - background\ int.dens.}{binary\ int.dens.} \times 100 \quad (1)$$

These values were reported in addition to values which corrected for the autofluorescence of the fibers (0 μM quercetin loading).

## 2.4 Characterization of Quercetin Loading and Glyoxal Cross-linking on PVA

Since the glyoxal reaction proceeds via formation of acetal linkages, this reaction should be quantifiable by analysis of chemical environments. Two main methods for this type of analysis are NMR and IR spectroscopy, which both provide information about the chemical environments present in the materials and how these may be modified. NMR requires materials to be dissolved at fairly high concentration in deuterated solvents for analysis, whereas IR can analyze the polymeric fibers directly. Redissolving the fibers may disrupt acetal linkages or release quercetin. Thus, a more complete description of the chemical environments present in the PVA fibers can be obtained via IR analysis. Specifically, hydroxyl stretching is represented by broad stretches in IR spectra around 3000-3500 $cm^{-1}$. This stretch provides a useful indicator for analysing the addition of glyoxal and the effectiveness of glyoxal in reaction with free hydroxyls to form acetal linkages.

### 2.4.1 IR Spectroscopy for Quantification of Glyoxal Cross-linking

To quantify the degree of cross-linking in PVA, the cross-linking reaction was completed as described by Zhang *et al*. (77). PVA was added to distilled water and the mixture was heated at 60°C until the PVA had dissolved to form a clear solution. Glyoxal (40% wt solution, Sigma-Aldrich) was added at 0, 20, 40, 60, and 100% mol effective amounts and the pH was lowered through dropwise HCl addition to 4.0. Solutions were allowed to react at 60°C for 2 h. The viscous polymer mixtures were then poured onto polydimethylsiloxane (PDMS, Slygard® 184) to form thin films which were allowed to air dry overnight. The films were dried in a dry gravity convection oven at 40°C for 2 h prior to infrared (IR) spectroscopy. IR spectra were collected using a Thermo Scientific Nicolet iZ10 Spectrometer using the Thermo Scientific Smart iTX

attenuated total reflection (ATR) sampling accessory. 16 scans were collected using the KBr beam splitter with a resolution of 4.00, resulting in data point spacing of 0.482137/$cm^{-1}$. Samples were scanned from 400 to 4000 $cm^{-1}$ and the OMNIC software suite was used to view and process the spectral data. The advanced ATR correction algorithm within the OMNIC software was used to process spectra, to correct data points for relative shifts in band intensity and absolute shifts in frequency introduced by the instrument configuration (84). The algorithm uses a library of transmission spectra to help correct for these effects (84).

### 2.4.2 IR Spectroscopy for Analysis of Quercetin Loading

To assess any molecular changes to PVA or quercetin during the contact drawing approach, fibers were pulled according to previously reported contact drawing protocols. Fibers were pulled with 20% one pot addition of glyoxal and 12 h of vapor-assisted cross-linking. Fibers were pulled with 0, 50, 100, and 200 μM of final quercetin loading to the viscous polymer solution prior to contact drawing. Fibers were allowed to dry overnight after vapor assisted cross-linking. Fibers were dried in a 40°C dry gravity convection oven for 30 min prior to IR analysis. Samples of pure quercetin powder and stock glyoxal solution were also prepared. IR spectra were collected using a Thermo Scientific Nicolet iZ10 Spectrometer using the Thermo Scientific Smart iTX ATR sampling accessory. 16 scans were collected using the KBr beam splitter with a resolution of 4.00, resulting in data point spacing of 0.482137/$cm^{-1}$. Samples were scanned from 400 to 4000 $cm^{-1}$ and the OMNIC software suite was used to view and process the spectral data. The advanced ATR correction was used to process data (84).

## 2.5 Quercetin Release Studies

For efficacy *in vitro* or *in vivo*, quercetin should be released from the PVA fibers for quercetin to act as an antioxidative agent and protect cells from oxidative damage. To model

drug release, choosing a mimetic bodily fluid for cumulative release studies can be a strong indicator for the response of the drug-eluting material. For quercetin release, bulk scaffolds of PVA fibers could be incubated in artificial cerebrospinal fluid (aCSF) to mimic a spinal cord injury environment. The Cold Spring Harbour Protocols recipe for aCSF was used to prepare a solution of 119 mM NaCl, 26.2 mM $NaHCO_3$, 2.5 mM KCl and 1 mM $NaH_2PO_4$ in distilled water and a solution of 1.3 mM $MgCl_2$ and 10 mM glucose in distilled water (85). These two solutions could be stored separately at 4°C until combined in equal parts to yield aCSF.

Bulk scaffolds were fabricated according to previously reported contact drawing, glyoxal cross-linking, and quercetin loading protocols. Two types of scaffolds were fabricated – quercetin free with 20% (mol effective) glyoxal one pot addition following by 12 h vapor bath cross-linking at 60°C and identical scaffolds loaded with 200 μM of quercetin. These materials were allowed to dry overnight after vapor assisted cross-linking. The bulk scaffolds were washed in 10 mM glycine buffer (in phosphate buffered saline) to inactivate residual free aldehydes. Scaffolds were then dried in gravity convection oven at 40°C for 2 h before dry weight measurements were collected. Scaffolds were then placed into 10 mL aliquots of aCSF and incubated at 37°C for 10 days. After 1, 4, 8, 40, 66, 114, and 240 h scaffolds were removed from aCSF, rinsed with distilled water, and oven dried at 40°C until weight measurements were stable. Weight measurements were used to calculate percent of original scaffold remaining over time according to:

$$Scaffold\ remaining\ (wt\ \%) = \frac{dry\ weight}{original\ dry\ weight} \times 100 \quad (2)$$

These experiments were completed in triplicate (N=3) and so averages were calculated for both scaffolds at all time points. Scaffold retention (wt%) was plotted over time for these values to

yield degradation profiles. Corresponding error bars for 90% confidence intervals of each data point were included.

### 2.5.1 Ultraviolet-Visible Spectroscopy for Quantification of Quercetin Release

Based on literature precedents, ultraviolet-visible spectroscopy (UV-Vis) appeared to provide a sensitive (low limit of detection) and accurate (low degree of error) method for analysis of drug-eluting biomaterials. For example, quercetin has been observed in UV-Vis in a release study via analysis of absorbance at a $\lambda_{max}$ of 375 nm (86). For quantification of quercetin release via UV-Vis, a standard curve is necessary. Quercetin powder (Sigma-Aldrich) was dissolved into DMSO to produce a stock solution of 100 mM. Samples containing 2, 5, 10, 25, 50, and 75 μM quercetin were prepared in aCSF. Non-linear derivations from the standard curve were observed at quercetin concentrations ≥100 μM. This could be a result of concentration-based deviations from Beer-Lambert Law. Spectra were collected on an Olis 8452A Diode Array Spectrophotometer. 10 × 4 × 45 mm acryl cuvettes (Sarstedt) were used. Three scans were collected between 200 and 700 nm for data collection. Olis GlobalWorks software was used to collect, view, and process spectral data. Absorbances values at 375 nm were plotted against corresponding quercetin concentrations to generate the standard curve (Figure 11).

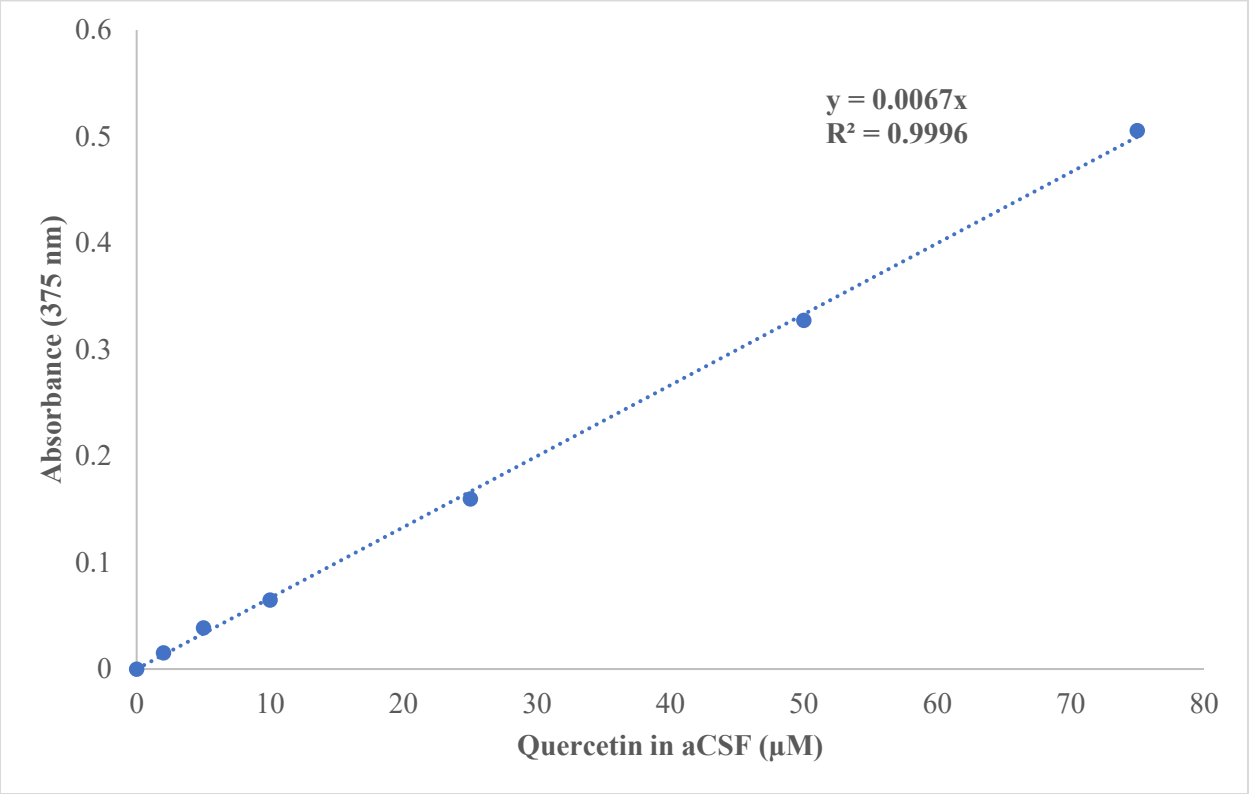


**Figure 11 Standard curve for quercetin in aCSF.**

Bulk scaffolds were incubated in aCSF at 37°C. Samples of aCSF from the incubations at 1, 4, 8, 16, 40, 66, 114, and 240 h of both scaffolds (+/- quercetin loading) were collected for analysis of quercetin release. Spectra were acquired identically to the methods previously described using an Olis 8452A Diode Array Spectrophotometer.

A series of calculations were used to determine quercetin release in the commonly used cumulative drug release format. First, the standard curve (Figure 11) was used to convert absorbance to drug concentration ($C$, µM) in aCSF. The absorbance ($A$) used for this conversion was previously corrected according to the absorbance of the scaffold without quercetin. Note that the constant (0.0067) is an experimentally determined value via standard curve construction (Figure 11):

$$C(\mu M) = \frac{A}{0.0067} \quad (3)$$

Next, the concentration ($C$, μM) could be converted to moles ($n$, nmol) using the total volume of the incubations (10 mL):

$$n\ (nmol) = C(\mu M)(10\ mL) \quad (4)$$

Weight of quercetin released ($m_r$, $\mu$g) was calculated according to:

$$m_r(\mu g) = n\ (nmol) \times \frac{302.236\ g}{mol} \times \frac{1\ \mu g}{10^3\ ng} \quad (5)$$

To compare the amount of quercetin released to the quercetin initially loaded into the scaffold, the initial quercetin content was calculated based on the loading concentration and final weight of the scaffold. The quercetin loading ($L_{Qu}$, μg/mL) was expressed for a quercetin concentration ($C_{Qu}$, $\mu M$) by:

$$L_{Qu}(\mu g/mL) = C_{Qu}\ (\mu M) \times \frac{302.236\ g}{mol} \times \frac{1L}{10^3\ mL} \quad (6)$$

For example, the quercetin loaded at 200 μM would correspond to 60.4 μg/mL loading (assuming 100% loading efficiency). The quercetin content would be relatively insignificant in the conversion from dry to original PVA volume since one milliliter of PVA would dry to form 125 mg of scaffold for a 12.5% (wt/wt) solution of PVA (compared to the 0.0604 mg of quercetin per 1 mL). Thus, the conversion from dry scaffold weight ($m_{sc}$, mg) to wet scaffold volume ($V_{sc}$, mL) quantities can be calculated according to:

$$V_{Sc}\ (mL) = m_{sc}\ (mg) \times \frac{1\ mL}{125\ mg} \quad (7)$$

This wet scaffold volume ($V_{sc}$, mL) and quercetin loading ($L_{Qu}$, μg/mL) can be used to calculate the quercetin load ($m_l$, μg) based on the weight of the dry scaffold.

$$m_l(\mu g) = L_{Qu}(\mu g/mL) \times V_{sc}\ (mL) \quad (8)$$

Finally, the ratio between quercetin released ($m_r$, $\mu$g) and quercetin loaded ($m_l$, µg) was converted into cumulative drug release (%):

$$Cumulative\ drug\ release\ (\%) = \frac{m_r\ (\mu g)}{m_l\ (\mu g)} \times 100 \quad (9)$$

### 2.5.2 Scanning Electron Microscopy for Morphological Analysis

Bulk scaffolds were incubated in aCSF at 37°C. After 1 h, 1 day, 3 days and 10 days, scaffolds were removed for sampling. A scalpel was used to slice surface and cross-sectional segments from the scaffolds. These slices were then placed onto adhesive carbon tape stubs. Samples were sputter coated with gold/palladium (80/20) nanoparticles using a LEICA EM 600 high vacuum sputter coater at a current of 30 mA and a sputter rate of 0.03 nm/sec until a coating depth of 12.19 nm was reached. Images were acquired using a ZEISS Sigma 300 Field Emission Scanning Electron Microscope. Samples were subject to an accelerating voltage of 5.00 kV and viewed using the secondary electron detector.

## 2.6 Characterization of Quercetin Loaded, Glyoxal Cross-Linked PVA Fibers

In addition to understanding how PVA, glyoxal, and quercetin influence the characteristics of the bulk material, characterization of the fibers was also conducted. Understanding the factors influencing fiber formation will be important considerations for manufacture of bulk materials and optimizing protocols for this polymer system.

### 2.6.1 Overview of Apparatus for Observing Single Fiber Formation

The fiber formation behaviour for contact drawing of a polymer system can be characterized using an apparatus developed previously (62). This apparatus has a viscous polymer solution loaded into a caddie, and a translational stage with a microneedle (Figure 12). This translational

stage can be moved along a fixed axis by a motor, under computer control (Thorlabs Kinesis® Software). The motor brought the needle into contact with the viscous polymer solution and after a short delay, moved the translational stage at a controlled speed back to the point of origin. The pull speed was the main parameter modified to understand the nature of fiber formation for a polymer system.

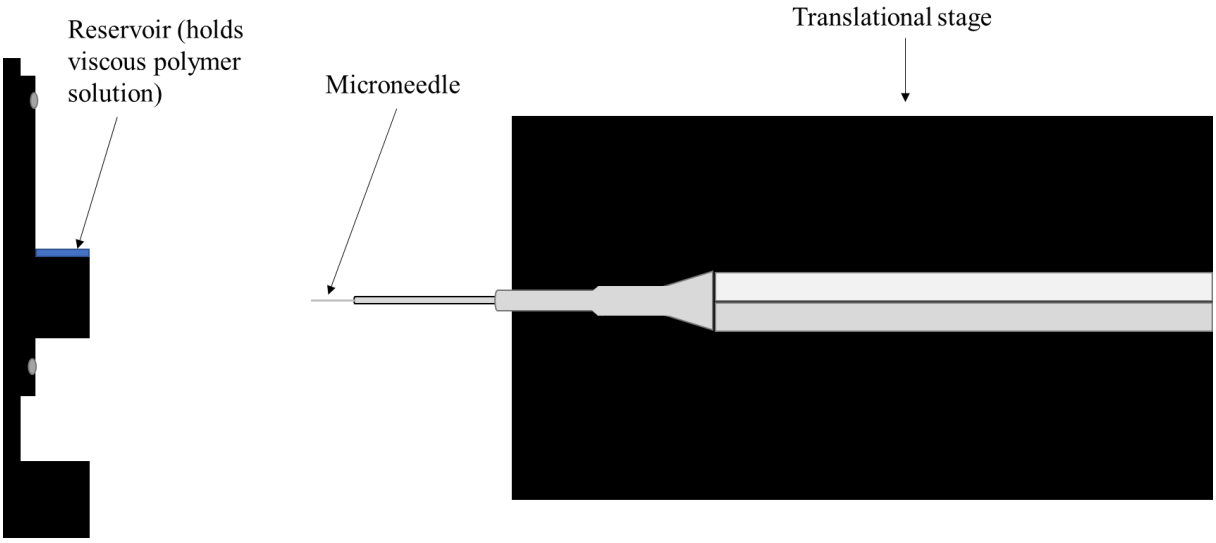


**Figure 12 Reservoir-microneedle based system for single fiber formation analysis.** Figure adapted from Chowdhry *et al*. (62).

For the PVA-based polymer system, the effects of pull speed on failure rate will help to elucidate the effects that PVA concentration, glyoxal cross-linking, and quercetin loading will have on fiber formation behaviour.

### 2.6.2 Failure Rate Analysis of Fiber Formation

Fibers pulled using the reservoir-microneedle based apparatus were assessed to elucidate fiber formation and the parameters affecting this process. All data were collected using an Ultra Micro-Needle, straight, tip radius 20 µm, 0.50 mm (Ted Pella, Inc). Data were collected in a binary system where the result is either success (liquid bridge becomes stable fiber as

microneedle pulls away from reservoir) or failure (fiber does not begin to form or fails as the microneedle pulls away from the reservoir). Each experiment was conducted from complete success (N=10, all fibers form) to complete failure (N=10, all fibers fail). For most polymer systems, the trend seems to be that as pull speed decreases, polymer entanglement will also decrease, and this will result in increased failure rate. To complete these analyses, the initial pull speed was set to >500 mm/s (uncorrected pull speed, input for Thorlabs Kinesis® Software). Data were collected for each pull speed, decreasing in 50 mm/s input increments until fibers ceased to form (i.e., 10 failures for a given pull speed were recorded). If the incremental steps became difficult to resolve (e.g., went from complete or almost complete success to complete or almost complete failure in one increment), more data were collected at 10, 12.5, or 25 mm/s increments.

The PVA systems for this analysis described modifications to three main parameters – PVA concentration (wt% in aqueous solution), glyoxal concentration (fixed PVA concentration and fixed time following addition of cross-linker), and time period following addition of glyoxal (fixed PVA and glyoxal concentrations). PVA concentrations tested were 7.5, 10.0, 12.5, 15.0, and 17.5% PVA (wt/wt). Glyoxal concentrations tested were 5, 10, 20, 50, and 100% glyoxal additions where the PVA concentration was fixed at 12.5% and the time following glyoxal addition prior to loading into the reservoir was 15 min. Finally, the time period following glyoxal addition was modified at 5-minute intervals between 15 and 45 min when the PVA concentration was fixed at 12.5% and the glyoxal concentration was fixed at 20% mol effective. To alleviate any confounding variables with solvent evaporation and timing concerns the 50 μL aliquot was replaced in the reservoir whenever the pull speed was adjusted (10 pulls, ~1 minute).

The modifiable pull speed was correcting using data obtained from an Edgertronic high-speed camera to adjust the input pull speed to actual pull speed. The desired pull duration ($\tau_{pull}$) was then calculated according to:

$$\tau_{pull} = \frac{path\ length}{pull\ speed} \tag{10}$$

Failure rate was calculated according to:

$$failure\ rate\ (\%) = \frac{number\ of\ failed\ trials}{number\ of\ total\ trials} \times 100 \tag{11}$$

The corresponding failure rate plots were generated using Minitab statistical analysis software. The data were modelled using the best fit of a Weibull Growth distribution for each unique PVA system.

### 2.6.3 Scanning Electron Microscopy Fiber Diameter Analysis

Fibers were also pulled using the reservoir-microneedle apparatus for analysis of fiber diameter via scanning electron microscopy (SEM). At least 25 fibers were collected at 260, 320, and 365 mm/s pull speeds to first determine the effects of pull speed on fiber diameter. At least 25 fibers were also collected for each of 5, 10, and 20% (mol effective) glyoxal additions both in the absence and presence of quercetin (final loading concentration of 200 μM) at a constant pull speed of 365 mm/s. Fibers were collected directly onto SEM carbon tape stubs. Samples were sputter coated with gold/palladium (80/20) nanoparticles using a LEICA EM 600 high vacuum sputter coater at a current of 30 mA and a sputter rate of 0.03 nm/sec until a coating depth of 6.21 nm was reached. Images were collected using a ZEISS Sigma 300 Field Emission Scanning Electron Microscope. Samples were subject to an accelerating voltage of 5.00 kV and viewed using the secondary electron detector.

Images were analyzed using ImageJ, where fiber diameters were measured using particle analysis and the provided scale bars/given magnification for the SEM images. Each fiber was measured in three separate locations to yield an average fiber diameter for n=25 fibers. The average of these diameters was calculated and reported with 95% confidence intervals to compare statistical significance among treatment groups.

### 2.6.4 Fiber Swelling

Fibers were pulled onto clear glass slides for analysis of swelling according to previously reported contact drawing, glyoxal cross-linking, and quercetin loading protocols. A solution of 12.5% PVA was used to pull fibers containing 20% (mol effective) glyoxal through one pot addition and a subsequent 12 h of vapor-assisted glyoxal cross-linking. Fibers were dried overnight and washed with 10 mM glycine solution (in phosphate buffered saline) to remove any residual glyoxal before being dried again for 2 h in a 40°C dry gravity convection oven. Fibers were immersed in aCSF for 7 days at 37°C. Fibers were visualized using the 20X objective of a Nikon Eclipse Ti optical microscope at 0, 1, 2, 4, 8, 12, 18, 24, 48, 72, 120, and 168 h following rehydration. Fiber diameters were obtained according to the same image processing analysis as mentioned previously.

## 2.7 Cell-based experiments

To model the novel biomaterial for the intended use, a suitable cell assay is required to determine the potential cytotoxicity of the PVA-based fibers and potential efficacy for quercetin release from these fibers. PC12-Adh cells are the adherent phenotype of the PC12 cells derived from pheochromocytoma of the adrenal rat medulla. These cells have origins in the neural crest and are a mix of neuroplastic and eosinophilic cells. These cells respond well to a variety of

neurotrophic factors, acting as an excellent model for neurotoxicity, neuroprotection, neurosecretion, neurodifferentiation, neuroinflammation, and synaptogenesis studies.

### 2.7.1 PC12Adh Cell Culture

Cells were brought out of liquid nitrogen storage and thawed at 37°C for approximately 2 min. Cells were pelleted by centrifugation at 200 × g for 5 min, with the pellet retained and the cryoprotectant (DMSO) removed with the supernatant. Cells were resuspended in complete culture medium. Cells were cultured in standard 150 mm (diameter) × 25 mm (height) Corning® tissue-culture treated culture dishes and kept in an incubator at 37°C and 5% $CO_2$. Two distinct media – complete cell culture medium (passaging and subculture) and differentiation medium (experimental media) were used. Both media used Kaighn's Modification of Ham's F-12 Medium (F-12K; Corning), supplemented with 1% antibiotic solution. The complete cell culture media also incorporated 2.5% fetal bovine serum (FBS) and 15% horse serum whereas the differentiation media had 1% horse serum. Culture medium was replaced every 3 days.

Subculture and passaging were completed at 90% confluency for PC12Adh cells. Media was removed and residual media was washed with phosphate buffered saline. 5 mL of 0.05% trypsin and 0.53 mM ethylenediaminetetraacetic acid (EDTA) in Hank's balanced salt solution (Corning) were added to the culture dish and placed into the incubator at 37°C for 5 min. Plates were assessed visually to assess morphological changes in cells to indicate release from culture dish. Trypsin was quenched with 5 mL of complete cell culture media and the cell suspension was transferred to 15- or 50-mL conical tubes (VWR). Tubes were centrifuged at 200 times the force of gravity for 5 min, allowing cells to form pellets in the bottom of the tubes. Supernatant was poured off and cells were resuspended using 1 mL of fresh complete cell culture media.

Cells were quantified using Countess II FL cell counter before being added to new culture dishes or plated for experiments.

### 2.7.2 Initial Cytotoxicity Screening for PVA Fiber Formulations

To understand how novel fiber formulations may affect PC12Adh cells, an experiment was designed to determine potential cytotoxic effects. PC12Adh cells were seeded directly into 96-well tissue culture treated culture plates in differentiation medium at a density of ~$10^4$ cells. Fibers were pulled onto PDMS sheets, and a biopsy punch was used to make punches for placement in the wells. Treatment groups included the well plate (no PDMS or fibers), PDMS control (PDMS blanks), PVA fibers without and with the addition of 100 and 200 µM of quercetin (on PDMS punches, 20% mol effective one-pot glyoxal addition and 12 h vapor-assisted cross-linking). Representative images were taken using a Nikon Eclipse Ti Epifluorescence Microscope and later processed with ImageJ for normalizing to cell densities. Cells were placed back in the incubator for 72 h before assessment of cell viability using Cell Titer Glo® 2.0 Cell Viability Assay (Promega). This single reagent assay quantifies cellular adenosine triphosphate (ATP) to determine cell viability. Cell medium was removed from wells and wells were washed with phosphate buffered saline. 100 µL of Cell Titer Glo® Reagent were added to the wells and placed on the agitator for 20 min. Total luminescence (all wavelengths) was measured using the Molecular Devices FilterMaxF5 Multimode Microplate Reader and processed using SoftMax Pro 6.5. Raw data for luminescence was corrected for cell density and then normalized to cell viability for cells cultured without PDMS or fibers. Each data point was the average of a triplicate and error bars represent 95% confidence intervals.

# 3. Results

## 3.1 Polymer Selection – Preliminary Screening for Stability Following Rehydration

Fibers were successfully pulled for dextran (50% by weight), poly(2-ethyl-2-oxazoline) (P2E2O, 50% by weight), and poly(vinyl alcohol) (12.5% by weight). The pin array tool with pins of dimensions 0.75 mm columns with 0.5 mm spacing was suitable for testing production of contact drawn fibers. This pin spacing was robust enough for reuse (i.e., the device could be reapplied to the polymer solution to pull many fibers without running into issues like pin breaking or clogging causing inconsistent fiber formation). Although the cross-linked dextran fibers showed some swelling and resistance to dissolution, the fibers were completely dissolved after a few minutes (Figure 13). The 50% P2E2O showed no signs of cross-linking as there was no change between the fibers before and after cross-linking following rehydration with distilled water (Figure 13). Glyoxal is known to cross-link free hydroxyls (in acetal formation) or free amine groups (in Schiff base formation). Thus, a reaction between the carbonyl groups present in P2E2O was not expected. Finally, for 12.5% PVA fibers, there was significant swelling and resistance to dissolution of cross-linked fibers compared to fibers that were not cross-linked (Figure 13). This indicated some degree of cross-linking between PVA molecules via acetal formation.

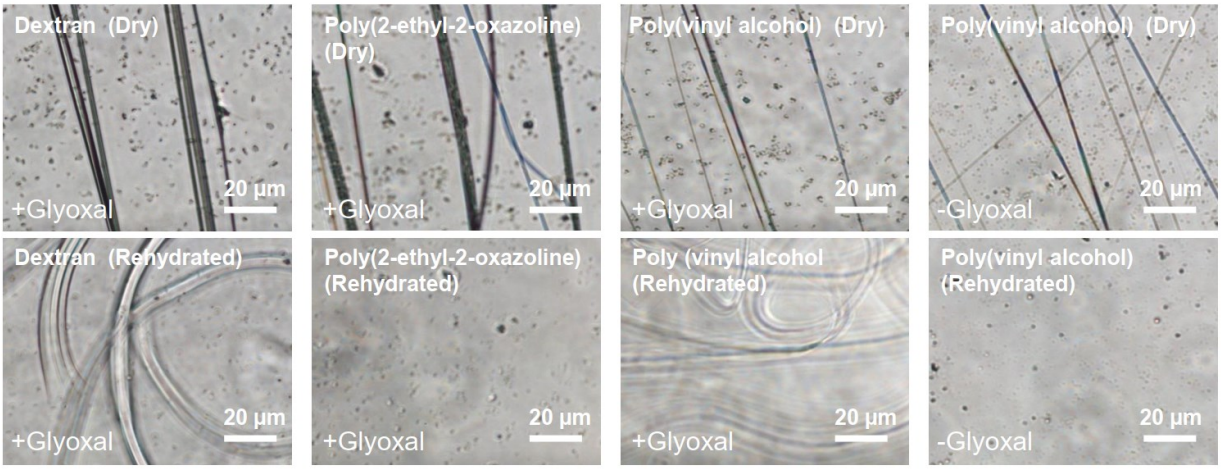


**Figure 13 Rehydration experiments for various polymer fibers.**
Fibers pulled with and without cross-linking via glyoxal addition (5% by weight) following rehydration with distilled water. Rehydrated images were acquired 1 min post-rehydration.

The initial rehydration experiments indicated that PVA and dextran could both be suitable polymers of choice for use in the proposed research. PVA has a simpler monomer than dextran, indicating potential steric hinderance may be less of a concern for chemical cross-linking by glyoxal. The simplest dialdehyde may require unfavourable molecular conformations of dextran for formation of acetal linkages. In addition to avoiding potential steric issues, PVA has a higher relative amount of free hydroxyl groups available for cross-linking. Therefore, PVA was selected as the polymer for further cross-linking experiments.

### 3.2 Optimization of Cross-linking Protocol

With PVA selected as the polymer of choice for the proposed research, the glyoxal cross-linking reaction was studied more in depth to optimize it for the contact drawing process. Cross-linking was pursued as a route to make the PVA fibers more resistant to hydrolysis and hydrolytic degradation. This was so the fibers could exist in an aqueous environment (and thus *in vivo*) over the course of the nerve regeneration following injury.

In this work, the so-called “one-pot addition” method was used, whereby the cross-linking agent glyoxal was added directly to the viscous PVA polymer solution along with HCl since lowering the pH promotes acetal formation via proton shifts (87). A one-pot method displays favourable kinetics and intermolecular interactions when the reacting species are in solution. In other words, chemical reactions proceed at reasonable rates when in solution since the number of collisions between molecules is greatly increased proportional to the same reaction between solid materials. Since PVA needs to be dissolved into an aqueous solution for contact drawing, the one-pot method is compatible with this process.

The second method explored for cross-linking of PVA fibers was through glyoxal vapour exposure. This method of cross-linking has more stringent requirements for the cross-linker. For example, vapour-assisted cross-linking requires a cross-linking agent that can exist as a vapour at reasonable vapour pressures and working conditions (i.e., pressures below 760 mm Hg are ideal). Glyoxal has a vapour pressure of 255 mm Hg at room temperature and this pressure increases as a function of temperature (88). The boiling point of glyoxal (51°C) is also lower than water, and glyoxal is almost always sold as an aqueous solution (88). Thus, at the right temperature, the vapour chamber will contain an extremely high proportion of glyoxal vapour relative to water vapour. Furthermore, the high heat capacity of water helps to absorb excess heat and keep the vapour chamber at a safe temperature and pressure. Collisions between molecules in gaseous states are even more likely than those in solution, making this method viable for chemical cross-linking. To accommodate glyoxal cross-linking through vapor-assisted cross-linking, PVA fibers were placed in vapor chambers for various times to further modify fibers after contact drawing. The effectiveness of vapor-assisted cross-linking and one-pot cross linking is shown below

through rehydration experiments in distilled water (Figure 14).

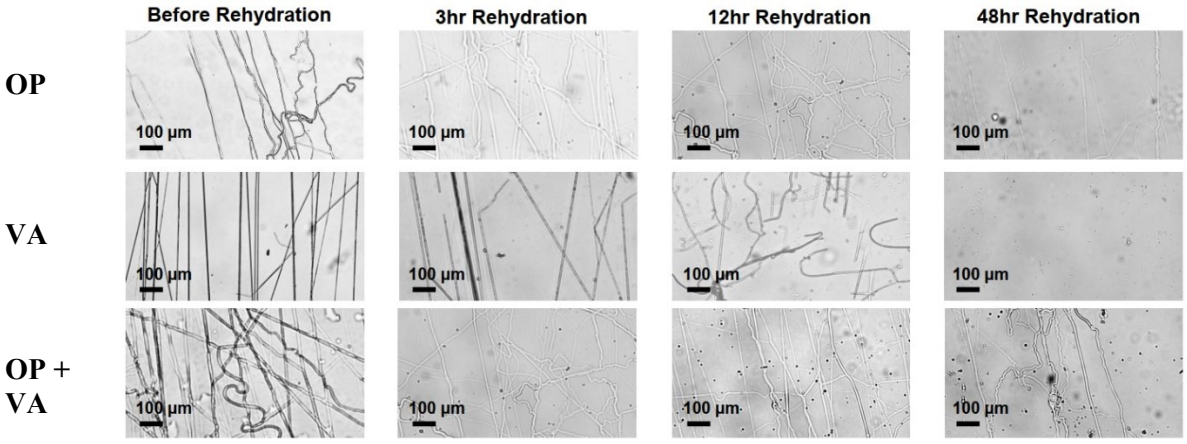


**Figure 14 Rehydration experiments for cross-linking methods.**
Conditions for cross-linking include OP – one-pot addition of glyoxal to viscous polymer solution prior to contact drawing and VA – vapor-assisted glyoxal cross-linking of fibers following contact drawing in vapor chambers at 60°C for 12 h. Presence of fibers (hydrated or dry) is indicative of cross-linking success (to which there are varying degrees) since fibers resist dissolution.

The one-pot and vapour-assisted methods indicate formation of acetal linkages between PVA chains to produce acetal linkages which made fibers less susceptible to hydrolysis and dissolution. The one-pot method produced fibers that were more resistant to hydrolysis and degradation than the vapour-assisted method, with the combination of approaches producing fibers that were still present 48 h after rehydration in distilled water. Fibers were essentially non-existent at 48 h for the vapour-assisted approach, whereas some of the fibers began to show broken segments for the one-pot method at 48 h that were similar to the broken fibers at 3 and 12 h for the vapour-assisted method.

### 3.3 Quercetin Loading – Dose Response

With successful approaches developed to cross-link PVA fibers following contact drawing, the potential to load the fibers with a model small molecule during the contact drawing

process was investigated. Small molecules like quercetin can be loaded into biomaterials in two main ways – before or after the fabrication step. Quercetin is soluble in many organic solvents, so loading following fiber formation could potentially proceed through a soaking process in a quercetin-containing solvent. It is also possible to load quercetin directly into the viscous polymer solutions prior to contact drawing. To explore the latter, various final concentrations of quercetin were added to the viscous polymer solution in combination with glyoxal. Although quercetin is insoluble in water, it has high solubility in DMSO. Thus, small volumes of concentrated quercetin in DMSO were added to the polymer solution before fiber formation. The microscopy images (brightfield and fluorescence of rehydrated fibers) for quercetin loading at 0, 50, 100, and 150 μM final concentrations show an increase in fluorescence proportional to the amount of quercetin present in the polymer solution, indicating that quercetin is readily incorporated into the contact drawn fibers (Figure 15).

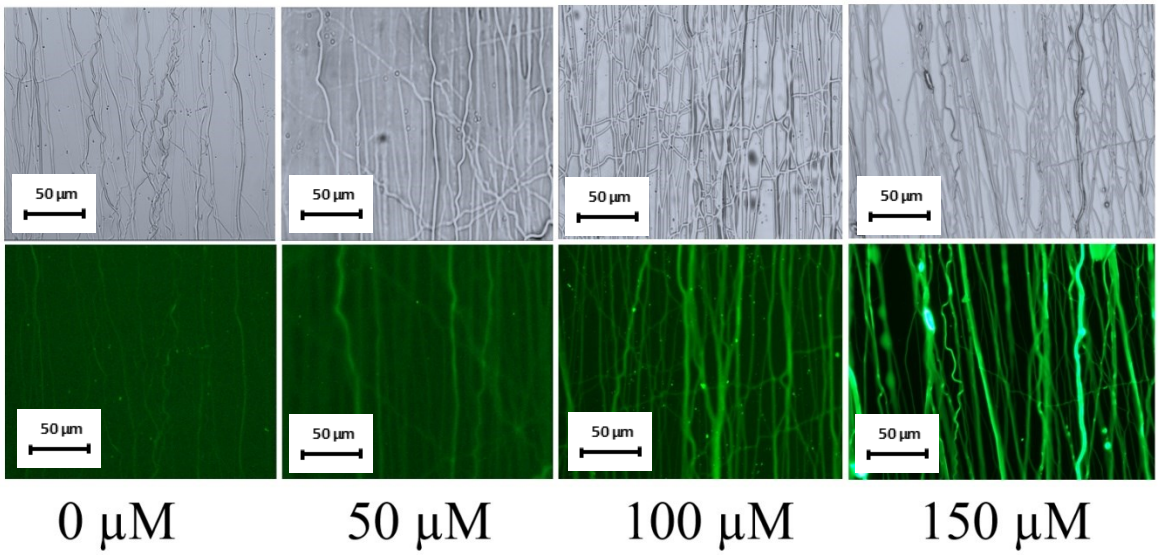


**Figure 15 Quercetin loading – dose response.**
PVA fibers pulled with various quercetin additions though one-pot addition of DMSO stock to viscous polymer solution.

Quercetin itself is an active fluorophore which provides an excellent indicator of loading via analysis of fluorescence (81). There is some autofluorescence observed for the fibers without any quercetin addition (Figure 15). Although autofluorescence is mostly encountered in the instance of biological autofluorescence (natural emission of light by biological structures), the autofluorescence of polymers is also known for many polymers across the visible spectrum (89,90). The degree of fluorescence could be quantified for each loading condition using ImageJ and fiber fluorescence for those containing quercetin can be corrected for autofluorescence (Figure 16).

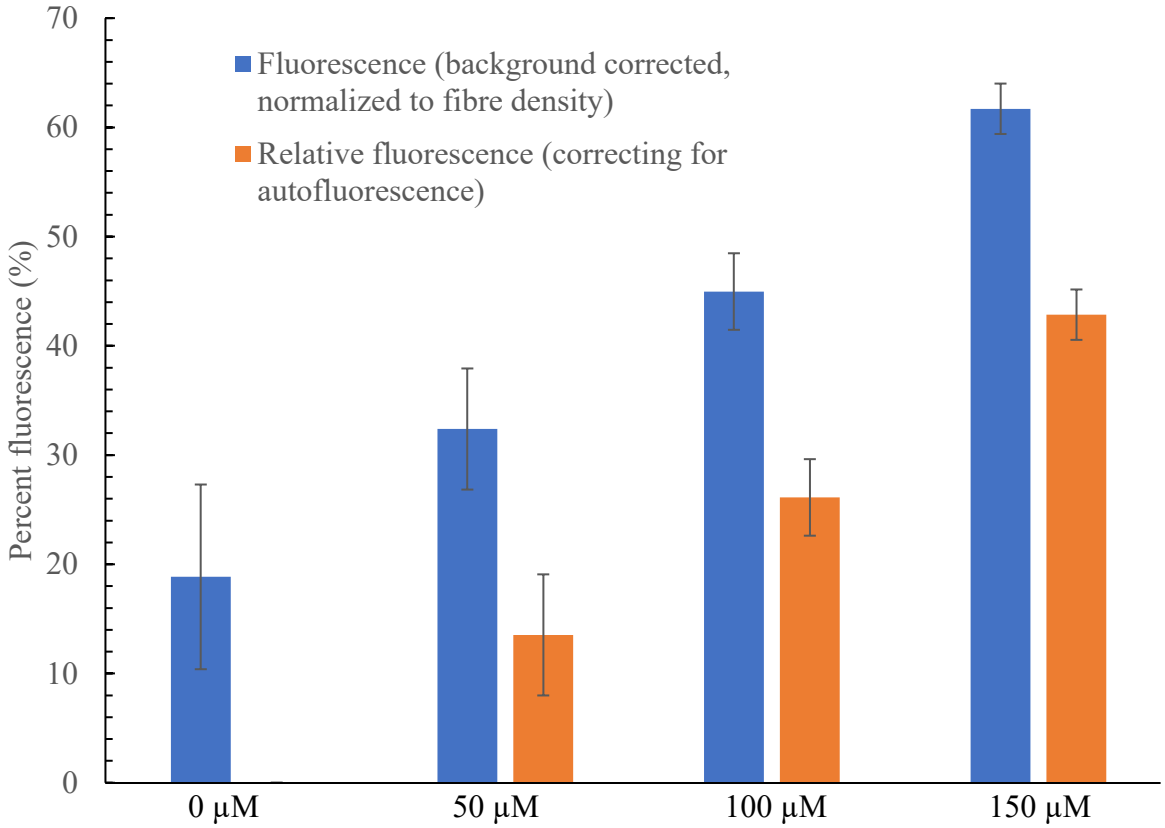


**Figure 16 Fluorescence quantification.**
Absolute fluorescence and relative fluorescence (correcting for autofluorescence) for fluorescence images of PVA fibers loaded with various final concentrations of quercetin prior to contact drawing. Error bars indicate signal to noise ratios for each loading concentration (signal being integrated density of the fibers and noise being integrated density of the background).

### 3.4 Characterization

Physical and chemical characterization of the material will help understand any significant modification to the base PVA polymer through glyoxal cross-linking and quercetin loading. Identifying the molecular changes from the addition of quercetin and glyoxal can help elucidate many useful experimental factors. For the purposes of this analysis, the focus was on the quantification of the cross-linking reaction and any significant changes to the base PVA which may affect future *in vitro* and *in vivo* applicability.

### 3.4.1 IR Spectroscopy for Quantification of Glyoxal Cross-Linking

The first characterization involved using films rather than fibers, to ensure ample material would be present for detection via ATR-FTIR. Material processing mimicked preparation of viscous polymer solutions prior to contact drawing but instead of pulling fibers the polymer solution were poured onto PDMS to make thin films for analysis. The films consisted of varying amount of glyoxal to understand how the cross-linking agent modified the PVA (Figure 17).

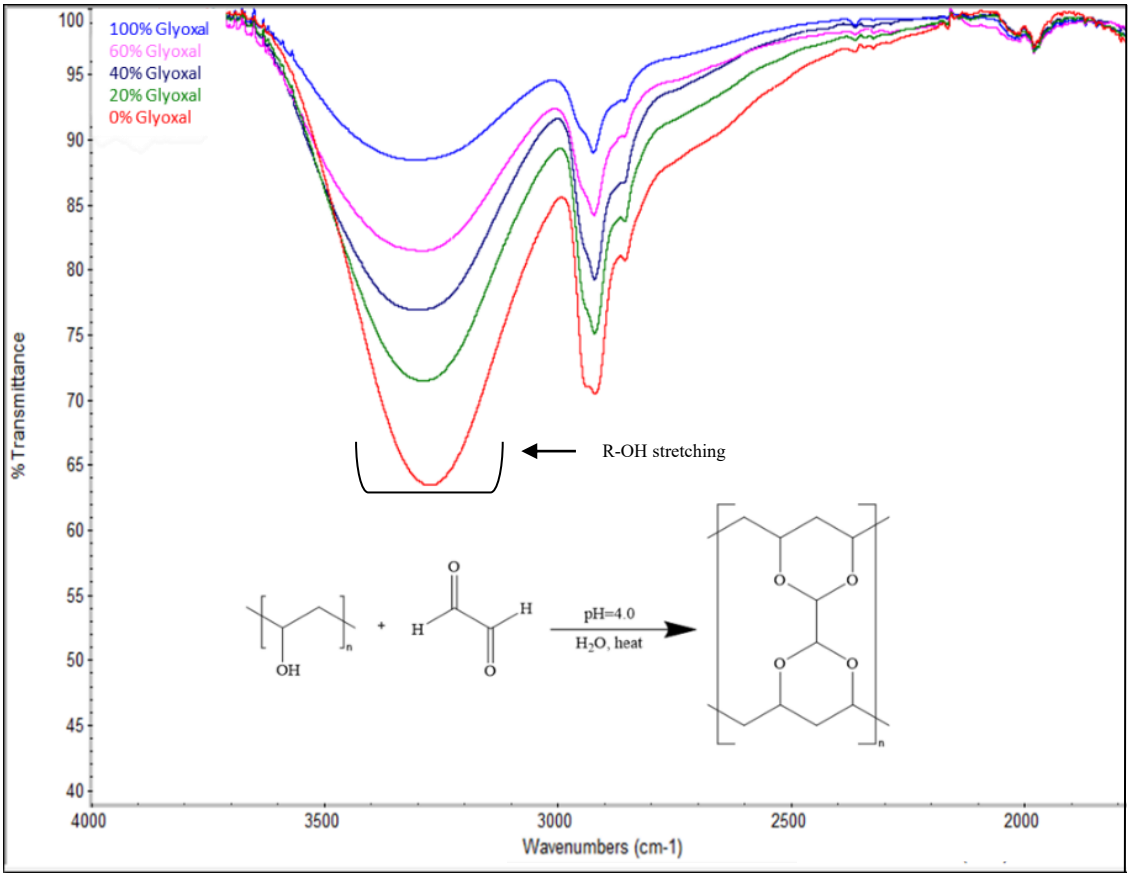


**Figure 17 Quantification of glyoxal cross-linking via IR.**
From bottom to top, films loaded with 0 (red), 20 (green), 40 (dark blue), 60 (pink), and 100 (blue) percent glyoxal (mol effective).

As the glyoxal concentration was increased, the presence of a broad band consistent with hydroxyl stretching from 3000-3500 $cm^{-1}$ decreased in intensity. This corresponds to a depletion

of hydroxyl groups that would initially be present in PVA, indicating that they formed acetal linkages.

### 3.4.2 IR Spectroscopy for Analysis of Quercetin Loading

IR can also be used to assess the PVA fibers following the addition of glyoxal and quercetin. Namely, IR can be indicative of different chemical functionalities through differences in vibrational signatures. IR spectra were collected for fibers with 0, 50, 100, and 200 µM of quercetin and compared to pure PVA (Figure 18). Spectra were mainly dominated by the PVA present in each samples when comparing groups to pure PVA (Figure 18). To compare with the IR spectrum of quercetin, see Appendix B.

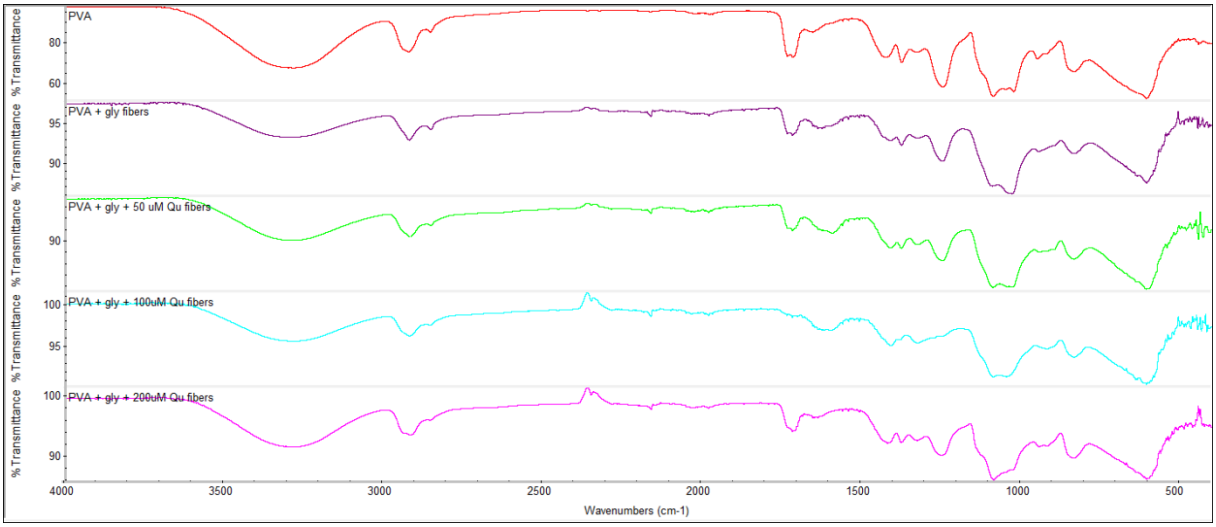


**Figure 18 IR spectra for PVA fibers loaded with quercetin.**
Spectra were collected from 400-4000 $cm^{-1}$. All fibers were pulled with 20% glyoxal addition (one-pot) and 12 h of vapor assisted cross-linking. Fiber spectra were compared to the spectrum of PVA alone. Spectra (top to bottom) are pure PVA, glyoxal cross-linked PVA fibers, glyoxal cross-linked PVA fibers with 50 µM of quercetin, glyoxal cross-linked PVA fibers with 100 µM of quercetin, and glyoxal cross-linked PVA fibers with 200 µM of quercetin.

The increasing intensity of stretching between 3000 and 3500 $cm^{-1}$ with the addition of quercetin may be a result of the many hydroxyl groups present in the structure of quercetin, indicating successful incorporation within our PVA fibers.

## 3.5 Quercetin Release

With quercetin showing promising results for loading into contact drawn PVA fibers, the logical progression was to assess whether the material releases quercetin *in vivo*. To model this, bulk scaffolds of the fibrous PVA materials were placed in aCSF to mimic conditions surrounding implantation following a traumatic nerve injury.

### 3.5.1 Degradation and Cumulative Drug Release Profiles

PVA scaffolds were incubated in aCSF at 37°C for 10 days. At 1, 4, 8, 16, 40, 66, 114, and 240 hours, the aCSF was assessed for quercetin release and at 1, 4, 8, 16, 40, 66, 114, 170 and 240 hours the weight of the scaffold was measured to assess degradation (Figure 19).

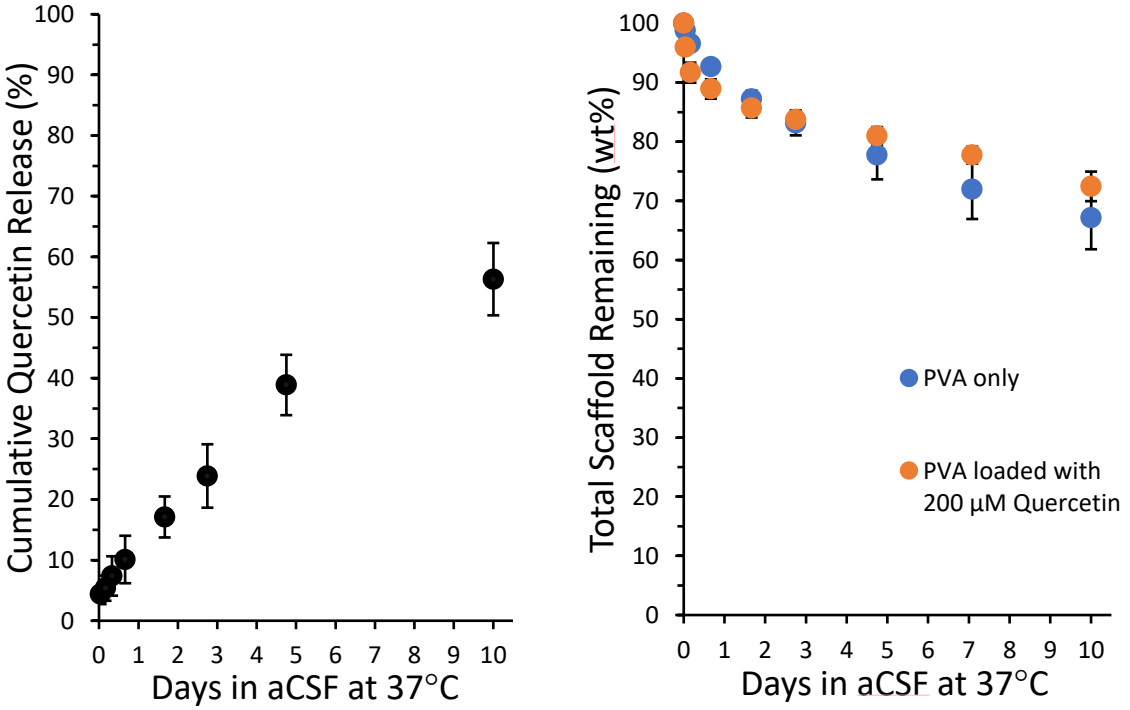


**Figure 19 Cumulative drug release and degradation profiles.**
Cumulative drug release (left) and degradation profile (right) for PVA fibers loaded with 200 µM of quercetin. Cumulative drug release over 10 days is calculated from UV-Vis absorbance at 375 nm (normalized to absorbance of scaffold without quercetin addition). Degradation profile

shows weight percent of original scaffold remaining over the course of 10 days. Data represent the average of 3 replicates (N=3) and corresponding 90% confidence intervals.

A short burst release of quercetin is indicated by the sharp increase in quercetin release to ~5% in the first few h following incubation in aCSF. Following this burst, the release pattern becomes more sustained and indicates a slow release of quercetin to a maximum of 56 ± 6% (average of three replicates). Degradation profiles indicate a relatively stable material, with degradation reaching 27 ± 3% for scaffolds loaded with quercetin and 33 ± 5% for those without quercetin.

### 3.5.2 Morphological Analysis of Scaffolds via SEM

In addition to quantifying quercetin release and degradation behaviour, analysis of fibrous scaffolds through the course of the incubations can yield valuable information about the release and degradation mechanisms at play. Scaffolds with and without quercetin from the incubations in aCSF at 37°C were also used for morphological analysis via SEM at 1 h and 1, 3, and 10 days (Figure 20).

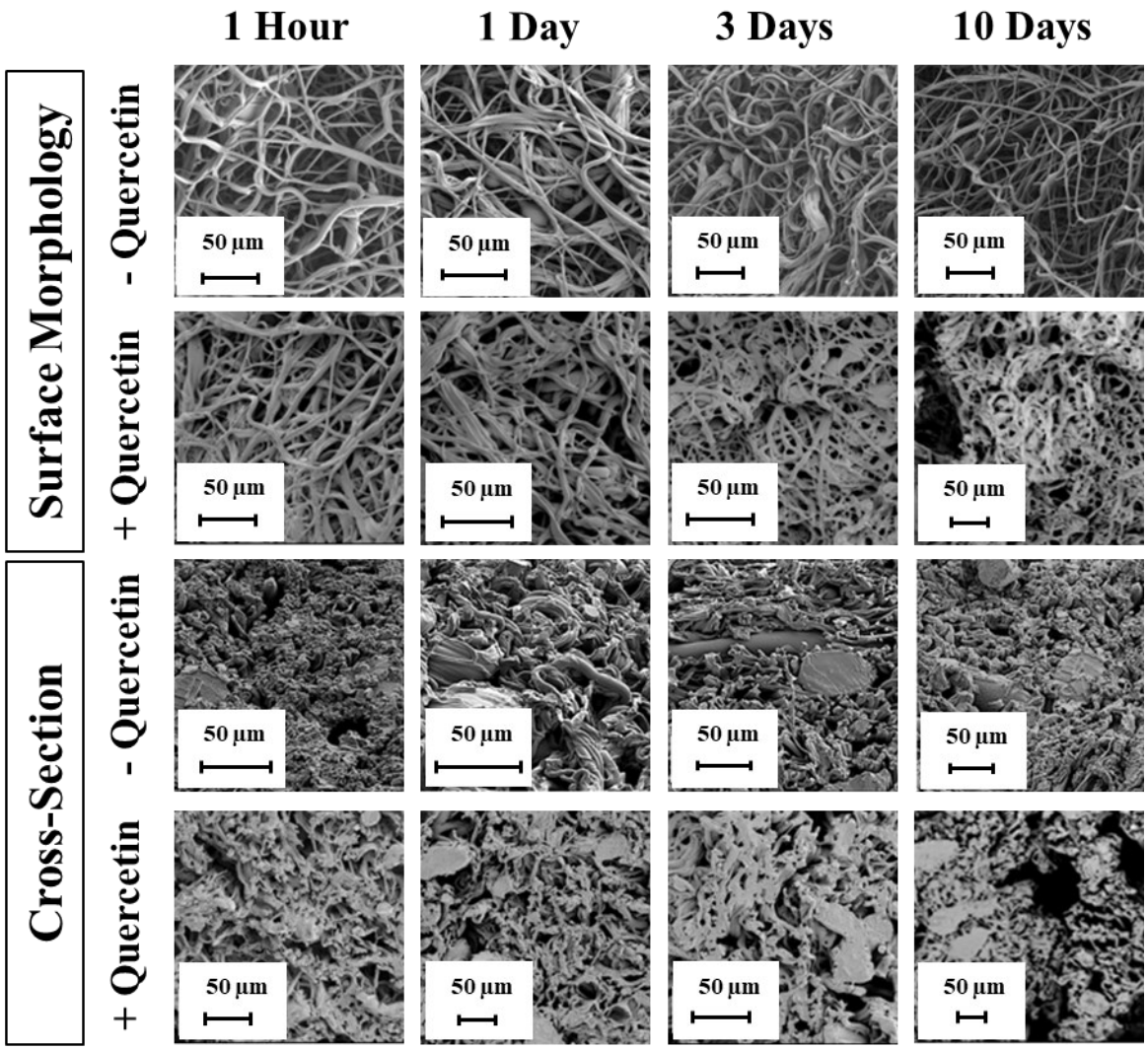


**Figure 20 SEM analysis of fibrous scaffolds following incubation in aCSF.**
Fibrous scaffolds without (-Qu, top two rows) and with (+Qu, bottom two rows) 200 µM quercetin addition. Surface and cross-sectional profiles of scaffolds are shown for both conditions.

Scaffolds without addition of quercetin appear to have highly retained fibrous morphologies, indicating degradation is likely to occur primarily through surface erosion of polymer fibers. Fibers without quercetin appear to shrink noticeably by day 10, further indicating surface erosion as a potential mechanism of bulk material loss. On the other hand, quercetin-

loaded scaffolds appear to become more porous over time and fibers appear to fuse together, becoming a lattice network of PVA fibers.

## 3.6 Fiber Formation Behaviour

Using a motorized stage for contact drawing, a better understanding of the fiber formation of the PVA polymer system can be obtained. Polymer entanglement drives fiber formation and the entanglement of polymers within a system can be influenced by many factors. Using the single fiber-forming needle-reservoir based system, we can assess the effects of a few of these factors: PVA concentration, glyoxal concentration, and time following glyoxal addition to the PVA solution.

### 3.6.1 PVA Concentration Effects

Chowdhry *et al*. showed that for solutions of dextran, increasing the concentration of dextran increased polymer entanglement and allowed stable liquid bridges (and thus dry fibers) to form at slow pull speeds (i.e., or long $\tau_{pull}$ values). To elucidate the effects of PVA concentration on fiber formation, aqueous solutions of PVA (205 kDa) at 7.5, 10.0, 12.5, 15.0, and 17.5% (wt/wt) were assessed (Figure 21). Fibers did not form at any pull speeds (maximum pull speed of the apparatus is ~400 mm/s) for 7.5% PVA. The pull speed required for polymer entanglement to drive fiber formation at the lowest tested concentration of PVA (7.5%) was likely beyond the capability of the motorized stage.

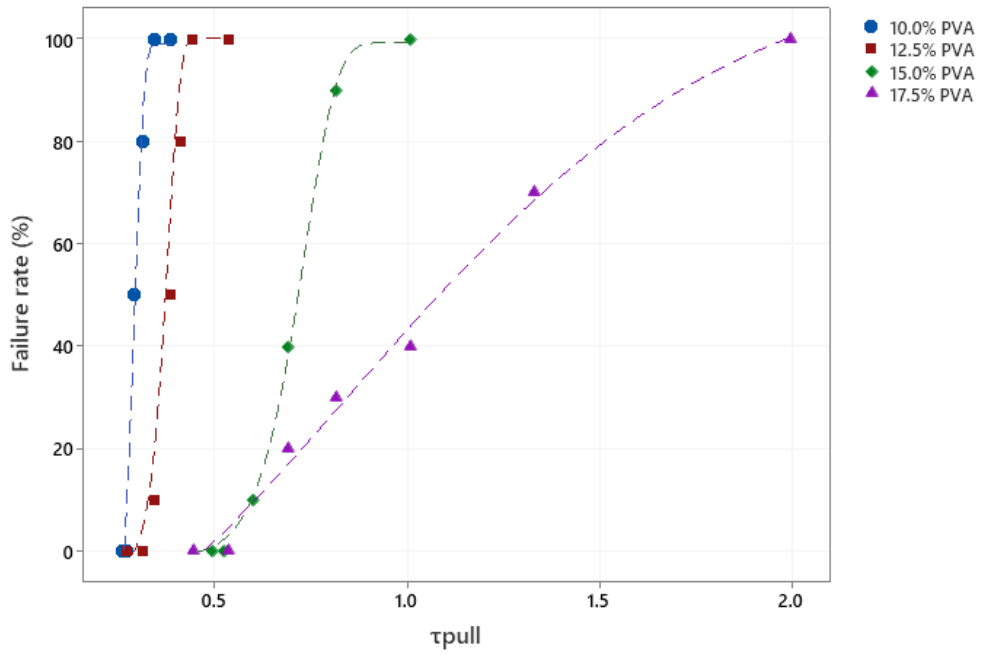


**Figure 21 Failure rate analysis for PVA concentration effects on fiber formation.**
Failure rate as a function of $\tau_{pull}$ for various PVA concentrations (no cross-linking). Each data set is fit using a Weibull cumulative distribution function (shown in dashed lines). Each data point is the percentage of failures from 10 trials.

With increasing PVA (wt%), the distribution curve displays a shift to the right toward larger $\tau_{pull}$ values, indicating fibers are more likely to form at slower pull speeds. The data indicated that polymer entanglement also increases for PVA polymer systems as the amount of polymer in solution is increased. If fibers can form at slower pull speeds, the entanglement of the polymer system must also be increasing.

### 3.6.2 Glyoxal Concentration Effects

Although the needle-reservoir system has been used to assess polymer concentration effects on fiber formation, this system has not been used previously to assess how the addition of a cross-linker may affect fiber formation. For this analysis, PVA concentration was fixed at 12.5% and the time was fixed at 15 min following the addition of glyoxal for running trials.

Trials were completed for 0, 5, 10, 20, 50, and 100% glyoxal additions (mol effective). Fibers did not form at any pull speeds for 100% glyoxal addition. This was likely the result of polymer entanglement increasing to the point where movement of polymer chains become too restricted for liquid bridge formation.

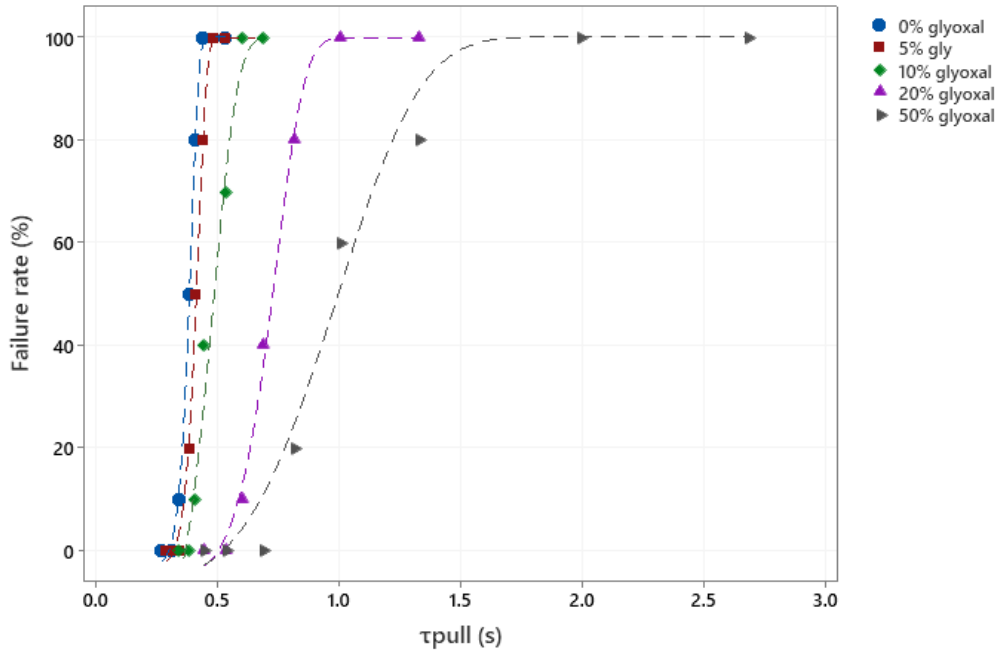


**Figure 22 Failure rate analysis for glyoxal concentration effects.**
Failure rate as a function of $\tau_{pull}$ for various glyoxal concentrations. Each data set is fit using a Weibull cumulative distribution function (shown in dashed lines). Each data point is the percentage of failures from 10 trials.

Similar to the increasing polymer content, as the amount of glyoxal is increased the failure rate distributions for polymer systems shift to the right. This indicates that fibers can form at larger $\tau_{pull}$ values, indicating polymer entanglement must be increasing for increasing glyoxal additions. Although a similar shift is indicated, the trend is less pronounced than the increasing PVA concentration. The subtle shift due to cross-linking (compared to PVA concentration

effects) indicates a less pronounced effect on polymer entanglement compared to addition of more polymer chains to the system.

### 3.6.3 Time Following Glyoxal Addition Effects

The final parameter explored for this polymer system was the time allotted following the addition of glyoxal to the PVA polymer solution. For this analysis, the amount of glyoxal was fixed at 20% (mol effective) and the PVA concentration was fixed at 12.5% (wt/wt). Trials were initially conducted for 15, 30, and 45 minute periods following glyoxal addition. However, the data indicated increased fiber formation at 30 min and comparable formation behaviour for 15 and 45 min. To explore this unexpected result, time periods at 5 min intervals between 15 and 45 min were collected (Figure 23, 24).

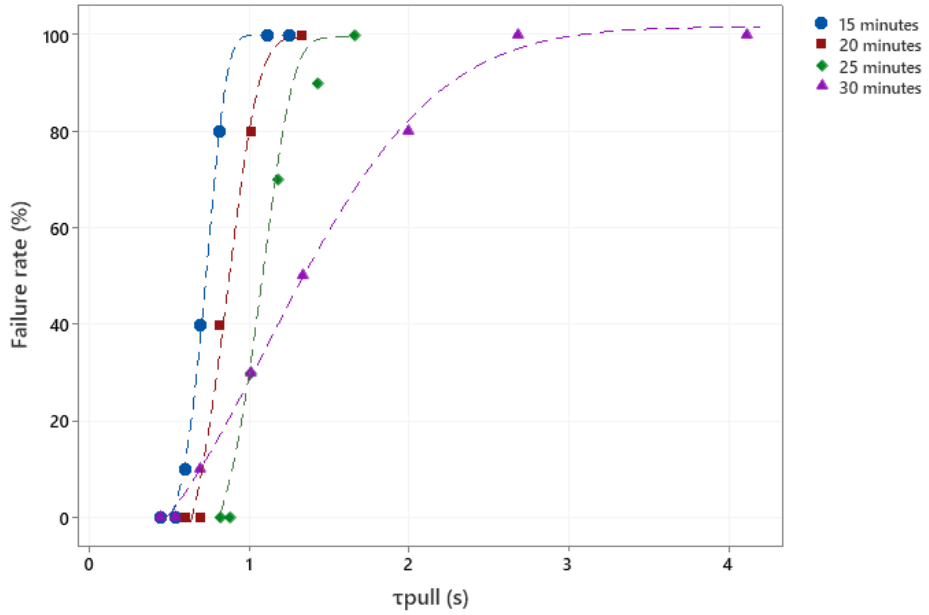


**Figure 23 Failure rate analysis for time periods following glyoxal additions on fiber formation (15-30 min).**
Failure rate as a function of $\tau_{pull}$ for various time periods following glyoxal additions. Each data set is fit using a Weibull cumulative distribution function (shown in dashed lines). Each data point is the percentage of failures from 10 trials.

For the first set of trials, polymer entanglement appears to drive fiber formation in a similar manner to the trend seen in both glyoxal and PVA additions. As the cross-linking reaction proceeds, the entanglement increases and intuitively fibers begin to form at slower pull speeds (larger $\tau_{pull}$ values). The same rightward shift of the distributions is present for these data sets.

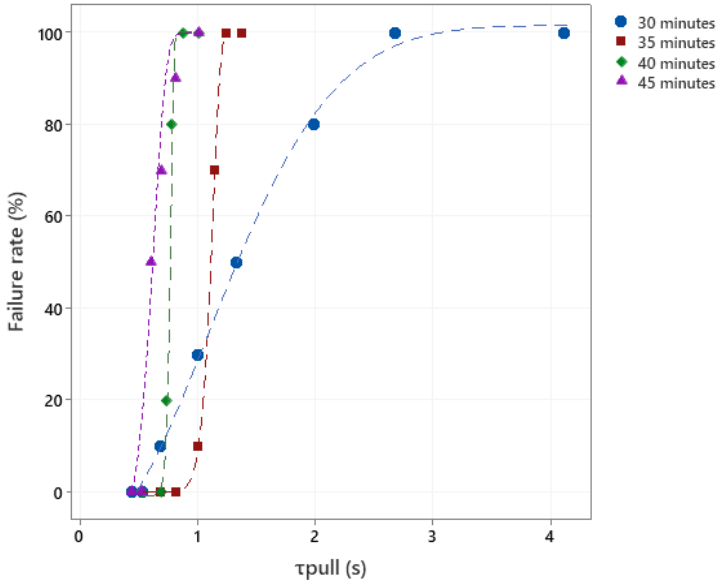


**Figure 24 Failure rate analysis for time periods following glyoxal additions on fiber formation (30-45 min).**
Failure rate as a function of $\tau_{pull}$ for various time periods following glyoxal additions. Each data set is fit using a Weibull cumulative distribution function (shown in dashed lines). Each data point is the percentage of failures from 10 trials.

In the data sets for the time points beyond 30 min, the opposite trend is observed. The cross-linking reaction is still progressing; thus, polymer entanglement is likely increasing. In this case, it was expected that the trend would continue as seen from Figure 23, yet the opposite trend is observed. One possible explanation for this is that the polymer system has begun to form a gel but has not completely gelled. This may result in localized areas where polymer chains are incorporated into a gel network and the areas outside of these gel regions actually have lower

apparent viscosity than the system as a whole. In this case, the fibers observed are likely due to the needle coming into contact with these areas in the reservoir to form liquid bridges and then dry fibers.

## 3.7 Fiber Diameter Analysis

With a better understanding of how fibers form as a function of different processing conditions, this was next related to the degree to which each PVA fiber type differed in physical character. Fiber diameter is a key parameter for biomaterial fibrous scaffolds, since fiber diameter can control a variety of factors including (but not limited to) pore size, cell adhesion and interaction, diffusion of nutrients, and degradation characteristics.

### 3.7.1 Pull Speed Effects

To understand how other factors (i.e., glyoxal cross-linking and quercetin loading) were affecting fiber diameters, a baseline of fiber diameter measurements was taken. For this analysis., the needle-reservoir apparatus was used to pull fibers at various pull speeds to determine the potential effects of pull speed on fiber diameter. Chowdhry *et al*. indicated that dextran did not show any significant effects on fiber diameter due to pull speed. To determine if this was also true for PVA fibers, fibers were pulled from 12.5% PVA at 260, 320, and 365 mm/s (Figure 25).

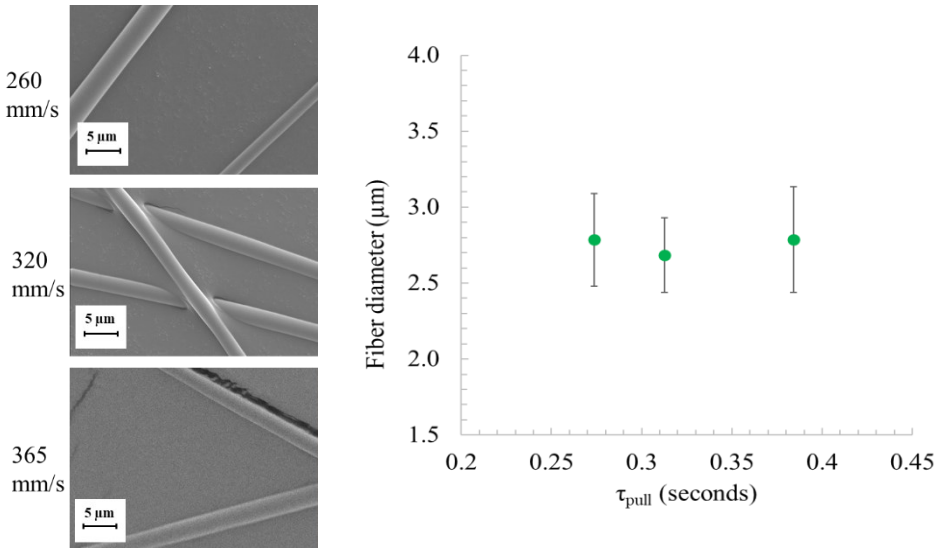


**Figure 25 Pull speed effects on PVA fiber diameters.**
Representative images of fibers pulled at (left, top to bottom) 260, 320, and 365 mm/s. Scale bars represent 10 µm. Fiber diameter as a function of $\tau_{pull}$ (right). Each data point is the average of at least 25 fibers and error bars indicate 95% confidence intervals.

Average fiber diameters were reported as 2.79 ± 0.34, 2.68 ± 0.24 and 2.79 ± 0.30 µm for pull speeds of 260, 320, and 365 mm/s respectively (corresponding to $\tau_{pull}$ values of 0.38, 0.31, and 0.27 respectively). These data did not show any significant differences in fiber diameter among pull speeds based on 95% confidence intervals. These pull speeds were chosen since a sufficient pull speed was required for fiber formation of 12.5% PVA, slower pull speeds may have resulted in partial formation of fibers and collection of loose fiber ends that could skew data. Although possible, it is unlikely pull speed plays a major role in fiber diameters for the contact drawing process since chain entanglement plays a major role in stabilizing fibrous structure. With increasing pull speeds, fibers could potentially approach 100% failure events due to chain relaxation time being too slow for polymer chains to slide past one another. Since polymer entanglement is the driving mechanism of fiber formation, it is likely the main determinant of fiber diameters as well.

### 3.7.2 Glyoxal Cross-linking and Quercetin Loading Effects

Although fiber diameter was not affected by pull speed (260-365 mm/s), it is possible that glyoxal cross-linking and quercetin loading may play a role in determining fiber diameters. Since pull speed did not lead to significant differences in diameter between 260-365 mm/s, fibers to test for glyoxal and quercetin effects were pulled at 365 mm/s. First, fibers were pulled with the introduction of glyoxal at 5, 10, and 20% (mol effective) (Figure 26). At the same concentrations of glyoxal, fibers were also loaded with quercetin (200 µM) to determine potential effects of glyoxal cross-linking and quercetin loading on fiber diameter (Figure 26).

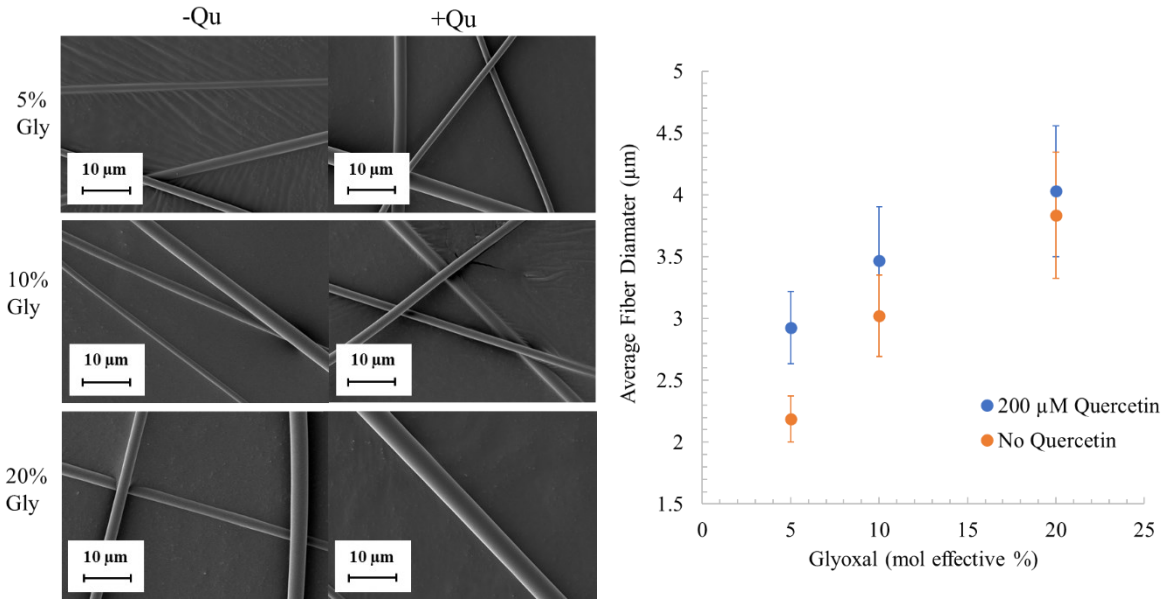


**Figure 26 Glyoxal cross-linking and quercetin loading effects on PVA fiber diameters.** Representative images of fibers pulled at (left, top to bottom) 5, 10, and 20% glyoxal (mol effective). Images of fibers pulled with (+Qu) and without (-Qu) 200 µM quercetin addition. Scale bars represent 10 µm. Fiber diameter as a function of glyoxal loading (mol %) (right). Each data point is the average of at least 25 fibers and error bars indicate 95% confidence intervals.

PVA fibers showed a trend of increasing fiber diameter with increased glyoxal loading. Fiber diameters were measured at 2.18 ± 0.18, 3.02 ± 0.33, and 3.83± 0.51 µm for glyoxal

concentrations of 5, 10, and 20% (mol effective), respectively. Fibers also exhibited increasing diameter with the addition of quercetin, at 2.92 ± 0.29, 3.46 ± 0.43, and 4.03 ± 0.53 μm for glyoxal concentrations of 5, 10, and 20% (mol effective) respectively. The only significant difference based on 95% confidence intervals was the fiber diameter increase from 5 to 10% glyoxal (without quercetin) and the difference with and without quercetin at 5% glyoxal. Although the data indicate increasing fiber diameter for increasing glyoxal concentrations and increasing fiber diameter with the addition of quercetin, the increasingly large range of fiber diameters for increasing glyoxal concentrations and quercetin addition resulted in wide 95% confidence intervals.

### 3.8 Fiber Swelling Experiments

The swelling response of a material is one facet of the material response and is an important consideration for hydrogels and other hydrophilic materials. PVA is considered to be highly hydrophilic due to the abundance of hydroxyl groups present in the side chains of the polymer. As a result, PVA materials can swell substantially in aqueous environments. The effect of swelling in aCSF was studied for the glyoxal cross-linked PVA fibers with and without addition of quercetin (Figure 27).

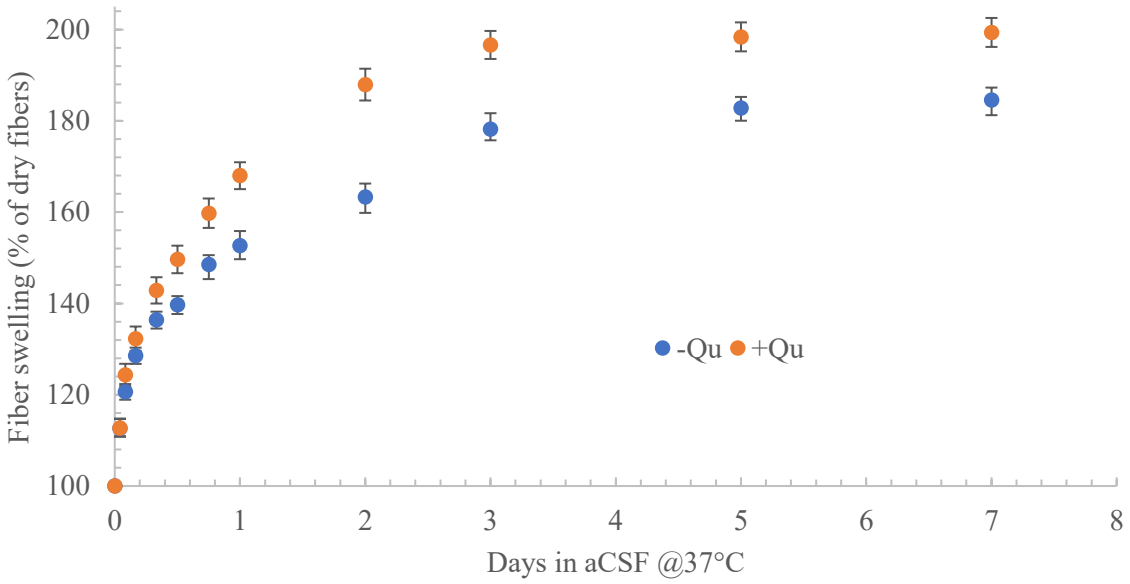


**Figure 27 Fiber swelling in aCSF.**
Fibers pulled with and without quercetin were incubated at 37°C in aCSF for 7 days. Fiber swelling assessed using fiber diameters and reported as percentage of the dry fiber diameter. Each data point is the average of 25 fibers and taken as a ratio of the initial average fiber diameter (for dry fibers). Error bars indicate 95% confidence intervals of swelling ratios.

Fiber swelling during the first 24 h of incubation reached values of up to 152.6 ± 2.9% and 168.0 ± 3.5% for fibers loaded without (-Qu) and with (+Qu) respectively. Swelling appeared to reach a plateau event after 3 days of incubation in aCSF with a maximum swelling after 7 days of 184.5 ± 3.3% and 199.4 ± 3.3% for fibers loaded without (-Qu) and with (+Qu) respectively. Fibers loaded with quercetin diverged from fibers without at 4 h and became significantly more swollen from 8 h onward.

### 3.9 Cell Viability Evaluation

The final objective of the proposed research was to determine efficacy of the PVA fibers in a cell-based assay. To properly determine efficacy based on intended use of this material, an assay (using PC12Adh cells as the model cell line) was developed. Cell viability would be an

indicator of the neuroprotective efficacy of the glyoxal-cross linked, quercetin loaded, PVA fibers.

### 3.9.1 Cell Viability – Screening Potential Cytotoxic Fiber Formulations

Before assessing the PVA fibers in the more complex neuroprotective assay, the fibers were screened for general cell viability in culture with PC12Adh cells. Fibers were washed with excess glycine buffer to remove any residual aldehydes from the bulk scaffolds prior to culturing. Representative images of the fibers are shown below (Figure 28).

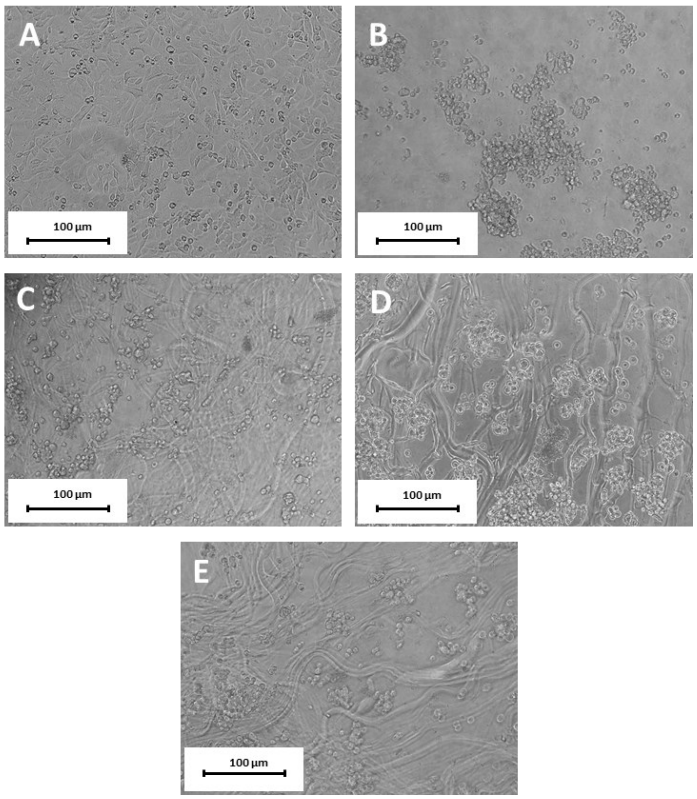


**Figure 28 PC12Adh cells grown with PVA fibers.**
Cells grown in (left to right) A) well plate (no PDMS), B) PDMS blank, C) PVA fibers with glyoxal, D) PVA fibers with glyoxal and 100 µM quercetin and E) PVA fibers with glyoxal and 200 µM quercetin. All PVA fibers were cross-linked with 20% glyoxal (one-pot addition) and 12 h of vapor assisted cross-linking. Images were taken before cell viability assessed at 3 days.

Fibers grown on the PDMS blank appeared to aggregate in clumps and displayed more spherical morphologies rather than the more dispersed and flattened morphologies expected for PC12Adh cells (Figure 28A). Cells also appeared more spherical for those grown alongside PVA fiber formulations (Figure 28C-E). Since these fibers were situated onto PDMS punches within the 96-well plates this is likely a result of the PDMS rather than the fibers. Cell viability results for the experiment indicate this as well (Figure 29).

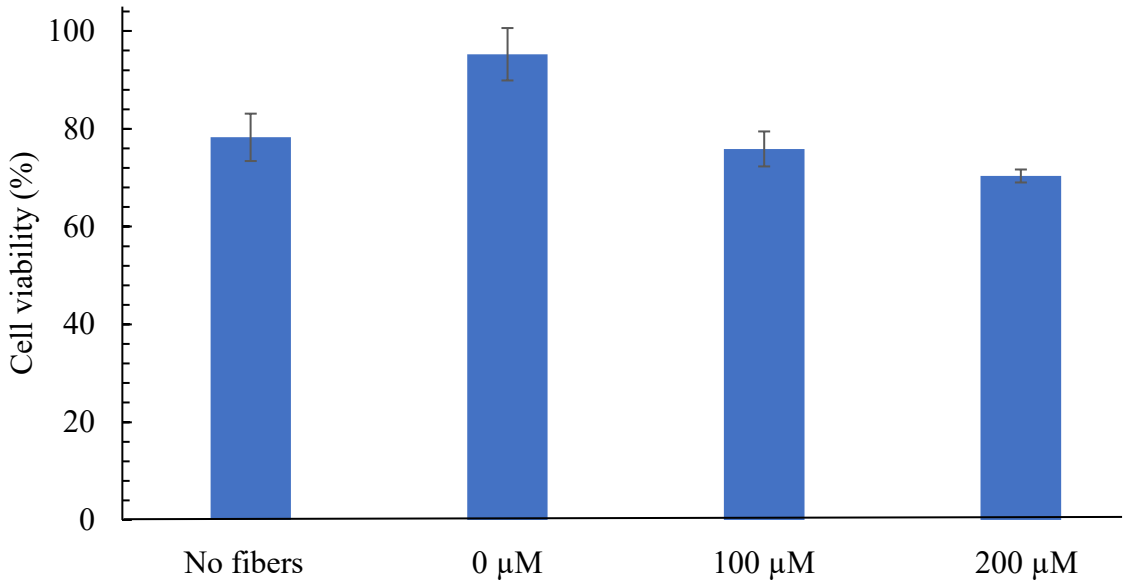


**Figure 29 Cell viability results for PC12Adh cells cultured with PVA fibers.**
Cells grown in (left to right) PDMS blank, PVA fibers with no quercetin (0 µM), PVA fibers with 100 µM quercetin (100 µM), and PVA fibers with 200 µM quercetin (200 µM). All PVA fibers were cross-linked with 20% glyoxal (one-pot addition) and 12 h of vapor assisted cross-linking. Viability data were normalized to cell viability of cells grown in absence of PDMS (well plate only condition from Figure 28) and reported as the average of triplicate trials (N=3). Error bars represent 95% confidence intervals. x

Cell viability results indicated fiber formulations were not cytotoxic toward PC12Adh cells. Cell viability for groups were reported as 78.3 ± 4.8%, 95.3 ± 5.4%, 75.9 ± 3.58%, and 70.4 ± 1.3% for cells grown with PDMS blanks, PVA fibers with no quercetin, PVA fibers with 100 µM quercetin, and PVA fibers with 200 µM quercetin, respectively. Cells grown with PVA

fibers alone indicated better cell viability than cells without fibers, potentially indicating a beneficial interaction between PVA fibers and PC12Adh cells. Cells grown with fibers loaded with quercetin showed comparable cell viability to those grown on PDMS blanks.

# 4. Discussion

As the data has been presented, three main sections of the work came together as a biomaterial development process – material fabrication and characterization, material response, and applicability of the material.

## 4.1 Material Fabrication and Characterization

Novel biomaterial development usually begins with an intended use in mind. This intended use often begins with theory-crafting, where obstacles or shortcomings of the current medical approach are known and documented. For example, improving regeneration and reinnervation following a nerve injury can provide significant improvements to a patient's prognosis, helping to restore motor and nerve function. To combat this problem with a novel biomaterial approach, a biocompatible material (with respect to nerve tissue) is required. Biomaterials science has advanced from materials that act as permanent implants which replace tissues or organs (e.g., metal alloy hip implants) to materials that provide support and are biodegradable/bioresorbable to allow/promote new tissue to replace dead/injured tissue (91). This is also true within the field of nerve repair applications since some of the first materials attempted (with extremely poor results) were not resorbable materials. To begin the material development process, PVA was selected as the polymer of choice for making contact drawn fibers. PVA has been widely used in tissue engineering applications and within various composites for a variety of tissues, including peripheral nerves (79). In addition to forming fibers through contact drawing, PVA is considered a bioabsorbable, which means it (or the degradation products) can be absorbed, metabolized, and/or excreted by the body (92,93). Once PVA was identified as the polymer of choice, glyoxal cross-linking was optimized and quantified. Next,

quercetin was successfully incorporated into fibers, and the effects of modifications to the contact drawing process were explored through fiber formation behavior and fiber diameters.

### 4.1.1 Hybrid cross-linking protocol and quantification

Although the choice of biomaterial is an important starting point, modifications to the design and fabrication process can have drastic effects in improving the success of a material *in vivo*. Cross-linking of biomaterials is one of the most powerful techniques for modifying these properties. Cross-links between polymer chains can affect the physical and chemical properties of a given polymer (94). Furthermore, the number of cross-links (or cross-linking density) can be modified to fine tune various chemical, physical, and mechanical properties. What is most interesting about many of these properties is that they are based on a spectrum. For PVA, the complete absence of cross-linking will cause contact drawn fibers to dissolve within seconds when placed in an aqueous environment, yet the incorporation of cross-linking can allow fibers to exist for more than 10 days in an aqueous environment. Thus, varying the amount of cross-linking could allow for desirable levels of solubility depending on the size of transected nerve, the extent of damage, and the gap between proximal and distal portions. Complex interactions *in vivo* can be hard to dictate and control, being able to selectively modify the biomaterial for an intended use allows for tailoring a polymeric biomaterial to a nerve regeneration application.

The hybrid approach of cross-linking contact drawn fibers through glyoxal addition in a one-pot fashion and through vapor-assisted cross-linking seemed to provide the best results for fibers resisting hydrolytic degradation and dissolution. The hybrid approach allows glyoxal to be incorporated withing the PVA solution to enhance homogeneity of cross-linking and incorporates enhanced surface cross-linking (95). Protecting the surface of the fibers is likely to slow the degradation by limiting the effects of surface erosion which lead to bulk material loss

and increased sites for hydrolytic degradation to proceed (96). Since the contact drawing also proceeds at room temperature, subjecting the fibers to heated glyoxal chambers for an extended period aids the kinetics of this reaction, allowing potentially unreacted glyoxal to react within PVA fibers.

As mentioned, the ability to fine tune a polymeric material through cross-linking is extremely beneficial for controlling specific chemical or mechanical properties of interest to maximize effectiveness. Through quantification via IR (although a semiquantitative technique) the amount of glyoxal incorporated can directly influence the hydroxyl stretching around 3260 $cm^{-1}$. This quantification method was also shown by Zhang *et al*. (77). The decreasing intensity of hydroxyl stretching indicates incorporation of these groups into acetal linkages. The amount of cross-linking will directly affect the solubility and many other characteristics of the biomaterial. A method for determining the degree of cross-linking can help to correlate how these properties are going to be affected and help predict outcomes for the material based on cross-linking density. The hybrid approach also involves glyoxal vapors which could be difficult to quantify without a method that can assess the biomaterial following this modification.

### 4.1.2 Quercetin loading

The major obstacle for regenerative medicine with respect to nerves is a lack of intrinsic regenerative capability (97). Researchers are still exploring the cellular microenvironments present following a nerve injury (peripheral or central) to determine the potential mechanisms at play which cause the stark differences in a regenerating nerve compared to regenerating bone or skin tissue. Potential issues at the cellular level include cell types becoming inactivated due to lack of electrical activity, inability to clear cellular debris (more pronounced for larger axons and in CNS), and over or under expression of signaling pathways involved in proper degeneration

and regeneration of axons (15,98). At the tissue scale, these issues may manifest as misguided growth and scar tissue formation before the gap between proximal and distal ends of a transected nerve can be connected by regenerating axons (25). One way to potentially avoid scar tissue formation is to thwart a potential foreign body response, by preventing apoptotic cell death that can trigger fibrosis (99). This was the intended goal through the addition of quercetin to PVA fibers. Quercetin is a known antioxidant and neuroprotectant when preventing oxidative damage in a nervous tissue environment (74).

Quercetin was successfully loaded and identified in PVA fibers through fluorescence microscopy, indicating a dose-dependent response via fluorescent signal. Quercetin could be loaded at concentrations up to 200 μM prior to contact drawing for incorporation in fibers. Above concentration of 200 μM, fibers did not successfully form, indicating quercetin was affecting the PVA polymer system. It may be that quercetin was interacting with polymer chains as a physical impedance, interrupting normal reptation and polymer flow that allowed fibers to form through contact drawing. It is also possible that the quercetin was reacting chemically with the PVA system, increasing polymer entanglement to the point where polymer chains could no longer freely flow to form stable liquid bridges. Numerous NMR experiments were conducted to try to elucidate the potential chemical modifications to quercetin or PVA, with little success. The first experiments included a preliminary release experiment to identify the product (quercetin or related derivative) released from the fibers. Due to small loading concentrations and relative quantities potentially released from the fibers, the solvent and PVA-related degradation products dominated these NMR spectra, providing no useful information about the nature of the released agent. Experiments were also conducted where excess quercetin was left to react with limiting amounts of PVA. These experiments showed excess quercetin present for the most part, either

indicating the relative amount of a reacted product was not detectable compared to excess quercetin, or potentially that quercetin was not being chemically modified by either glyoxal or PVA.

### 4.1.3 Experimental factors affecting PVA fiber formation and diameters

One of the biggest issues with any biomaterial development project is the trouble with scalability and translating a bench top procedure to bulk processing for widespread use. Exploring the PVA polymer system and understanding fiber formation as a function of PVA concentration, glyoxal cross-linking, and time periods following glyoxal addition provides valuable information to developing standard protocols for bulk production of these materials through contact drawing methods. For the needle-reservoir experiments that produced failure distribution curves, these data can be used to identify the best PVA concentration, glyoxal concentration, and time period allotted for cross-linking to produce fibers. Most of the failure distribution curves showed sharp transitions between failure and success, indicating a narrow range of pull speeds (and corresponding $\tau_{pull}$ values) for which fibers may or may not form. Within these mostly narrow ranges, failing fibers could pose an issue for bulk production of fibers in contact drawing apparatus, where the free ends of a failing liquid bridge could disrupt other liquid bridges and cause large aggregations of material before fibers have a chance to dry. As a result, it is best to avoid these pull speeds and the experimental conditions which may have slower transitions to complete failure events to avoid such phenomena. Since fibers were pulled by hand, pull speeds empirically determined from the fiber formation data were used as guidance for developing the best technique for fabrication.

Experimental conditions with sharp transitions from 0 to 100% failures and pull speeds clear of potential transition points were ideal for bulk fiber pulling. These conditions should

avoid fiber failure events which may lead to fiber tangles, large bead structures, or other undesirable fabrication artifacts. The working conditions developed from this analysis used for making bulk scaffolds for examining the material response included 12.5% PVA, 20% mol effective glyoxal addition, and a cross-linking time of 15 min at ambient temperature prior to pulling fibers. 10.0 and 12.5% PVA showed a much sharper transition from 0 to 100% failure than 15.0 and 17.5% PVA, making both suitable choices for use in contact drawing. 20% glyoxal was the largest loading of glyoxal concentration tested that showed a relatively sharp transition in failure analysis. Finally, the most difficult parameter to assess was the cross-linking duration because the results were largely unexpected. A similar trend to PVA and glyoxal concentration was predicted for increasing duration of cross-linking. Polymer systems and the associated polymer entanglement and free movement of polymers is complex process and is influenced by many factors. A sufficient degree of cross-linking was desired to create a biomaterial fiber resistant to degradation as to persist within the environment of a regenerating nerve for the course of the recovery. As a result, one-pot cross-linking alone with 20% mol effective cross-linking for 15 min may not produce sufficiently cross-linked fibers even though the conditions are beneficial for contact drawing. This is why the hybrid protocol for cross-linking is so valuable, allowing fibers to be subsequently cross-linked after fabrication of fibers and subsequently modifying fibers to become more resistant to degradation whilst not impeding optimal fiber formation conditions.

In addition to playing a large role in the formation of fibers (failure or success), these conditions can also influence fiber diameters. Fiber diameter within the scope of a biomaterial scaffold can influence a variety of interactions including (but not limited to) release of adjuvants (like quercetin), cell interactions, nutrient and bulk material flow, and cell interactions, and

porosity within the scaffold. All of these can have a significant effect on the success of a drug-eluting fibrous scaffold. The addition of quercetin and increased glyoxal additions was observed to cause an increase of average fiber diameters. Almost a two fold increase in fiber diameter was noted when increasing from 5 to 20% glyoxal additions (2.18 ± 0.18 to 3.83 ± 0.51 μm) for fibers pulled in the absence of quercetin. This effect was less dramatic when quercetin was present (2.92 ± 0.29 to 4.03 ± 0.53 μm). Quercetin also showed significant changes to fiber diameters when comparing 5% glyoxal addition groups (+/- quercetin), with fibers increasing from to 2.18 ± 0.18 to 2.92 ± 0.29 μm. This effect became insignificant (with respect to 95% confidence intervals) at increasing concentrations of glyoxal, indicating glyoxal had a stronger effect on fiber diameters than quercetin.

Fiber diameters were notably smaller at the similar pull speeds for experiments testing pull speed effects without the addition of glyoxal or quercetin. One possible explanation is that the initial addition of glyoxal causes a more sterically favourable orientation of neighbouring chains, allowing increased polymer chain movement based on polymer entanglement theory. As the cross-linking increases, this initial increase in polymer movement is now countered by increasing cross-linking density which results in increased effective molecular weight and effectively increases polymer entanglement. Another possible explanation for this difference is variability in ambient temperature and relative humidity within the lab during the days these experiments were conducted. If these two sets of fibers were collected on the same day it would be easier to draw conclusions about the fiber diameters as a function of polymer entanglement and reptation theory. The temperature and humidity have been postulated to affect polymer systems and the molecular interactions governing fiber formation.

## 4.2 Material Response

In addition to developing detailed protocols and for fabrication and characterisation of biomaterials, the intended use demands an iterative design process where the behaviour of the material *in situ* can have researchers revisiting the design process to optimize material characteristics for more desirable responses. For example, placing the contact drawn PVA fibers in an aqueous environment only to discover they have completely dissolved after 4 h requires a more robust cross-linking reaction for a nerve regeneration application. Observing a one-off or complete burst release of quercetin loading may not have the neuroprotective effects required to prevent fibrosis and scar tissue formation following apoptotic events. The novel biomaterial fibers were observed in mimetic models to gain an understanding of how the material is likely to respond *in vivo* as to further develop and optimize the fiber formulation.

### 4.2.1 Degradation of fibrous scaffolds

Preliminary experiments for studying the response of contact drawn fibers included simple rehydration experiments in distilled water to assess solubility and resistance to hydrolysis. The hydrophilic PVA would resolubilize rapidly with no modifications to the PVA pre- or post-contact drawing. Once the cross-linking protocols had been updated to include increased amounts of glyoxal in one pot addition and subsequent vapor assisted cross-linking, fibers were significantly more stable in distilled water (persisting for at least 48 h). At this point, bulk scaffolds were assessed in a more biomimetic aqueous environment – aCSF. The scaffold degradation was assessed in two ways – quantitatively through weight measurements of bulk scaffolds after incubation and qualitatively through analysis of cross-sectional and surface slices of scaffolds. Compared to a similar material, the contact drawn PVA fibers persisted much longer than the electrospun PVA fibers cross-linked in glutaraldehyde bath Alhosseini *et al*. (79).

At 10 days, the materials were essentially completed degraded whereas more than two thirds of the original scaffolds of hybrid cross-linked PVA fibers remained by weight after 10 days in aCSF at 37°C. It is likely that the material will need to persist for longer than 10 days through the course of a nerve regeneration event, although this time period is variable and may require a case-by-case analysis of many variables (e.g., size of gap, diameter of injured nerve) to determine the appropriate degradation rate. Since the degree of cross-linking can be selectively modified for the approach, the degradation rate can also be correspondingly modified.

The qualitative degradation studies include interesting morphological differences observed between contact drawn scaffolds loaded with and without quercetin. Scaffolds without quercetin did not show significant changes to fiber structures, and original fiber morphologies were extremely well retained following 10 days in aCSF. It was noted the fiber diameters seem to decrease noticeably by 10 days, potentially indicating a shrinkage of fibers and loss of material as a result of surface erosion. On the other hand, quercetin scaffolds appeared to lose their original fibrous structure over time, melding or fusing with neighbouring fibers. This was observed as an increasingly latticed and porous network from surface perspectives, with original fiber traces becoming part of the lattice network that appeared increasingly spongiform over time. This was also indicated in the cross-sectional images as observed by larger super-structures of fibers present than seen during fabrication and increasingly large gaps presenting over time in the interior of these scaffolds. This process could be the result of slightly more favourable interactions between fibers loaded with quercetin, encouraging their association with one another over time in the aqueous environment.

There is a significant amount of PVA-based scaffold materials, mostly those fabricated through electrospinning (100). Many scaffolds also represent composite designs – including

additions of chitosan, carbon nanotubes, or other polymers (100,101). These additions usually function to impart increased mechanical or material responses depending on the intended use. Applications within tissue engineering are also well varied, everything from bone to nerve to cardiac tissue engineering approaches are detailed (100–102). There is also a variety of cross-linked PVA scaffolds including those cross-linked with genipin, glutaraldehyde and glyoxal. Electrospun PVA scaffolds cross-linked in glutaraldehyde baths from Alhosseini *et al*. showed almost complete degradation by 10 days (103). On the other hand, PVA scaffolds cross-linked with glutaraldehyde vapours and surface modified with polydopamine (to increase cell adherence) were claimed as insoluble scaffolds (104). The PVA scaffolding presented in this project falls in between these two PVA-based scaffolds, indicating the tunability of dialdehyde cross-linking for intended use.

### 4.2.2 Quercetin release

Whereas glyoxal was incorporated into PVA fibers for increased chemical properties of the material, addition of quercetin was proposed as a route creating a localized neuroprotective effect following surgical intervention of a nerve injury. Although quercetin loading showed promising results, the neuroprotective effects quercetin is known for may not reign true if the small molecule is not released from PVA fibers. To model release, incubations of bulk scaffolds were completed in aCSF at 37°C. Ultraviolet-visible spectroscopy provided a sensitive technique for identifying quercetin release over time in the surrounding aCSF. Quercetin release was reached a maximum release of 56±6% by the tenth day. The slower, sustained released indicates the quercetin is well integrated within the PVA fibers. This may be through significant hydrogen bonding or possibly even covalent linkages which hydrolyze over time to see quercetin released into the surrounding environment.

When compared to other polymeric materials designed for drug release, the quercetin loaded PVA fibers show a similar release profile to various porous scaffolds, electrospun fibers, and nanoparticles loaded with similar small molecules. Cao *et al*. prepared core-shell PVA/silk fibroin nanoparticles via electrospraying to release doxorubicin (anticancer drug) at up to 90% cumulative release by 72 h (105). One of the most similar materials encountered was the core-shell silk/PVA nanofibers which released amoxicillin (antibacterial agent) at 60% cumulative release by 12.5 days (106). Degradation of these fibers were significantly greater than PVA fibers with nearly 75% degradation by 10 days (106). Rather than cross-linking, surface modification via $O_2$ plasma was used to modify material to decrease solubility (106). Another similar material with even more sustained release was the dexamethasone (anti-inflammatory agent) releasing copolymer network of poly(ethylene oxide terephthalate) and poly(butylene terephthalate) (107). Release of drug shows sustained release over a period of 30 days, with burst release noted over the first 24 h and then sustained release approaching 60% cumulative release (107). These examples all use drugs which have very similar structures to quercetin, often an inclusion of various hydroxyl groups and aromatic and heterocyclic rings. These molecules also have relatively low molecular weights (all around or below 500 g/mol), especially in relation to the molecular weights of polymers they are incorporated within.

When compared to polymer materials specific to quercetin loading and release, there exists a variety of potential applications. Quercetin can be incorporated into food packaging films for suitable long-term inhibition of lipid oxidation in food (108). A slower sustained release was noted for quercetin in this instance when compared to the lipid-like molecule tocopherol which is also loaded into the polymer films for food packaging applications (108). Increasingly hydrophilic polymers indicated faster release of quercetin (108). A similar study

utilized various polymer formulations and cross-linking reactions to create both slow- and fast-releasing quercetin tablets for oral administration (109). The release rates in both studies indicated a PVA-based polymer should release quercetin more rapidly than observed in this study. This indicated the quercetin may have been chemically incorporated within the PVA polymer system for slower release or the sustained release was due to the significant chemical modification of PVA through the hybrid glyoxal cross-linking procedure. Comparisons to nanoparticle polymer systems releasing quercetin appear to have some of the most similar release characteristics. When comparing to poly-D,L-lactide nanoparticles loaded with quercetin via sonification and emulsification to reach a release of quercetin around 80-90% by 5 days (110). A burst release toward 60% was noted in the first few hours (110). Another instance of quercetin loading into polylactic acid shows burst release to 30% cumulative quercetin release and then a plateau event following this burst (111). These instances of quercetin release from similar polymer systems indicate our release characteristic does not include the large burst release observed in other quercetin release profiles. The release of quercetin from our PVA fibers indicated modification via glyoxal cross-linking likely played a significant role in controlled release of quercetin from the fibers.

The ideal release profile will depend on the intended use – for a material releasing an anticancer agent, a burst release to bombard cancerous cells may be preferred over a slower, sustained release pattern. On the other hand, a material developed for protecting a regenerating nerve from oxidative damage which could interfere with healthy tissue growth, a slower sustained release is likely beneficial to continue to protect the fragile tissue environment as the axons regrow. The absolute amount of drug released is also an important consideration, since many drugs have a range of concentrations where they are effective, yet above or below this

'sweet spot' can lead to toxicity or ineffective concentrations. Quercetin, although neuroprotective for certain concentrations, exhibits a neurotoxic effect when concentrations exceed the neuroprotective threshold (74). This is also true for the dexamethasone example provided earlier – healthy cell populations show significant increase in proliferation up to 1% dexamethasone loading, with a significant decrease in healthy cell viability at 2% dexamethasone loading . Proceeding to *in vitro* testing for analysis of efficacy will aid the ongoing design process and determine if the release profile indicates efficacy for the intended use.

### 4.2.3 Swelling

An intriguing quality of hydrophilic, polymeric biomaterials is that the materials can experience significant swelling due to water absorption. The hydrophilic nature of PVA allows for dissolution in water to form the viscous polymer paste used for contact drawing. Although the hydrophilicity is decreased to some extent through glyoxal cross-linking, the material is still capable of absorbing water and swelling when placed into an aqueous environment. Since the bulk scaffolds used in the quercetin release studies may have the ability to hold water not only within the fibers but in the porous spaces created in the fibrous scaffold, a wet weight-dry weight analysis may not be suitable for this material. Swelling can still be assessed for individual fibers by observing the change in fiber diameters as a function of time in an aqueous system. Understanding the swelling behaviour of any hydrophilic biomaterial is important since swelling is an indicator of hydrophilicity. The degree of hydrophilicity and how materials like these fibers will swell may influence cellular interactions, porosity, and drug-elution characteristics.

For the swelling of quercetin-free and quercetin-loaded PVA fibers, fibers were incubated in aCSF (37°C) once again to mimic a nerve tissue environment. After three days fiber swelling

appeared to plateau and reach a maximum swelling of 184.5 ± 3.3% and 199.4 ± 3.3% for fibers loaded without (-Qu) and with (+Qu) respectively after seven days. Quercetin itself has a large number of free hydroxyl groups yet the molecule alone is relatively insoluble. Quercetin loading may have increased the hydrophilic character of the fibers through increased hydrogen bonding acceptors or through fabrication artifacts. Without details about the mechanism at play via quercetin loading into PVA fibers it is difficult to determine how the increased hydrophilic character is achieved. This increased hydrophilic character may be part of the explanation for the morphological differences observed for the fiber loaded with and without quercetin.

## 4.3 Material Application

The next progression in the iterative design process of a biomaterial is testing the material in an *in vitro* context prior to exploration in an *in vivo* model. Any undesirable effects at this stage will also require further inspection or modifications to existing fabrication and development to fit the criteria for intended use. If the material appears to invoke a cytotoxic response, it may be required to deactivate potentially harmful or reactive species during material fabrication. In the case of the novel PVA fibers, a different approach for cross-linking, small-molecule loading, or biomaterial selection may be required if biological assays indicate deleterious responses *in vivo* or *in vitro*.

### 4.3.1 Efficacy *in vitro* as neuroprotective biomaterial

The first biological assay required for most biomaterial developments includes some type of cell-based assay for general cytotoxicity testing. For this work, the model cell line was chosen as PC12Adh cells to determine potential cytotoxicity and material. If the material causes an undesired response (e.g., induces cell death in otherwise healthy cell culture), potential solutions will need to be devised to solve this issue. Residual aldehydes were the main concern based on

the proposed fabrication of PVA fibers, which can be easily removed and inactivated through washing with glycine, since the free aldehydes will reaction with the free amines to form a Schiff base. Cell viability was greater than 70% for all treatment groups in preliminary cell viability screening, indicating promising deactivation of any free aldehydes from the PVA fibers. Since viability was normalized to a condition in the absence of PDMS, the reduced cell viability in most cases was likely the result of the PDMS present in the well plates. If normalized to the condition with PDMS plugs and no fibers, all cell viability results for cultures containing fibers would be greater than 90% - extremely promising results for the first experiments with cells grown alongside the PVA fibers.

The next assay planned for the PVA fibers is a more complex assay, which includes the use of 6-OHDA to potentially induce apoptosis. Quercetin is a known neuroprotectant which can prevent cell damage through sequestration of reactive oxygen species produced by 6-OHDA (73,74,112). This assay will be used to screen the neuroprotective efficacy of PVA fibers loaded with various amounts of quercetin.

### 4.3.2 Translation to use in NGC for *in vivo* explorations

One of the major issues with regenerating nerves is misguided growth. The nerve guidance conduit has been proposed as a solution to combat misguided growth (26,31,113). These conduits have emerged as a potential alternative to the traditional nerve repair strategies and have been successful in both management and functional recovery of peripheral nerve injuries. Nerve conduits are a tissue-engineering based approach to traditional surgical interventions, where a biomaterial-based wrap is sutured on the proximal and distal ends of the damaged nerves. The biomaterial conduit functions to guide the proximal shoots toward the Büngner bands (Figure 30).

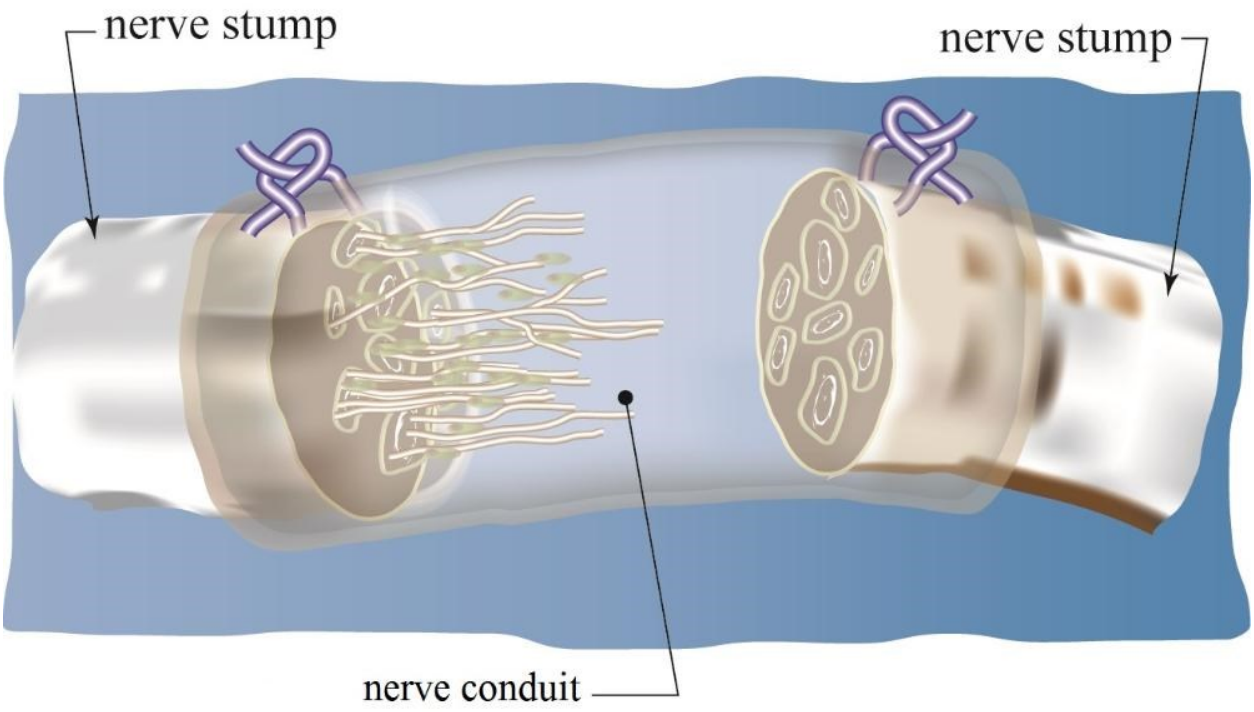


**Figure 30 A nerve guidance conduit guides the growing shoots of the proximal end of a nerve injury toward the Büngner bands of the distal stump** (28)**.**

The fabrication of NGCs and the potential design strategies can also play a large role in the clinical outcomes. Many of the potential design strategies involve variations in the interior structure of the nerve guidance conduit. Some of the most popular approaches have been hydrogel loading and nanofiber loading in the hopes of these material providing guidance cues for regenerating axons. Other strategies that are more conceptual or in the early stages of research include magnetically aligned fibril loaded, micro-grooved luminal deign, intraluminal guidance, luminal surface functionalization, unidirectional freeze drying, shell-core filament loaded, microfilament loaded, and rolled up pattern loaded (16).

In addition to various design and fabrication modifications, the NGCs can be loaded with small molecules, various neurotrophic factors, and even different extracellular matrix proteins. These ECM components provide natural cellular attachment cues to guide regenerating shoots of

the proximal end of a nerve lesion. These cells express specific integrins ($\alpha_1\beta_1$, $\alpha_2\beta_1$, $\alpha_6\beta_1$, $\alpha_6\beta_4$, $\alpha_5\beta_1$, $\alpha V\beta_3$) that bind to ECM proteins to promote myelination through their interaction (114,115). A variety of ECM components have been shown to play a major role in nerve guidance and attachment, including fibronectin, laminin, collagen, and vitronectin (113,114,116). Furthermore, some of these ECM proteins have exhibited synergistic effects, specifically fibronectin and laminin (115). Various synergies have also been observed for the interaction of various neurotrophic factors with ECM proteins.

With all of this in mind, imagine a multifunctional nerve guidance conduit that has been purposed to combat some of the main issues surrounding nerve tissue regeneration. The nerve conduit itself creates a localized environment for promoting healing and proper guidance of regenerating axons. The inner space of the nerve guidance conduit has been fashioned to further enhance nerve guidance using specific binding cues and ECM matrix proteins either using repurposed ECM or ECM-loaded biomaterial. In addition to this, the nerve guide incorporated with the novel contact drawn, glyoxal cross-linked PVA fibers which serve as a neuroprotectant within the nerve guide, on the surface of the nerve guide or both. The slowly quercetin loaded PVA fibers help to prevent apoptotic cell death and limit the foreign body response to prevent inhibiting of regeneration through minimizing scar tissue formation. There are many variables to explore and test when it comes to nerve guidance conduits, and finding the ideal design, fabrication, and biomaterial will be a challenge. The NGC can also be enhanced with gene and cell transplant therapies, physical therapy, electrical stimulation, and other types of adjuvant treatments. It is likely that the ideal solution will be a combination of a variety of these techniques and treatments, with the contact drawn PVA fibers with potential neuroprotective efficacy as one of the constituents.

# 5. Conclusions

## 5.1 Significance and Future Directions

With respect to this work, the main avenue for further exploration involves continuing and completing cell-based experiments to screen fiber formulations for neuroprotective efficacy. As mentioned previously, the translation to *in vivo* studies following promising results from cell-based assays would also be a logical progression for this work. One of the biggest things to remember with the development of a biomaterial like this is the iterative design process that continues throughout the project. This feedback continues to modify design inputs even after clinical trials and successful implementation within the context of a nerve guidance conduit.

This material has promise for use as a neuroprotectant through the addition of quercetin; however, the work has provided a template through the development of the PVA system and glyoxal cross-linking. Within the scope of intended use, the proposed PVA fibers could represent one part of a multifunctional nerve guide. The quercetin incorporation allows for protection from adverse events and promoting healing following a nerve injury. These PVA fibers can be modified with other adjuvants and small molecules, or even incorporated with various ECM proteins to allow cells to directly adhere with proper topological guidance cues and help guide regenerating axons. This is analogous to using dextran to template collagen fibrils for guiding cell growth. Since the major issues surrounding failed reinnervation for nerve injuries are misguided growth, the multifunctional nerve guide should look to promote guidance of regenerating axons at the tissue, cellular, and macromolecular levels. Aligned fibers could be made (with PVA or another similar polymer) to provide guidance channels within the nerve guidance conduit to guide regenerating axons toward the distal stump (tissue level guidance).

The loading or surface modification of these fibers would promote guidance and cellular adhesion through proper topographical guidance cues (cell level guidance). Finally, other small molecules or growth factors could be loaded into a PVA polymer fiber or directly into aligned fibers to promote guidance cues and proper signaling pathways at a macromolecular level. The PVA polymer system may be a possible template for the pursuit of other pieces of the composite, multifunctional NGC.

In addition to the intended use proposed for this project, it should be noted an antioxidant eluting biomaterial fiber can have a variety of potential applications, especially within the field of regenerative medicine. The fine-tuning of cross-linking allows the material to be specifically fabricated for other tissue engineering approaches or more generic applications. In addition to acting as a template for various modifications to increase efficacy in a nervous tissue engineering approach, these PVA fibers could easily translated for other tissues of interest, wound dressing materials, bioresorbable sutures. With the proper groundwork and iterative design process the fundamental characterization of the PVA polymer system with respect to contact drawing allows for bulk fiber fabrication for a multitude of potential uses.

## 5.2 Future Perspectives in Nerve Tissue Engineering

Although there are many facets and dimensions associated with neural regeneration, a main theme for future studies appears throughout much of the literature – the nerve guidance conduit. It is likely that this will be the focus of neural tissue engineering and will eventually be implemented in place of the nerve autograft, due to ease of availability and simplicity of implementation. Advances in other scientific fields including (but not limited to) biomaterials science, cell and molecular biology, polymer science, biochemistry, chemical biology, pathophysiology, and molecular neuroanatomy will provide insight for tissue engineering

approaches of peripheral nerves. The breadth and depth of knowledge required for biomaterials scientists and those working in regenerative medicine is incredible – to fully comprehend a biomaterial approach to tissue engineering, one must be a chemist, biologist, engineer, healthcare professional, biochemist, and cell biologist. Thus, collaboration among fields and specialties and those with experiences in these fields present great candidates for working toward a real solution for nerve tissue engineering.

Peripheral nerves present a much easier target than the central nervous system, and it is likely that a clinically relevant technique will be in place for peripheral nerves before any major breakthroughs can be made in central nervous system tissue engineering. As for the central nervous system, spinal cord injuries represent an extremely challenging yet rewarding task. The benefits of a breakthrough in central nervous system tissue engineering include partial or complete functional recovery for those suffering from para- and tetraplegia. There are many challenges associated with CNS tissue engineering, primarily the delayed cellular responses surrounding Wallerian degeneration and the rate of clearing for myelin and other cellular debris. The role of Schwann cells in nerve regeneration is slowly beginning to be unraveled, and their absence in the CNS is well noted – oligodendrocytes cannot compete with their PNS counterparts. As a result, gene therapies and cell transplants may be required for proper CNS treatment, due to a lackluster intrinsic regenerative capability. Furthermore, the proper tissue engineering approach may include gene therapy and other interventions to increase the rate of Wallerian degeneration and myelin clearance in the CNS, thus preparing the lesion for further surgical intervention . With improvements in surgical techniques, the clinical outcome of a spinal cord injury has been improved to some degree of paralysis. Until WWII, this type of injury was almost always fatal (117). Through the advancement of modern tissue engineering approaches,

the clinical outcome for these individuals may be continuously improved to the point of complete functional recovery.

## Works Cited


1. Devivo MJ. Epidemiology of traumatic spinal cord injury: Trends and future implications. In: Spinal Cord. Nature Publishing Group; 2012. p. 365–72.

2. Noonan VK, Fingas M, Farry A, Baxter D, Singh A, Fehlings MG, et al. Incidence and prevalence of spinal cord injury in Canada: A national perspective [Internet]. Vol. 38, Neuroepidemiology. 2012 [cited 2020 Apr 11]. p. 219–26. Available from: http://www.ncbi.nlm.nih.gov/pubmed/22555590

3. Chronic Diseases and Injuries in Canada - Canada.ca [Internet]. [cited 2020 Apr 11]. Available from: https://www.canada.ca/en/public-health/services/reports-publications/health-promotion-chronic-disease-prevention-canada-research-policy-practice/vol-33-no-3-2013/economic-burden-traumatic-spinal-cord-injury-canada.html

4. Martyn CN, Hughes RAC. Epidemiology of peripheral neuropathy. Vol. 62, Journal of Neurology Neurosurgery and Psychiatry. BMJ Publishing Group; 1997. p. 310–8.

5. López-Cebral R, Silva-Correia J, Reis RL, Silva TH, Oliveira JM. Peripheral Nerve Injury: Current Challenges, Conventional Treatment Approaches, and New Trends in Biomaterials-Based Regenerative Strategies. Vol. 3, ACS Biomaterials Science and Engineering. 2017.

6. Strong OS, Elwyn A. Human neuroanatomy (2nd ed.). Human neuroanatomy (2nd ed.). Williams & Wilkins Co; 2011.

7. Andreatta RD. Neuroscience Fundamentals for Communication Sciences and Disorders [Internet]. Plural Publishing Inc. 2018 [cited 2020 Apr 16]. Available from: https://books.google.ca/books?hl=en&lr=&id=z5SFDwAAQBAJ&oi=fnd&pg=PA85&dq=understanding+the+neuroanatomy+and+division+of+the+PNS&ots=wrZ91g9TY-&sig=W4iXBHktzs1WtIzKrBKmIlKsG1E#v=onepage&q=understanding the neuroanatomy and division of the PNS&f=false

8. Branco T, Häusser M. The single dendritic branch as a fundamental functional unit in the nervous system. Vol. 20, Current Opinion in Neurobiology. Elsevier Current Trends; 2010. p. 494–502.

9. Jessen KR. Glial cells. Vol. 36, International Journal of Biochemistry and Cell Biology. Elsevier Ltd; 2004. p. 1861–7.

10. Chhabra A, Ahlawat S, Belzberg A, Andreseik G. Peripheral nerve injury grading simplified on MR neurography: As referenced to Seddon and Sunderland classifications. Indian J Radiol Imaging. 2014;24(3):217–24.

11. Sunderland S. Classification of Peripheral Nerve Injuries Producing Loss of Function. Brain [Internet]. 1951 [cited 2020 Apr 16];74(4):491–516. Available from: https://academic.oup.com/brain/article-abstract/74/4/491/323666

12. Seddon HJ. Peripheral Nerve Injuries. Glasgow Med J [Internet]. 1943 [cited 2020 Apr 16];61–75. Available from: https://www.ncbi.nlm.nih.gov/pmc/articles/PMC5950788/

13. Zayed R. MR Neurography: an emerging modality in the evaluation of the lumbosacral plexus and sciatic lesions. 2019 [cited 2021 Jul 16]; Available from: https://www.researchgate.net/profile/Rola-Zayed/publication/332329958_MR_neurograohy_an_emerging_modality_in_the_evaluation_of_lumbosacral_plexus_and_sciatic_lesions/links/5cae1d864585156cd78e1162/MR-neurograohy-an-emerging-modality-in-the-evaluation-of-lumbosacral-plexus-and-sciatic-lesions.pdf

14. Roberts TT, Leonard GR, Cepela DJ. Classifications In Brief: American Spinal Injury Association (ASIA) Impairment Scale. Clin Orthop Relat Res [Internet]. 2017 May 1 [cited 2020 Jun 23];475(5):1499–504. Available from: https://www.ncbi.nlm.nih.gov/pmc/articles/PMC5384910/

15. Avellino AM, Hart D, Dailey AT, Mackinnon M, Ellegala D, Kliot M. Differential macrophage responses in the peripheral and central nervous system during wallerian degeneration of axons. Exp Neurol. 1995;136(2):183–98.

16. Faroni A, Mobasseri SA, Kingham PJ, Reid AJ. Peripheral nerve regeneration: Experimental strategies and future perspectives. Vol. 82, Advanced Drug Delivery Reviews. Elsevier; 2015. p. 160–7.

17. Faroni A, Mobasseri SA, Kingham PJ, Reid AJ. Peripheral nerve regeneration: Experimental strategies and future perspectives. Vol. 82, Advanced Drug Delivery Reviews. 2015.

18. Vargas ME, Barres BA. Why Is Wallerian Degeneration in the CNS So Slow? Annu Rev Neurosci [Internet]. 2007 Jul 28 [cited 2020 Apr 16];30(1):153–79. Available from: http://www.annualreviews.org/doi/10.1146/annurev.neuro.30.051606.094354

19. Palin K, Cunningham C, Forse P, Perry VH, Platt N. Systemic inflammation switches the inflammatory cytokine profile in CNS Wallerian degeneration. Neurobiol Dis. 2008 Apr 1;30(1):19–29.

20. Hopkins TM, Little KJ, Vennemeyer JJ, Triozzi JL, Turgeon MK, Heilman AM, et al. Short and long gap peripheral nerve repair with magnesium metal filaments. J Biomed Mater Res - Part A. 2017 Nov 1;105(11):3148–58.

21. Ray WZ, Mackinnon SE. Management of nerve gaps: Autografts, allografts, nerve transfers, and end-to-side neurorrhaphy. Vol. 223, Experimental Neurology. NIH Public Access; 2010. p. 77–85.

22. Ko CC, Tu TH, Wu JC, Huang WC, Tsai YA, Huang SF, et al. Functional improvement in chronic human spinal cord injury: Four years after acidic fibroblast growth factor. Sci Rep. 2018 Dec 1;8(1):12691–12691.

23. Curtis E, Martin JR, Gabel B, Sidhu N, Rzesiewicz TK, Mandeville R, et al. A First-in-Human, Phase I Study of Neural Stem Cell Transplantation for Chronic Spinal Cord Injury. Cell Stem Cell [Internet]. 2018 Jun 1 [cited 2020 Apr 13];22(6):941-950.e6. Available from: http://www.ncbi.nlm.nih.gov/pubmed/29859175

24. Tajdaran K, Chan K, Gordon T, Borschel GH. Matrices, scaffolds, and carriers for protein and molecule delivery in peripheral nerve regeneration. Vol. 319, Experimental Neurology. Academic Press Inc.; 2019. p. 112817.

25. Chiono V, Tonda-Turo C. Trends in the design of nerve guidance channels in peripheral nerve tissue engineering. Vol. 131, Progress in Neurobiology. Elsevier Ltd; 2015. p. 87–104.

26. Daly W, Yao L, Zeugolis D, Windebank A, Pandit A. A biomaterials approach to peripheral nerve regeneration: Bridging the peripheral nerve gap and enhancing functional recovery. Vol. 9, Journal of the Royal Society Interface. Royal Society; 2012. p. 202–21.

27. Sarker M, Naghieh S, McInnes AD, Schreyer DJ, Chen X. Strategic Design and Fabrication of Nerve Guidance Conduits for Peripheral Nerve Regeneration. Vol. 13, Biotechnology Journal. Wiley-VCH Verlag; 2018.

28. Nguyen DY, Tran RT, Costanzo F, Yang J. Tissue-Engineered Peripheral Nerve Guide Fabrication Techniques. In: Nerves and Nerve Injuries. Elsevier; 2015. p. 971–92.

29. Gu X, Ding F, Williams DF. Neural tissue engineering options for peripheral nerve regeneration. Biomaterials. 2014 Aug 1;35(24):6143–56.

30. Patel NP, Lyon KA, Huang JH. An update-tissue engineered nerve grafts for the repair of peripheral nerve injuries. Vol. 13, Neural Regeneration Research. Medknow Publications; 2018. p. 764–74.

31. Sarker MD, Naghieh S, McInnes AD, Schreyer DJ, Chen X. Regeneration of peripheral nerves by nerve guidance conduits: Influence of design, biopolymers, cells, growth factors, and physical stimuli. Vol. 171, Progress in Neurobiology. Elsevier Ltd; 2018. p. 125–50.

32. Jesion I, Skibniewski M, Skibniewska E, Strupiński W, Szulc-Dąbrowska L, Krajewska A, et al. Biotechnology & Biotechnological Equipment Graphene and carbon nanocompounds: biofunctionalization and applications in tissue engineering. Taylor Fr [Internet]. 2015 [cited 2021 Jun 9];29(3):415–22. Available from: http://dx.doi.org/10.1080/13102818.2015.1009726

33. Mouriñ V, Cattalini JP, Boccaccini AR. Metallic ions as therapeutic agents in tissue engineering scaffolds: an overview of their biological applications and strategies for new developments. royalsocietypublishing.org [Internet]. 2012 Mar 7 [cited 2021 Jun 9];9(68):401–19. Available from: https://royalsocietypublishing.org/

34. Kato-Negishi M, Onoe H, Ito A, Takeuchi S. Rod-Shaped Neural Units for Aligned 3D Neural Network Connection. Adv Healthc Mater [Internet]. 2017 Aug 9 [cited 2020 Apr 10];6(15):1700143. Available from: http://doi.wiley.com/10.1002/adhm.201700143

35. Antman-Passig M, Shefi O. Remote Magnetic Orientation of 3D Collagen Hydrogels for Directed Neuronal Regeneration. Nano Lett. 2016 Apr 13;16(4):2567–73.

36. Anderson MA, O'Shea TM, Burda JE, Ao Y, Barlatey SL, Bernstein AM, et al. Required growth facilitators propel axon regeneration across complete spinal cord injury. Nature. 2018;561(7723):396–400.

37. Du J, Liu J, Yao S, Mao H, Peng J, Sun X, et al. Prompt peripheral nerve regeneration induced by a hierarchically aligned fibrin nanofiber hydrogel. Acta Biomater. 2017 Jun 1;55:296–309.

38. Hua Y, Gan Y, Zhang Y, Ouyang B, Tu B, Zhang C, et al. Adaptable to Mechanically Stable Hydrogels Based on the Dynamic Covalent Cross-Linking of Thiol-Aldehyde Addition. ACS Macro Lett. 2019 Mar 19;8(3):310–4.

39. Papadimitriou L, Manganas P, Ranella A, Bio ES-MT, 2020 undefined. Biofabrication for neural tissue engineering applications. Elsevier [Internet]. [cited 2021 Jun 9]; Available from: https://www.sciencedirect.com/science/article/pii/S259000642030003X

40. Huang C, Ouyang Y, Niu H, He N, Ke Q, Jin X, et al. Nerve guidance conduits from aligned nanofibers: Improvement of nerve regeneration through longitudinal nanogrooves on a fiber surface. ACS Appl Mater Interfaces [Internet]. 2015 Apr 8 [cited 2021 Jun 22];7(13):7189–96. Available from: www.acsami.org

41. Wu T, Li D, Wang Y, Sun B, Li D, Morsi Y, et al. Laminin-coated nerve guidance conduits based on poly(l-lactide-: Co-glycolide) fibers and yarns for promoting Schwann cells' proliferation and migration. J Mater Chem B [Internet]. 2017 May 3 [cited 2021 Jun 22];5(17):3186–94. Available from: https://pubs.rsc.org/en/content/articlehtml/2017/tb/c6tb03330j

42. Hou Y, Wang X, Zhang Z, Luo J, Cai Z, Wang Y, et al. Repairing Transected Peripheral Nerve Using a Biomimetic Nerve Guidance Conduit Containing Intraluminal Sponge Fillers. Adv Healthc Mater [Internet]. 2019 Nov 1 [cited 2021 Jun 21];8(21). Available from: https://pubmed.ncbi.nlm.nih.gov/31583854/

43. Jeffries EM, Wang Y. Incorporation of parallel electrospun fibers for improved topographical guidance in 3D nerve guides. Biofabrication [Internet]. 2013 Sep 14 [cited 2021 Jun 22];5(3):35015–23. Available from: https://iopscience.iop.org/article/10.1088/1758-5082/5/3/035015

44. Dinis TM, Vidal G, Jose RR, Vigneron P, Bresson D, Fitzpatrick V, et al. Complementary effects of two growth factors in multifunctionalized silk nanofibers for nerve reconstruction. PLoS One [Internet]. 2014 [cited 2021 Jun 22];9(10):109770. Available from: www.plosone.org

45. Design Control Guidance For Medical Device Manufacturers | FDA [Internet]. [cited 2020 Jun 18]. Available from: https://www.fda.gov/regulatory-information/search-fda-guidance-documents/design-control-guidance-medical-device-manufacturers

46. BV Polyganics. Neurolac nerve guide - 510(k) summary. Vol. 510. 2011.

47. Integra LifeSciences Corporation. Neurogen Nerve Guide - 510(k) summary. 2001.

48. Kehoe S, Zhang XF, Boyd D. FDA approved guidance conduits and wraps for peripheral nerve injury: A review of materials and efficacy. Vol. 43, Injury. Elsevier; 2012. p. 553–72.

49. Perez-Puyana V, Jiménez-Rosado M, Romero A, Guerrero A. Polymer-based scaffolds for soft-tissue engineering [Internet]. Vol. 12, Polymers. MDPI AG; 2020 [cited 2021 Jun 9]. p. 1566. Available from: www.mdpi.com/journal/polymers

50. Rahmati M, Mills DK, Urbanska AM, Saeb MR, Venugopal JR, Ramakrishna S, et al. Electrospinning for tissue engineering applications. Vol. 117, Progress in Materials Science. Elsevier Ltd; 2021. p. 100721.

51. Hsu CC, Serio A, Amdursky N, Besnard C, Stevens MM. Fabrication of Hemin-Doped Serum Albumin-Based Fibrous Scaffolds for Neural Tissue Engineering Applications. ACS Appl Mater Interfaces [Internet]. 2018 Feb 14 [cited 2021 Jun 9];10(6):5305–17. Available from: www.acsami.org

52. Girão AF, Sousa J, Domínguez-Bajo A, González-Mayorga A, Bdikin I, Pujades-Otero E, et al. 3D Reduced Graphene Oxide Scaffolds with a Combinatorial Fibrous-Porous Architecture for Neural Tissue Engineering. ACS Appl Mater Interfaces [Internet]. 2020 Sep 2 [cited 2021 Jun 9];12(35):38962–75. Available from: https://dx.doi.org/10.1021/acsami.0c10599

53. Li Y, Liao C, Tjong SC. Electrospun polyvinylidene fluoride-based fibrous scaffolds with piezoelectric characteristics for bone and neural tissue engineering [Internet]. Vol. 9, Nanomaterials. MDPI AG; 2019 [cited 2021 Jun 9]. p. 952. Available from: www.mdpi.com/journal/nanomaterials

54. Zhang B, Yan X, He HW, Yu M, Ning X, Long YZ. Solvent-free electrospinning: Opportunities and challenges [Internet]. Vol. 8, Polymer Chemistry. Royal Society of Chemistry; 2017 [cited 2021 Jun 22]. p. 333–52. Available from: www.rsc.org/polymers

55. Council NR. High Performance Synthetic Fibers for Composites [Internet]. 1992 [cited 2021 Jun 22]. Available from: https://books.google.com/books?hl=en&lr=&id=YBNZUJVGQToC&oi=fnd&pg=PR1&dq=High+Performance+Synthetic+Fibers+for+Composites+(1992)+Chapter:+3+Fiber-Forming+Processes:+Current+and+Potential+Methods&ots=TSXp2nM9gl&sig=Q2-749onWUBwe5LHW2T9qM2RP8w

56. Ye, Kuang, You, Morsi, Mo. Electrospun Nanofibers for Tissue Engineering with Drug Loading and Release. Pharmaceutics [Internet]. 2019 Apr 15 [cited 2020 Mar 4];11(4):182. Available from: https://www.mdpi.com/1999-4923/11/4/182

57. De Gennes PG. Reptation of a polymer chain in the presence of fixed obstacles. J Chem Phys [Internet]. 1971 Dec 9 [cited 2021 Jun 9];55(2):572–9. Available from: https://doi.org/10.1063/1.1699180

58. Qin J, Milner ST. Tubes, topology, and polymer entanglement. Macromolecules. 2014 Sep 9;47(17):6077–85.

59. McLeish TCB. Tube theory of entangled polymer dynamics. Adv Phys [Internet]. 2002 Sep [cited 2021 Jun 9];51(6):1379–527. Available from: https://www.tandfonline.com/action/journalInformation?journalCode=tadp20

60. Colby RH, Rubinstein M, Viovy JL. Chain Entanglement in Polymer Melts and Solutions. Macromolecules [Internet]. 1992 Mar 1 [cited 2021 Jun 9];25(2):996–8. Available from: https://pubs.acs.org/sharingguidelines

61. Lv Y, Lin Y, Chen F, Li F, Shangguan Y, Zheng Q. Chain entanglement and molecular dynamics of solution-cast PMMA/SMA blend films affected by hydrogen bonding between casting solvents and polymer chains. RSC Adv [Internet]. 2015 May 19 [cited 2021 Jun 9];5(56):44800–11. Available from: www.rsc.org/advances

62. Chowdhry G, Chang YM, Frampton JP, Kreplak L. Polymer entanglement drives formation of fibers from stable liquid bridges of highly viscous dextran solutions. Soft Matter [Internet]. 2021 Feb 21 [cited 2021 Jun 9];17(7):1873–80. Available from: https://pubs.rsc.org/en/content/articlehtml/2021/sm/d0sm01550d

63. Liu GY, Agarwal R, Ko KR, Ruthven M, Sarhan HT, Frampton JP. Templated Assembly of Collagen Fibers Directs Cell Growth in 2D and 3D. Sci Rep [Internet]. 2017 Dec 1 [cited 2021 Jun 22];7(1). Available from: /pmc/articles/PMC5575125/

64. de Ruiter GCW, Malessy MJA, Yaszemski MJ, Windebank AJ, Spinner RJ. Designing ideal conduits for peripheral nerve repair. Vol. 26, Neurosurgical Focus. NIH Public Access; 2009. p. 1–9.

65. de Luca AC, Lacour SP, Raffoul W, di Summa PG. Extracellular matrix components in peripheral nerve repair: How to affect neural cellular response and nerve regeneration? Neural Regen Res. 2014 Nov 15;9(22):1943–8.

66. Wang AG, Yen MY, Hsu WM, Fann MJ. Induction of vitronectin and integrin alphav in the retina after optic nerve injury. Mol Vis. 2006;12:76–84.

67. Konofaos P, Ver Halen JP. Nerve repair by means of tubulization: Past, present, future. J Reconstr Microsurg. 2013;29(3):149–63.

68. Du J, Liu J, Yao S, Mao H, Peng J, Sun X, et al. Prompt peripheral nerve regeneration induced by a hierarchically aligned fibrin nanofiber hydrogel. Acta Biomater. 2017;55.

69. Flora G, Joseph G, Patel S, Singh A, Bleicher D, Barakat DJ, et al. Combining neurotrophin-transduced schwann cells and rolipram to promote functional recovery from subacute spinal cord injury. Cell Transplant [Internet]. 2013 Dec 1 [cited 2020 Apr 16];22(12):2203–17. Available from: http://www.ncbi.nlm.nih.gov/pubmed/23146351

70. Guercio JR, Kralic JE, Marrotte EJ, James ML. Spinal cord injury pharmacotherapy: Current research & development and competitive commercial landscape as of 2015. J Spinal Cord Med [Internet]. 2019 Jan 2 [cited 2020 Jun 18];42(1):102–22. Available from: https://www.tandfonline.com/doi/full/10.1080/10790268.2018.1439803

71. Nie S, Xu Y, Chen G, Ma K, Han C, Guo Z, et al. Small molecule TrkB agonist deoxygedunin protects nigrostriatal dopaminergic neurons from 6-OHDA and MPTP induced neurotoxicity in rodents. Neuropharmacology. 2015 Aug 22;99:448–58.

72. Jang SW, Liu X, Chan CB, France SA, Sayeed I, Tang W, et al. Deoxygedunin, a natural product with potent neurotrophic activity in mice. PLoS One [Internet]. 2010 [cited 2021 Jun 9];5(7). Available from: https://pubmed.ncbi.nlm.nih.gov/20644624/

73. Zhang ZJ, Cheang LCV, Wang MW, Lee SMY. Quercetin exerts a neuroprotective effect through inhibition of the iNOS/NO system and pro-inflammation gene expression in PC12 cells and in zebrafish. Int J Mol Med [Internet]. 2011 Feb 1 [cited 2021 Jan 25];27(2):195–203. Available from: http://www.spandidos-publications.com/10.3892/ijmm.2010.571/abstract

74. Ossola B, Kääriäinen T, Raasmaja A, Toxicology PM-, 2008 undefined. Time-dependent protective and harmful effects of quercetin on 6-OHDA-induced toxicity in neuronal SH-SY5Y cells. Elsevier [Internet]. [cited 2021 Jun 9]; Available from: https://www.sciencedirect.com/science/article/pii/S0300483X08001662

75. Wright A, Miller C, Williams M, research GA-B, 2008 undefined. Microglial activation is not prevented by tacrolimus but dopamine neuron damage is reduced in a rat model of Parkinson's disease progression. Elsevier [Internet]. [cited 2021 Jun 9]; Available from: https://www.sciencedirect.com/science/article/pii/S0006899308009384

76. Kääriäinen T, Piltonen M, Ossola B, research HK-B, 2008 undefined. Lack of robust protective effect of quercetin in two types of 6-hydroxydopamine-induced parkinsonian models in rats and dopaminergic cell cultures. Elsevier [Internet]. [cited 2021 Jun 9]; Available from: https://www.sciencedirect.com/science/article/pii/S0006899308003041

77. Zhang Y, Zhu PC, Edgren D. Crosslinking reaction of poly(vinyl alcohol) with glyoxal. J Polym Res. 2010 Sep;17(5):725–30.

78. Nagasawa HT, Valentekovich RJ, Nagasawa SG, Nagasawa RH. Sequestration and Elimination of Toxic Aldehydes. Chem Res Toxicol [Internet]. 2020 Mar 16 [cited 2021 Jun 9];33(3):764–8. Available from: https://dx.doi.org/10.1021/acs.chemrestox.9b00373

79. Naghavi Alhosseini S, Moztarzadeh F, Kargozar S, Dodel M, Tahriri M. Development of Polyvinyl Alcohol Fibrous Biodegradable Scaffolds for Nerve Tissue Engineering Applications: *In Vitro* Study. Int J Polym Mater Polym Biomater [Internet]. 2015 Sep 22 [cited 2020 Mar 24];64(9):474–80. Available from: http://www.tandfonline.com/doi/full/10.1080/00914037.2014.977893

80. Nifli AP, Theodoropoulos PA, Munier S, Castagnino C, Roussakis E, Katerinopoulos HE, et al. Quercetin exhibits a specific fluorescence in cellular milieu: A valuable tool for the study of its intracellular distribution. J Agric Food Chem. 2007 Apr 18;55(8):2873–8.

81. Mishra B, Barik A, Priyadarsini I, Mohan H. Fluorescence spectroscopic studies on binding of a flavonoid antioxidant quercetin to serum albumins [Internet]. Vol. 117, J. Chem. Sci. 2005 [cited 2021 Jun 9]. Available from: https://link.springer.com/content/pdf/10.1007/BF02708293.pdf

82. Hartig SM. Basic image analysis and manipulation in imageJ. Curr Protoc Mol Biol. 2013;(SUPPL.102).

83. Nichele L, Persichetti V, Lucidi M, Continuum GC-O, 2020 undefined. Quantitative evaluation of ImageJ thresholding algorithms for microbial cell counting. osapublishing.org [Internet]. [cited 2021 Jun 9]; Available from: https://www.osapublishing.org/abstract.cfm?uri=osac-3-6-1417

84. Nunn S, Nishikida K. Advanced ATR Correction Algorithm.

85. ACSF (Artificial cerebrospinal fluid). Cold Spring Harb Protoc [Internet]. 2007 Feb 1 [cited 2021 Jun 21];2007(2):pdb.rec10804-pdb.rec10804. Available from: http://cshprotocols.cshlp.org/content/2007/2/pdb.rec10804.full

86. Sadhukhan P, Kundu M, Chatterjee S, Ghosh N, Manna P, Das J, et al. Targeted delivery of quercetin via pH-responsive zinc oxide nanoparticles for breast cancer therapy. Mater Sci Eng C. 2019 Jul 1;100:129–40.

87. Rudra R, Kumar V, Kundu PP. Acid catalysed cross-linking of poly vinyl alcohol (PVA) by glutaraldehyde: effect of crosslink density on the characteristics of PVA membranes used in single chambered microbial fuel cells. RSC Adv [Internet]. 2015 Sep 25 [cited 2021 Jun 22];5(101):83436–47. Available from: www.rsc.org/advances

88. Glyoxal | OHCCHO - PubChem [Internet]. [cited 2021 Jun 22]. Available from: https://pubchem.ncbi.nlm.nih.gov/compound/glyoxal

89. Chiu YC, Brey EM, Pérez-Luna VH. A study of the intrinsic autofluorescence of poly (ethylene glycol)-co-(L-lactic acid) diacrylate. J Fluoresc [Internet]. 2012 May [cited 2021 Jun 15];22(3):907–13. Available from: https://pubmed.ncbi.nlm.nih.gov/22218971/

90. Qi L, Knapton EK, Zhang X, Zhang T, Gu C, Zhao Y. Pre-culture Sudan Black B treatment suppresses autofluorescence signals emitted from polymer tissue scaffolds. Sci Rep [Internet]. 2017 Dec 1 [cited 2021 Jun 15];7(1):1–12. Available from: www.nature.com/scientificreports/

91. Migonney V. History of Biomaterials. In: Biomaterials [Internet]. Hoboken, NJ, USA: John Wiley & Sons, Inc.; 2014 [cited 2020 Apr 16]. p. 1–10. Available from: http://doi.wiley.com/10.1002/9781119043553.ch1

92. Gaudin R, Knipfer C, Henningsen A, Smeets R, Heiland M, Hadlock T. Approaches to peripheral nerve repair: Generations of biomaterial conduits yielding to replacing autologous nerve grafts in craniomaxillofacial surgery. Vol. 2016, BioMed Research International. 2016.

93. Chiellini E, Corti A, D'Antone S, Solaro R. Biodegradation of poly (vinyl alcohol) based materials. Vol. 28, Progress in Polymer Science (Oxford). 2003. p. 963–1014.

94. Lim KS, Klotz BJ, Lindberg GCJ, Melchels FPW, Hooper GJ, Malda J, et al. Visible Light Cross-Linking of Gelatin Hydrogels Offers an Enhanced Cell Microenvironment with Improved Light Penetration Depth. Macromol Biosci [Internet]. 2019 Jun 1 [cited 2020 Mar 4];19(6):1900098. Available from: https://onlinelibrary.wiley.com/doi/abs/10.1002/mabi.201900098

95. Mcmanus M, Boland E, Sell S. Cross-linking methods of electrospun fibrinogen scaffolds for tissue engineering applications Related content Electrospun fibrinogen for urinary tract reconstruction. 2008;

96. Gil-Castell O, Badia JD, Ontoria-Oviedo I, Castellano D, Marco B, Rabal A, et al. In vitro validation of biomedical polyester-based scaffolds: Poly(lactide-co-glycolide) as model-case. Polym Test. 2018 Apr 1;66:256–67.

97. López-Cebral R, Silva-Correia J, Reis RL, Silva TH, Oliveira JM. Peripheral Nerve Injury: Current Challenges, Conventional Treatment Approaches, and New Trends in Biomaterials-Based Regenerative Strategies. Vol. 3, ACS Biomaterials Science and Engineering. American Chemical Society; 2017. p. 3098–122.

98. Huang J, Hu X, Lu L, Ye Z, Zhang Q, Luo Z. Electrical regulation of Schwann cells using conductive polypyrrole/chitosan polymers. J Biomed Mater Res - Part A. 2010 Apr;93(1):164–74.

99. Alberts, B., Johnson, A., Lewis, J., Raff, M., Roberts, K. and Walter, P. Programmed Cell Death (Apoptosis). In: Molecular Biology of the Cell [Internet]. 2002 [cited 2019 Nov 15]. Available from: https://www.ncbi.nlm.nih.gov/books/NBK26873/

100. Kumar A, Han SS. International Journal of Polymeric Materials and Polymeric Biomaterials PVA-based hydrogels for tissue engineering: A review PVA-based hydrogels for tissue engineering: A review, International Journal of Polymeric Materials and Polymeric Biomaterials PVA-based hydrogels for tissue engineering: A review. Int J Polym Mater Polym Biomater [Internet]. 2017 Mar 4 [cited 2021 Jun 22];66(4):159–82. Available from: https://www.tandfonline.com/action/journalInformation?journalCode=gpom20http://dx.doi.org/10.1080/00914037.2016.1190930

101. Enayati MS, Behzad T, Sajkiewicz P, Rafienia M, Bagheri R, Ghasemi-Mobarakeh L, et al. Development of electrospun poly (vinyl alcohol)-based bionanocomposite scaffolds for bone tissue engineering. J Biomed Mater Res - Part A. 2018 Apr 1;106(4):1111–20.

102. Karimi A, Navidbakhsh M. Materials Technology Advanced Performance Materials Mechanical properties of PVA material for tissue engineering applications Mechanical properties of PVA material for tissue engineering applications. Taylor Fr [Internet]. 2013 Mar [cited 2021 Jun 22];29(2):90–100. Available from: https://www.tandfonline.com/action/journalInformation?journalCode=ymte20

103. Naghavi Alhosseini S, Moztarzadeh F, Kargozar S, Dodel M, Tahriri M. Development of Polyvinyl Alcohol Fibrous Biodegradable Scaffolds for Nerve Tissue Engineering Applications: *In Vitro* Study. Int J Polym Mater Polym Biomater [Internet]. 2015 Sep 22 [cited 2020 Mar 4];64(9):474–80. Available from: http://www.tandfonline.com/doi/full/10.1080/00914037.2014.977893

104. Roy S, Kuddannaya S, Das T, Lee HY, Lim J, Hu XM, et al. A novel approach for fabricating highly tunable and fluffy bioinspired 3D poly(vinyl alcohol) (PVA) fiber scaffolds. Nanoscale [Internet]. 2017 Jun 7 [cited 2021 Jun 22];9(21):7081–93. Available from: https://pubs.rsc.org/en/content/articlehtml/2017/nr/c7nr00503b

105. Cao Y, Liu F, Chen Y, Yu T, Lou D, Guo Y, et al. Drug release from core-shell PVA/silk fibroin nanoparticles fabricated by one-step electrospraying. Sci Rep [Internet]. 2017 Dec 1 [cited 2021 Jun 22];7(1):1–9. Available from: www.nature.com/scientificreports/

106. Ojah N, Saikia D, Gogoi D, Baishya P, Ahmed GA, Ramteke A, et al. Surface modification of core-shell silk/PVA nanofibers by oxygen dielectric barrier discharge plasma: Studies of physico-chemical properties and drug release behavior. Appl Surf Sci. 2019 May 1;475:219–29.

107. Gaharwar AK, Mihaila SM, Kulkarni AA, Patel A, Di Luca A, Reis RL, et al. Amphiphilic beads as depots for sustained drug release integrated into fibrillar scaffolds. J Control Release. 2014 Aug 10;187:66–73.

108. Chen X, Lee DS, Zhu X, Yam KL. Release kinetics of tocopherol and quercetin from binary antioxidant controlled-release packaging films. J Agric Food Chem [Internet]. 2012 Apr 4 [cited 2021 Jun 22];60(13):3492–7. Available from: https://pubs.acs.org/sharingguidelines

109. Lauro MR, Torre ML, Maggi L, De Simone F, Conte U, Aquino RP. Fast- and slow-release tablets for oral administration of flavonoids: Rutin and quercetin. Drug Dev Ind Pharm [Internet]. 2002 [cited 2021 Jun 22];28(4):371–9. Available from: https://www.tandfonline.com/action/journalInformation?journalCode=iddi20

110. Kumari A, Yadav SK, Pakade YB, Singh B, Yadav SC. Development of biodegradable nanoparticles for delivery of quercetin. Colloids Surfaces B Biointerfaces. 2010 Oct 15;80(2):184–92.

111. Kumari A, Kumar V, Yadav SK. Plant extract synthesized PLA nanoparticles for controlled and sustained release of Quercetin: A green approach. PLoS One [Internet]. 2012 Jul 23 [cited 2021 Jun 22];7(7):e41230. Available from: www.plosone.org

112. Carrasco E, Casper D, Werner P. Dopaminergic neurotoxicity by 6-OHDA and MPP+: Differential requirement for neuronal cyclooxygenase activity. J Neurosci Res [Internet]. 2005 Jul 1 [cited 2021 Jan 25];81(1):121–31. Available from: https://pubmed.ncbi.nlm.nih.gov/15931668/

113. Zhang Z, Zhang C, Li Z, Zhang S, Liu J, Bai Y, et al. Collagen/β-TCP nerve guidance conduits promote facial nerve regeneration in mini-swine and the underlying biological mechanism: A pilot in vivo study. J Biomed Mater Res - Part B Appl Biomater. 2019;107(4).

114. Santiago LY, Nowak RW, Rubin JP, Marra KG. Peptide-surface modification of poly(caprolactone) with laminin-derived sequences for adipose-derived stem cell applications. Biomaterials. 2006 May 1;27(15):2962–9.

115. Hersel U, Dahmen C, Kessler H. RGD modified polymers: Biomaterials for stimulated cell adhesion and beyond. Biomaterials. 2003;24(24):4385–415.

116. Ko HCH, Milthorpe BK, McFarland CD. Engineering thick tissues - The vascularisation problem. Vol. 14, European Cells and Materials. AO Research Institute Davos; 2007. p. 1–18.

117. Spinal Cord Injury: Hope Through Research | National Institute of Neurological Disorders and Stroke [Internet]. [cited 2020 Apr 16]. Available from: https://www.ninds.nih.gov/Disorders/Patient-Caregiver-Education/Hope-Through-Research/Spinal-Cord-Injury-Hope-Through-Research

118. Ding J, Chen M, Chen W, He M, Zhou X, Yin G. Vapor-assisted crosslinking of a FK/PVA/PEO nanofiber membrane. Polymers (Basel) [Internet]. 2018 Jul 6 [cited 2021 Jun 22];10(7):747. Available from: www.mdpi.com/journal/polymers

## Appendix A – Developing Vapour Chamber Protocol

For developing the vapour assisted method, the protocol for the Frampton lab needed to be developed as a an adaptation from models in the literature (118). The main requirement for the vapour bath was a sealed chamber which could hold the cross-linking agent. Aa the chamber was heated, the vapours should remain within the chamber, allowing cross-linking to proceed. The first prototype for this development was the use of sample vials. A small section of weight boat was fashioned to the top of the sample vial to hold the fibers above the liquid and allow vapours to react with the sample (Supplementary Figure 1).

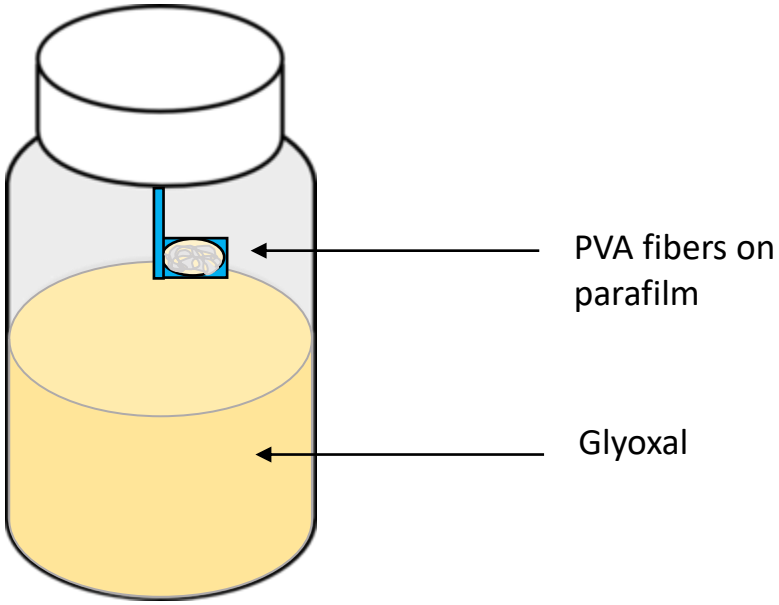


**Supplementary Figure 1.** Original prototype for glyoxal chambers for vapour-assisted cross-linking.

One of the main issues with this prototype was the imaging issues associated with parafilm during rehydration experiments. In Supplementary Figure 2, the issues with discerning synthetic polymer fiber from cellulose present in the parafilm became a significant issue.

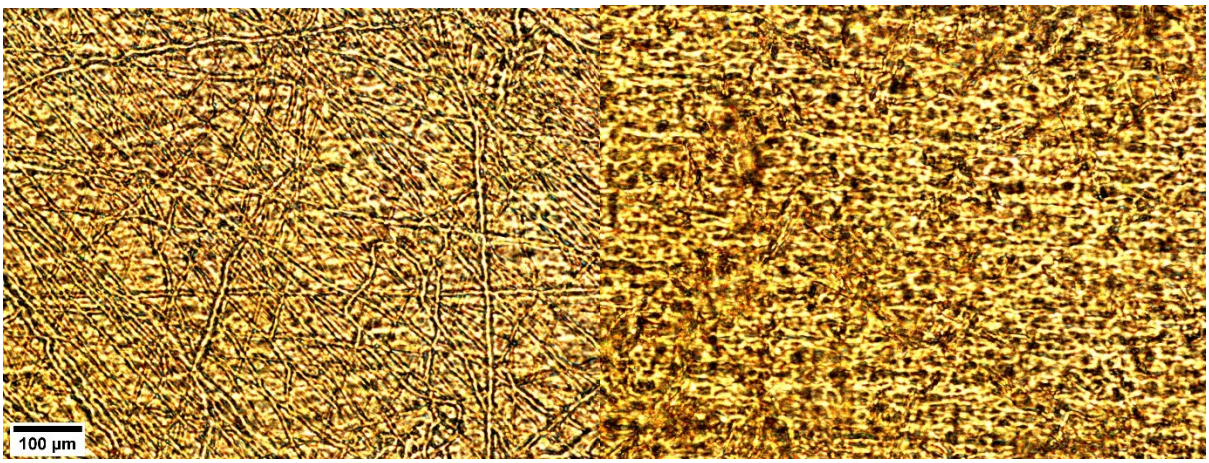


**Supplementary Figure 2.** Images of fibers on parafilm (left) and parafilm only (right).

To alleviate the issues associated with parafilm imaging, the next prototype developed involved the use of larger mason jars and pedestals that could hold weight boats or glass slides above the glyoxal (Supplementary Figure 3).

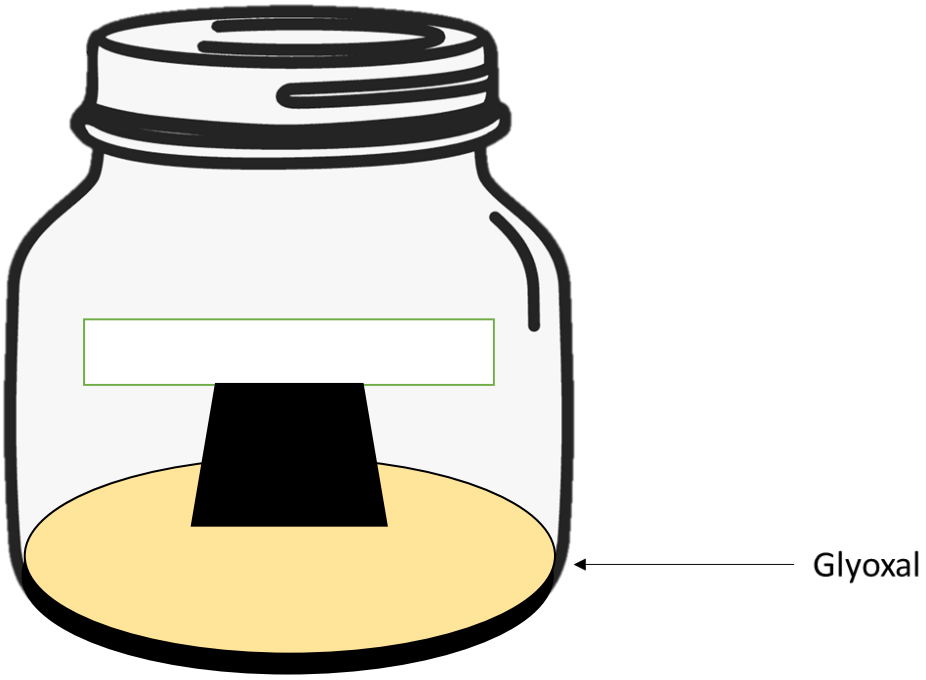


**Supplementary Figure 3.** Second prototype for glyoxal chambers for vapour-assisted cross-linking.

The main issue associated with these chambers was the large tops which during the hours under heat accumulated a large amount of condensation and these droplets were then splashed onto the fibers before they were sufficiently cross-linked and dissolved the fibers, creating a cross-linked film of PVA in the bottom of the weight boat or on the glass slide. This led to the final prototype for the vapour chambers, which included the addition of protecting glass slide "houses" (Supplementary Figure 4). Now with the final addition, the fibers could be effectively cross-linked with glyoxal and retain their fibrous morphology after this processing step.

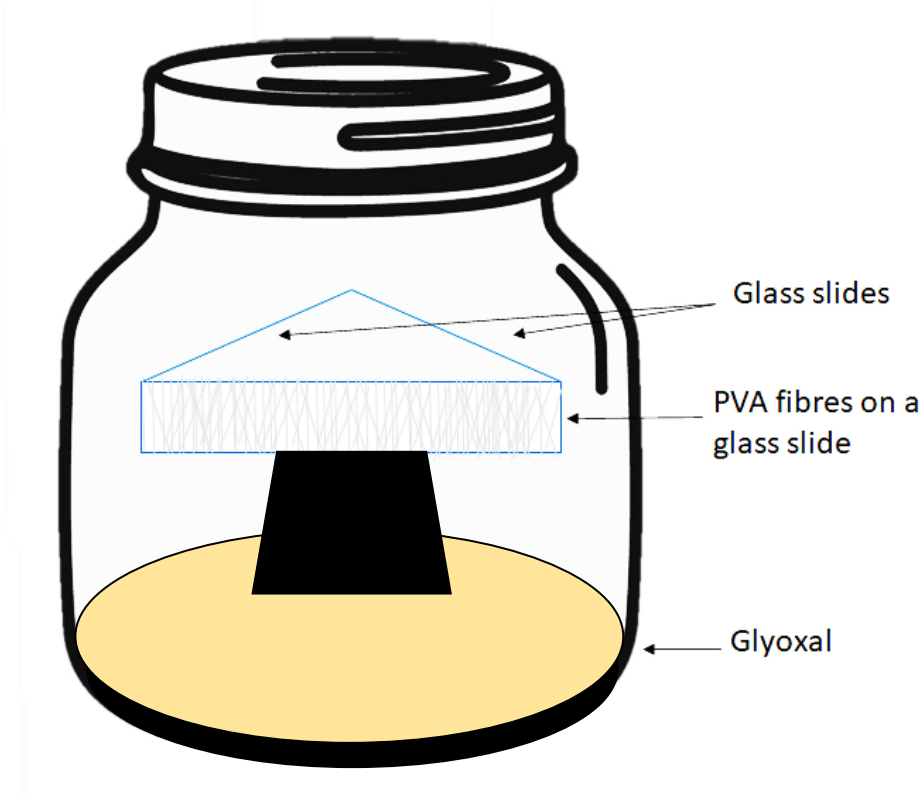


**Supplementary Figure 4.** Final prototype for glyoxal chambers for vapour-assisted cross-linking.

With this final addition, the incorporation of multiple levels for insertion of weigh boats and/or glass slides was possible, allowing for more fibers to be cross-linked in a single chamber.

## Appendix B – IR Spectrum for Quercetin